ADDIS ABABA UNIVERSITY
ADDIS ABABA INSTITUTE OF TECHNOLOGY
SCHOOL OF CIVIL AND ENVIRONMENTAL ENGINEERING

ANALYTICAL INVESTIGATION OF COMPOSITE COLUMN AND RC BEAM JOINT WITH INTEGRATED JOINT CONNECTIONS

A Thesis in Structural Engineering

By

Mahlet Wondwosen

GSR/4511/11

(January 2022)
Addis Ababa

A Thesis

Submitted to the School of Civil and Environmental Engineering in Partial Fulfillment of the Requirements for the Degree of Master of Science

The undersigned have examined the thesis entitled '**Analytical Investigation of Composite Column and RC Beam Joint with Integrated Joint Connections**' presented by **MAHLET WONDWOSEN**, a candidate for the degree of **Master of Science** and hereby certify that it is worthy of acceptance.

Prof. Girma Zerayohannes		Feb. 04/2022
Advisor	Signature	Date
Dr. Abraham Gebre		Feb. 02/2022
Internal Examiner	Signature	Date
Dr. Bedilu Habte		Jan 26/2022
External Examiner	Signature	Date
Dr.Ing. Mebruk Mohammed		
Chair person	Signature	Date

UNDERTAKING

I certify that research work titled “Analytical Investigation of Composite Column and RC Beam Joint with Integrated Joint Connections” is my own work. The work has not been presented elsewhere for assessment. Where material has been used from other sources it has been properly acknowledged /referred.

Mahlet Wondwosen

ABSTRACT

Hybrid structural frame systems, which combine the use of reinforced concrete and steel, are becoming a viable solution for high-rise buildings. But like all innovative solutions, this comes with the problem of connecting the reinforced concrete beam with these composite columns. In this study, the structural performance of concrete-encased composite columns and reinforced concrete beam joints for selected connection types are evaluated. The main objective of this research is to investigate the two common types of connection, passing through type and wing plate type, and the implementation of a combination of these connections at one joint on an interior steel-reinforced concrete composite column to reinforced concrete beam joint under repeated reverse cyclic loading. Furthermore, the effect of column axial load variation for the three connection types has been investigated under cyclic loading. Beam-column joint specimens are obtained from a published experimental study. A non-linear finite element model is then developed using a three-dimensional software, DuCOM-COM3, and validated using the experimental result. An interior steel-reinforced concrete composite column to reinforced concrete beam joint using the passing through and wing plate connection type has been validated and used as control specimens. A comparative study is conducted between the control specimens and the integrated type specimen. In addition, a total of 18 specimens are simulated by varying column axial load on the three connection types. The analytical result showed that the integrated type specimen exhibits increased ultimate shear capacity and ductility from the control specimens. The increase of column axial load up to 20% of the column capacity on the three connection types showed a slight enhancement in the ultimate storey shear capacity. However, the ultimate storey shear capacity decreased as the axial force increased because of the adverse effect of axial forces on the lateral stiffness of the column. Moreover, an increase in column axial load ratio showed a reduction in the ductility performance of the joints. For the wing plate type specimen, an increase in column axial load ratio showed a determinantal effect on the stiffness and the energy dissipation capacity of the joint.

Keywords: Beam-column joint, Steel reinforced concrete column, Column axial load ratio, DuCOM-COM3, Cyclic loading, Hysteretic response, Storey shear capacity, Ductility, Stiffness, Energy dissipation capacity

ACKNOWLEDGMENTS

First of all, I would like to thank God for giving me the strength and the patience to complete this thesis paper.

I would like to express my sincere appreciation, respect, and profound gratitude to my advisor Prof. Girma Zerayohannes, for his tremendous guidance, unending support, and consistent encouragement throughout this research. His guidance helped me in all the time of research and writing of this thesis.

I would like to express my heartfelt appreciation to Dr. Esayas Gebreyouhannes, who gave insight and knowledge that aided this research immensely and for always being there when I needed his support. He also provided me the DuCOM-COM3 software and through several discussions, taught and advised me on how to use it.

Next, I would like to acknowledge Dr.-Ing. Adil Zekaria and Dr. Abreham Gebre for their continuous encouragement and concern. I would also like to thank my colleagues Yisshak Tadesse for his assistance in formulating the thesis idea and Mohammed Sirage for his invaluable support and advice.

I would also like to thank my friend Natnael Ayele for all of his support and encouragement during difficult times. I am also grateful to my friends for their constant moral support and encouragement.

Last but not the least, I would like to express my deepest gratitude to my family for providing me continuous support and encouragement throughout my years of study and through the process of researching. I would also like to thank them for their unconditional love, patience, and prayer. This accomplishment would not have been possible without them.

TABLE OF CONTENTS

LIST OF TABLES

LIST OF FIGURES

LIST OF SYMBOLS

A_s	Area of the steel section
A_c	Area of concrete fill or encasement
A_{sr}	Area of continuous reinforcing bars
f'_c	Compressive strength of concrete
f_y	Yield stress of the steel section
f_{ysr}	Yield stress of reinforcing bars
V'_r	Longitudinal shear force
P_{rs}	External force
P_{no}	Composite section plastic capacity
h_{sc}	Depth of the web of steel column
t_w	Thickness of the web of steel column
f_{ce}	Effective concrete strength of the inner strut
h_c	Depth of the column
K_c	Confinement factor
b_f	Width of steel beam flanges
∅	Diameter
f_{cd}	Design concrete compressive strength
μ_Δ	Displacement ductility factor

LIST OF ABBREVIATIONS

RC	Reinforced concrete
SRC	Steel reinforced concrete
CFTs	Concrete filled tubes
AISC	American Institute of Steel Construction
TWSTCC	Thin-Walled Steel Tube Confined Concrete
CFST	Concrete Filled Steel Tube
ALR	Axial load ratio
ADE	Accumulated dissipated energy
FE	Finite element
EN	Eurocode

CHAPTER 1 INTRODUCTION

1.1 Background

The use of hybrid structural frame systems is becoming an alternative for high-rise structures. This is apparent in developing nations where reinforced concrete (RC) is the main construction unit and has a limited application for complex infrastructures. And the complete transition to steel or composite structures may have a socioeconomic implication which most developing nations are not ready to bear. Hence the use of conventional RC and composite and/or steel structures is a viable solution being implemented.

In high-rise buildings, integrating composite columns in RC structures is a common solution for problems that arise with a large amount of gravity load. The cross-section of the reinforced concrete column must be enlarged to carry the increased gravity load as the building's height increases, but having large dimensions is not acceptable from the architectural point of view. However, as with all novel solutions, there is the problem of connecting the RC beam to the composite columns.

To address this problem several alternatives are implemented. These can be categorized as being the passing through type, the wing plate type, the H-beam bracket type, and the mechanical coupler type (Ju & Chun, 2005) as shown in Figure 1-1.

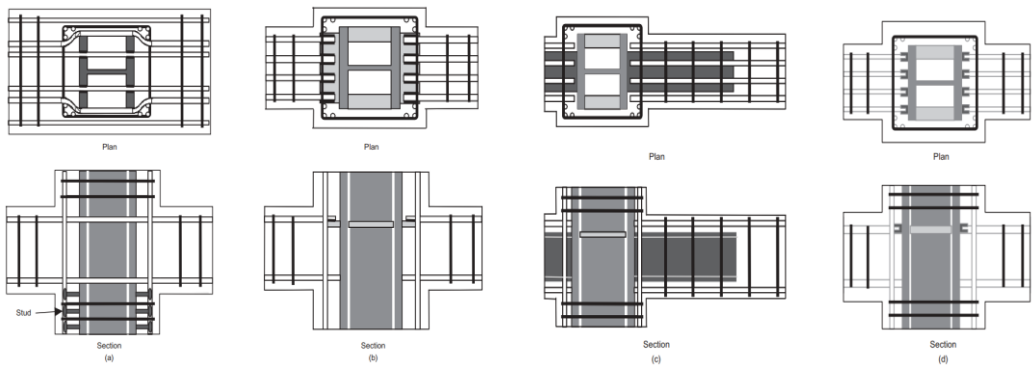

Figure 1-1 Connection types: (a) passing through type; (b) wing plate type; (c) H-beam bracket type; (d) coupler type (Ju & Chun, 2005)

The difficulty of providing the required complete anchoring of the RC beam's longitudinal reinforcement is still a concern in all situations except the passing through type. And in theory, the coupler type, depending on the mechanical splicer and the welding quality has good reliability as well. Providing the desired anchorage is vital for the plastic hinge formation in beams and the energy dissipative design. To ensure the hierarchy of plastic hinge formation in Capacity Design, as depicted in most design codes including the Eurocode 8 and the Ethiopian building code ESEN 1998,1-1(EBCS EN- 8 Part, 2014; Eurocode 8, 2003), understanding the behavior of these connections under seismic/cyclic forces is a must.

Furthermore, in practice, the provision of complete and exclusive use of one of these connection types is not feasible due to difficulty in construction and geometry at joints. Hence, an integrated application of two connections types is usually implemented.

In this research, the nonlinear finite element software DuCOM-COM3 was used to perform nonlinear finite element analysis of steel-reinforced concrete (SRC) composite column and reinforced concrete (RC) beam joints. All of the proposed investigations were preceded by comprehensive validation of the software against existing experimental results. Then, the nonlinear finite element investigation was divided into two parts. Part one focuses on the investigation of the two common types of connection, passing through type and wing plate type, and the implementation of a combination of these connections at one joint on an interior steel-reinforced concrete composite column to reinforced concrete beam joint under reverse cyclic loading with a constant column axial load is examined using nonlinear finite element analysis. In the second part, a parametric study is carried out to investigate the effect of column compressive axial load variations on the performance of SRC column - RC beam joints on three types of connections: passing-through, wing type, and the integrated use of the two connection types (integrated type) under cyclic loading.

1.2 Statement of the problem

The structural performance of concrete-encased composite column and reinforced concrete beam connection at moment-resisting frame joints is not clearly understood. For frame structures in seismic regions, this property is very important to the ductile response

of the building to ensure the energy dissipative design procedures taken are realized. In addition, providing the desired full anchorage of the longitudinal reinforcement of the RC beam is still an issue.

1.3 Objective

1.3.1 General Objective

The objective of the research is to understand the behavior of composite column and RC beam joints for selected types of connections under seismic actions (cyclic loading) using nonlinear finite element analysis, and in doing so to have an understanding with an acceptable level of certainty of the rigidity, strength, energy dissipative capacity, and ductility provided by these joints.

1.3.2 Specific Objective

The specific objectives of this study can be summarized as follows:

i. To predict and validate the numerical results of SRC column - RC beam joints obtained from DuCOM-COM3 simulation with existing experimental results through load-displacement response, peak load, and crack pattern.
ii. To understand the structural performance of SRC column - RC beam joints using the integrated type connection.
iii. To assess the influence of column compressive axial load variations on the seismic behavior of composite column and RC beam joints using nonlinear finite element analysis.

1.4 Significance of the study

Currently, the researches on this specific topic are limited and almost no discussions are put forward with regards to the specific performance and suitability of these joints for a frame in earthquake-prone regions. The existing experimental study focused on the application of these joints for underground structures and did not cover the integral use of these connections at one joint. This paper aims to focus on two common types of connections; passing-through and wing plate type connection. Their seismic performance and suitability will be assessed separately. Taking practical applications into consideration,

the implementation of a combination of these connections at one joint will also be a major question to address and this study also provides the influence of axial load variation on the response of SRC column and RC beam joints under cyclic loading on each connection types as a parametric study.

1.5 Scope of the study

- The floor slab contribution to the beam-column joint hysteretic response is not taken into account.
- Because of the constraints of laboratory test equipment, a 3D non-linear finite element analysis is carried out.
- Only reversed cyclic loading analysis is performed.
- To assess the joint performance, the storey shear force - storey displacement hysteretic response is investigated.
- Steel reinforced concrete (SRC) composite column is used in this study and a perfect bond is assumed between structural steel and concrete.

1.6 Thesis Layout

This thesis is composed of five chapters. Chapter 1 presents the background, statement of the problem, objectives, significance of the study, and scope of the study. Chapter 2 provides a literature review of the existing literature in the relevant field of the research in this thesis. It covers theoretical background on beam-column joints, load transfer mechanism of the composite column, shear strength model of SRC joints and it reviews existing literature on composite column and reinforced concrete beam joints. Chapter 3 provides the methodology used in this study. It discusses experimental specimens for model validation, specimens for the current numerical study and it also provides the material property, test setup, and restraint condition of the interior steel-reinforced composite column and reinforced concrete beam joint specimen. Finite element modeling using DuCOM-COM3 software and validation of the nonlinear finite element model with experimentally tested specimens is also discussed in this chapter. Chapter 4 presents the analytical result and discussions of the specimens. The final chapter, Chapter 5, presents the conclusions drawn from the findings of this study as well as recommendations for future work.

CHAPTER 2 LITERATURE REVIEW

2.1 General

This chapter provides a review of the existing literature in the relevant field of the research in this thesis. It attempts to present achievements and conclusions drawn from published research works and at the same time emphasize some gaps which are to be studied in this thesis. It starts with a theoretical background of joints, followed by load transfer mechanism in composite column, shear strength model in SRC joints, and then existing researches on composite column - reinforced concrete beam joints.

2.2 Theoretical Background

Joints are crucial components that join frame columns and beams. Joints maintain structural continuity and transmit forces existing at the ends of members. The beam-column joint is a critical component of RC structures because beams often fail at the beam-column joints. The reasons for their critical behavior include a sudden change in geometry and the intricacy of the stress distribution at the joint. A joint, which is the area where beams and columns meet, permits the linked elements to grow and retain their maximum capacity. The joints must be strong and rigid enough to withstand the internal forces of the frame elements.

The intended joint performance criteria can be stated as follows: (Paulay & Priestley, 1992).

i. The joint strength shall not be less than the maximum demand corresponding to the development of the structural plastic hinge mechanism for the frame. This eliminates the need for repair in a relatively inaccessible zone, as well as energy dissipation via joint mechanisms, which, as will be shown later, suffer severe stiffness and strength deterioration when subjected to cyclic actions in the inelastic range.
ii. The column's capacity should not be affected by potential strength deterioration within the joint. The joint is also an important and integral element of the column.

iii. The joint reinforcement required to guarantee good performance should not create additional construction challenges.

2.2.1 Failure Mechanism of Beam-Column Joint

Knowledge of stresses in joint and failure mechanisms is required for joint designs that can convey forces efficiently(Kaliluthin, Kothandaraman, & Ahamed, 2015). For reinforced concrete structures in seismic regions, beam-column joints are often designed using the widely recognized strong column weak beam philosophy. This is preferable because the inelastic movements occur in beam plastic hinges, whereas plastic hinges in columns, which might produce a soft story mechanism, are avoided.

Aside from other factors, the strength of the beam-column joint is determined by the compressive, shear, and bond strength of the concrete, as well as the tensile strength of the reinforcement at the joint. According to Al-zamel, H. S. and El-Ghazaly, H.A.et al.(1991) (El-Ghazaly & Al-Zamel, 1991), the primary causes of joint failure are anchorage failure, failure as a result of reinforcement yielding, failure as a result of concrete crushing, and Cracking due to diagonal tension.

The joint-to-member interfaces are critical sections for transferring member forces to the connection (Pinkham et al., 1985). Detailing also has a strong impact on the load transmission mechanism via bond.

Large horizontal shears inside the joint are caused by very strong lateral loads, notably from seismic forces. During load reversals, shear in the joint generates diagonal cracks, which combine to form a grid of inclined cracks. When the ultimate capacity of the adjoining members is developed, the diagonal tension can become extremely high, resulting in extensive diagonal cracking. As a result of this diagonal cracking, the beam-bar anchorage has deteriorated. In addition to diagonal cracking, the joint may experience flexural cracking. The majority of the crack damage in strong column-weak beam joints is focused on the beams towards the column face. The interface between beam ends and the column face is where the most flexural cracks occur. (Raffaelle, G.S. and Wight, 1992).

2.2.2 Structural Properties of Joint

The following are the specific structural properties that must be addressed.

i. **Stiffness**

If deformations caused by lateral forces are to be accurately assessed and then regulated, a realistic assessment of the relevant characteristic known as stiffness must be made (Paulay & Priestley, 1992). This quantity describes the relationship between loads or forces and the resulting structural deformations.

ii. **Strength**

To safeguard a concrete structure from damage during a specific seismic event, inelastic excursions during its dynamic reaction must be avoided. To withstand internal actions produced during the structural elastic dynamic response, the structure must be of sufficient strength. As a result, an elastic analysis based on stiffness properties is a suitable approach for evaluating earthquake-induced activities. The seismic actions, when combined with other loads on the structure, such as gravity, will result in the proportioning of structural elements, perhaps with minor changes (Hung-Jen Lee and Jen-wen ko, 2007). As a result, the designer can offer the necessary strength in terms of lateral force resistance.

iii. **Ductility**

Structures must be capable of sustaining a high proportion of their initial strength when a strong earthquake imposes significant deformations to prevent serious damage and assure the survival of buildings with modest resistance to lateral forces. These deformations might be well beyond the elastic limit. The ability of a structure or its components, or the materials employed, to provide resistance in the inelastic domain of response is referred to as ductility. This comprises the ability to withstand significant deformations as well as the ability to absorb hysteretic energy. This is why, in seismically active areas, the building designer prioritizes it as the most important property.

Ductility in structural components can only be developed if the constituent material is ductile in the first place. Thus, if resistance is given by steel in tension, achieving the necessary ductility is quite simple. When steel is compressed, however, precautions must

be taken to guarantee that early buckling does not interfere with the formation of the required large inelastic strain in compression (Paulay & Priestley, 1992).

2.3 Load transfer in composite column

Composite columns, which are made up of reinforced concrete and encased steel sections, combine the benefits of these two materials, allowing the strength of the concrete and steel sections to be fully utilized. Steel sections, typically with high yield strength and good ductility, contribute to the column's bearing capacity and ductility. The reinforced concrete, on the other hand, protects the steel sections against buckling and fire. The bearing capacity of the composite column is greater than the sum of the bearing capacities of the concrete and steel sections because of the composite action between the concrete and steel sections.

Composite columns are generally divided into two types: filled composite columns, also known as concrete-filled tubes (CFTs), and encased composite columns, also known as steel-reinforced concrete (SRC) columns. To establish a condition of internal balance of equilibrium and act in a composite way, force must be transmitted between the components of different materials.

Steel reinforced concrete (SRC) composite columns can be loaded by connecting directly to the concrete encasement, the steel member, or both materials at the same time. Figure 2-1 depicts examples of force introduction to SRC composite column. A beam can be connected to a steel form only by using extended shear tabs. Similarly, external forces can be delivered by concrete alone, or a cap plate can engage both materials at the same time. In the AISC manual, a plastic stress distribution model is used to determine the section strength of composite columns, indicating that both the steel and RC sections are expected to attain their yield and crushing strengths.

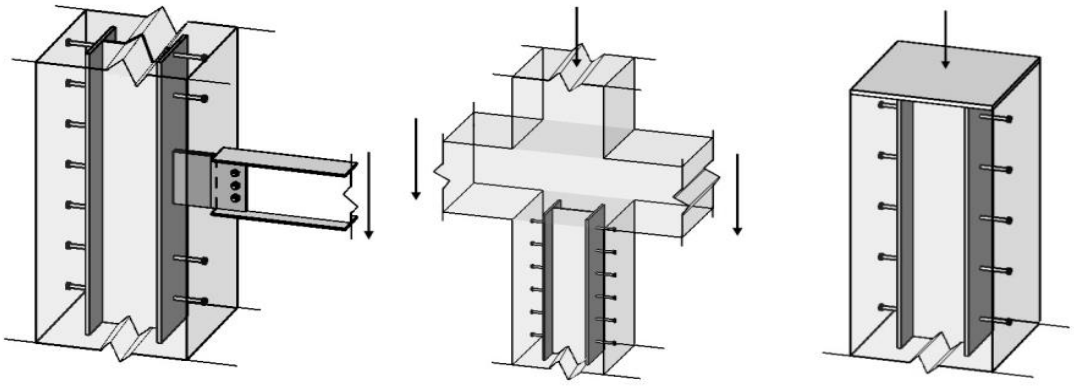

(a)	(b)	(c)
Load transfer to SRC with steel connection	Load transfer to SRC with concrete connection	Load transfer to SRC via concrete and steel concurrently

Figure 2-1 Force Introduction to SRC Columns (AISC, 2010)

This model for SRC columns is represented by the composite member section strength P_{no}, which is as follows (AISC, 2010).

$$P_{no} = A_s F_y + A_{sr} F_{ysr} + 0.85 A_c f'_c \quad (\mathbf{2.1})$$

Where: A_S denotes the area of the steel section, in^2 (mm^2); A_C denotes the area of concrete fill or encasement, in^2 (mm^2); A_{SR} denotes the area of continuous reinforcing bars, in^2 (mm^2); f'_C denotes the specified compressive strength of concrete, ksi (MPa); F_y denotes the specified minimum yield stress of the steel section, ksi (MPa); F_{ysr} denotes the specified minimum yield stress of reinforcing bars, ksi (MPa).

The AISC Specification mandates that the applied external forces be distributed within the composite section based on the same ratio of steel section strength to reinforced concrete section strength as described by the plastic capacity model.

If the whole external force is exerted on the steel segment:

$$V'_r = P_r (1 - A_s F_y / P_{no}) \quad \mathbf{(2.2)}$$

If the whole external force is exerted on the Concrete segment:

$$V'_r = P_r (A_s F_y / P_{no}) \quad \mathbf{(2.3)}$$

If the external force is exerted simultaneously to both materials:

$$V'_r = P_{rs} - P_r (A_s F_y / P_{no}) \quad \textbf{(2.4)}$$

Where: V'_r is the required longitudinal shear force to be transferred, kips (N); P_r is the required external force applied to the composite member, kips (N); $A_s F_y$ is the plastic capacity of steel section, kips (N); P_{rs} is the external force section applied to the steel, kips (N); P_{no} is the composite section plastic capacity as calculated by 2010 AISC Equations.

2.3.1 Mechanism for force transfer

After determining the longitudinal shear force, V'_r, a force transfer mechanism must be chosen to transport this force between steel and concrete. The force transfer mechanism methods specified by the AISC standard are direct bearing, shear connection, and direct bond interaction. For the SRC composite column, the standard allows the use of direct bearings or shear connections.

2.3.2 Load introduction length

Load introduction length is provided for the transfer of longitudinal shear force to take place. Because it is critical for this shear transfer to occur as quickly as possible to facilitate composite action, the AISC specification limits the load introduction length above and below the load transfer region to two times the minimum transverse dimension (or diameter for circular filled tubes). Figure 2-2 illustrates the load introduction length concept for SRC Column.

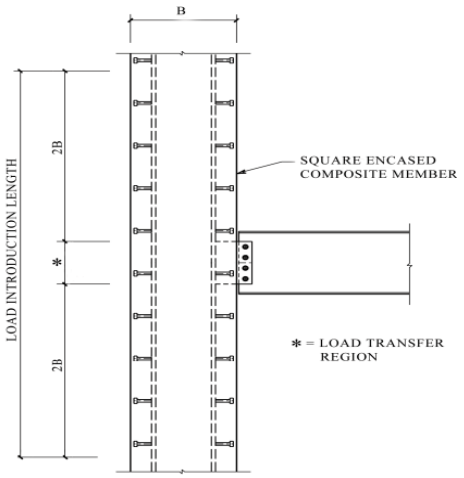

Figure 2-2 Load Introduction Length

2.4 Shear Strength model in SRC joints

In reinforced beam-column joint diagonal tension and compression stresses in the joint core are caused by the internal forces that are transferred from adjacent members as a result of horizontal and vertical shear forces. These shear forces are resisted by two mechanisms, the diagonal concrete strut, and truss mechanisms (Paulay & Priestley, 1992).

Jia et al.(2011) proposed a new model for predicting the horizontal shear strength of SRC column beam connections, in which the contribution of the steel web, inner concrete compression strut, and outer concrete compression strut is divided into three parts: steel web, inner concrete compression strut, and outer concrete compression strut (Jia et al., 2011). Figure 2-3 shows the strength mechanisms of the three parts of the joint.

$$V = V_w + V_{inner} + V_{outer} \quad \textbf{(2.5)}$$

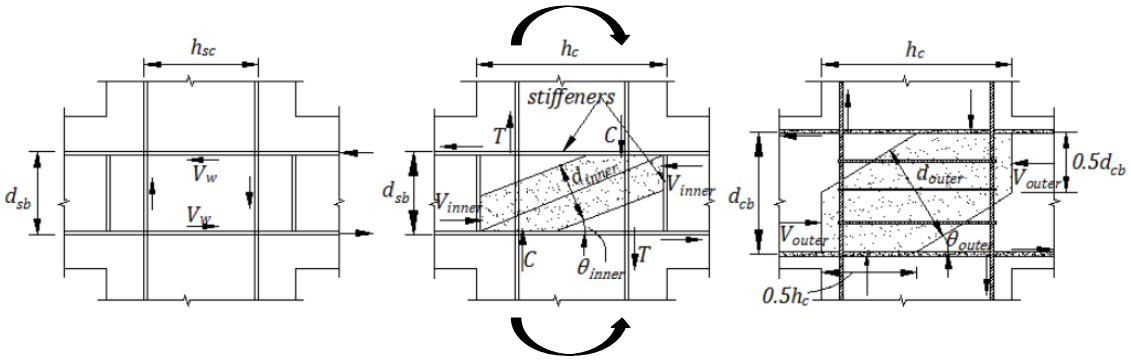

(a) Steel web panel (b) Inner concrete strut (c) Outer concrete strut

Figure 2-3 Strength Mechanisms in SRC joints (Jia et al., 2011)

2.4.1 Strength Contribution of Steel Web

The contribution of steel web to the horizontal shear strength of a joint is given by

$$V_w = \int_0^{h_{sc}} \tau_{web}\ (x) t_w dx = \frac{f_y}{\sqrt{3}} t_w h_{sc} \quad \textbf{(2.6)}$$

Where h_{sc} is the depth of the web of steel column, t_w is the thickness of the web of steel column and f_y is the strength of steel web column.

2.4.2 Strength Contribution of Inner Diagonal Concrete Strut

The web stiffeners or concrete of beam ends and the steel beam flanges are the ones that activate the inner diagonal concrete strut in the SRC connection. The horizontal shear strength of the connections contributed by the inner concrete strut is given by:

$$V_{inner} = 0.3\, f_{ce} h_c\, (b_f - t_w) \quad \textbf{(2.7)}$$

$$f_{ce} = k_c \beta\, f_c \quad \textbf{(2.8)}$$

Where f_{ce}: effective concrete strength of the inner strut

f_c: uniaxial compressive strength of concrete

h_c: depth of the column

k_c: confinement factor kc = 2 is assumed

$\beta = 0.6$ is suggested

t_w: thickness of the web of the steel column

b_f: width of steel beam flanges

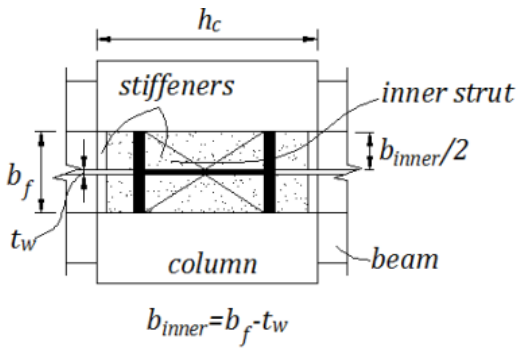

Figure 2-4 Inner strut width (Jia et al., 2011)

2.4.3 Strength Contribution of Outer Diagonal Concrete Strut

Force transferred from web stiffeners of a steel beam or concrete of beam ends to outer concrete in a SRC joint activate the outer diagonal concrete strut which works like the concrete strut in a reinforced concrete beam-column joints.

The horizontal shear capacity of the connections of the outer concrete strut is provided by:

$$V_{outer} = 0.6\, f_c\, b_{outer}\, d_{outer} \quad \textbf{(2.9)}$$

$$d_{outer} = d_{cb} h_c / \sqrt{(d_{cb}^2 + h_c^2)} \quad \textbf{(2.10)}$$

Where d_{cb}, is the outer joint depth, is the distance from the centroid of the beam tensile reinforcement to the centroid of the beam compression reinforcement.

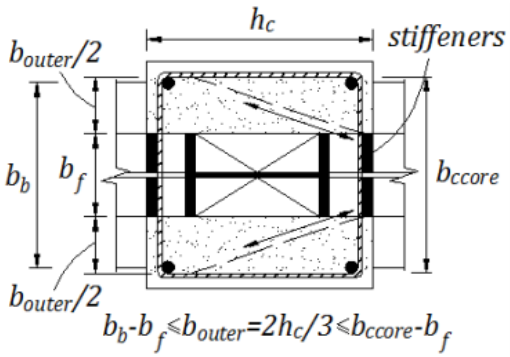

Figure 2-5 Outer strut width (Jia et al., 2011)

2.5 Existing Researches on Reinforced concrete beam - Composite Column joint

SRC columns are commonly employed in structures with superior elevations since they offer more capacity for bearing and higher ductility than conventional RC columns. As the story number of the building increases, the dimensions of mega-columns have to be enlarged to carry the increased gravity load. The importance of the beam-column connection problem emerged by increasing the use of composite columns. Because the connection zone between reinforced concrete beams and composite columns needs special attention, studies have been published in the relative areas. In these studies, many parameters are covered including column cross-sectional types, column axial load ratio, the effect of reinforcement ratio, joint type, the existence of RC slab or not. This section provides a review of relevant studies on the structural response of Composite columns to RC beam joints subjected to cyclic loading.

Han et al.(2009) carried out an experimental cyclic loading test on TWSTCC column to RC beam joints. The column types (Thin-Walled Steel Tube Confined Concrete or Concrete Filled Steel Tube), the column cross-sectional shape types (square column or circular column), and the amount of the relative axial load applied to the column (n=0.05, 0.3 and 0,6) have been identified and designed as parameters to examine the effect of the above altering parameters in two specimens. From the test result, some conclusions are drawn and it was found that the TWSTCC column to RC beam joints failed at the plastic hinges of the beams showing a mode of bending failure, while the CFST joints failed at the joint core zone due to shear failure plus the integrity and cyclic performance of the TWSTCC joints was generally better than that of CFST joints and has shown good seismic performance which can be adoptable in practical building structures, particularly in earthquake zone (Han, Qu, Tao, & Wang, 2009). The details of tested joints are shown in Figure 2-6.

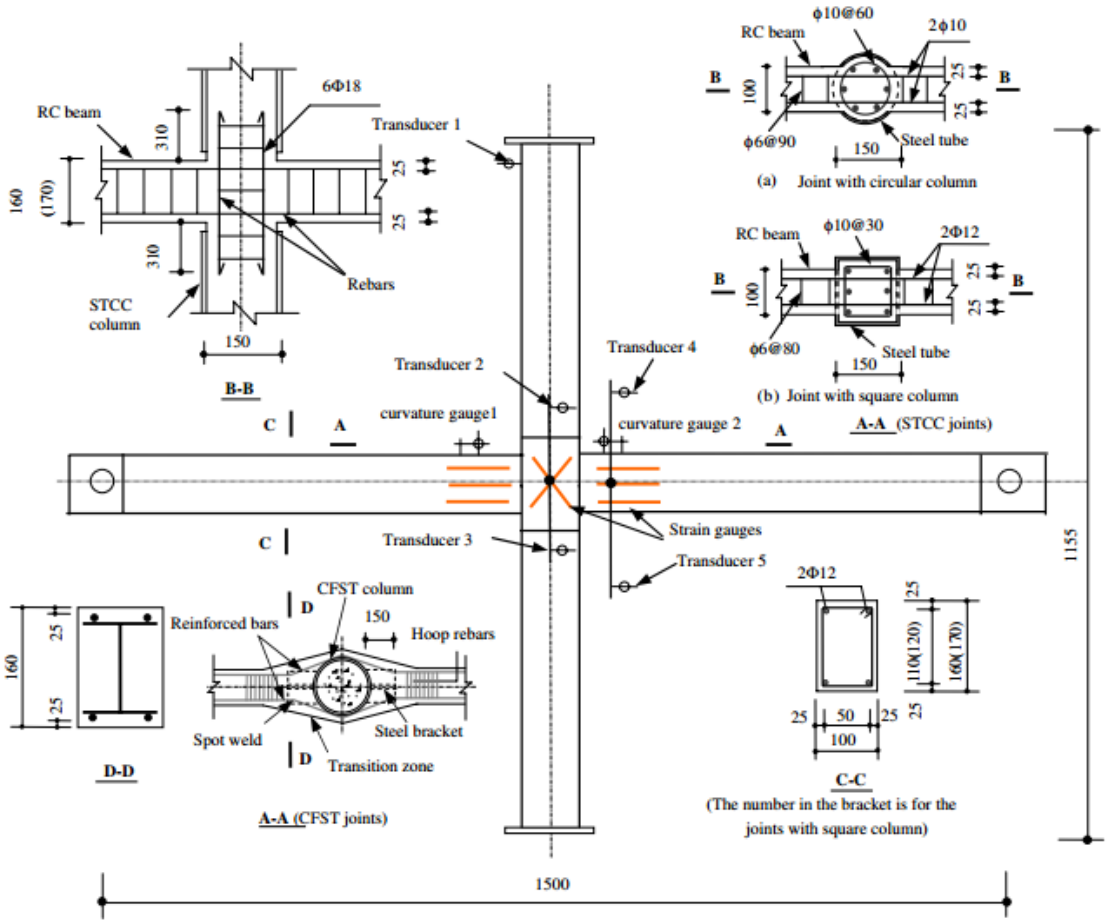

Figure 2-6 Details of TWSTCC (STCC) and CFST test joints (unit: mm) (Han et al., 2009)

Nie et al.(2008) proposed a new connection for a concrete-filled steel tube composite column and RC beams, where the steel tube is interrupted for through-beam by the steel reinforcement bars in the RC beam to be continuous in the floor. He conducted an axial compression test and reversed cyclic loading test on three interior column and three corner column specimens to evaluate the new beam-column system. He experimentally observed that that effective confinement can be achieved by the stiffening ring, and an excellent axial bearing capacity can be obtained, as well as a superior ductility and energy dissipation capacity (Bai, Nie, & Cai, 2008).

Chen et al.(2014) investigated the seismic and post-seismic behavior of a new type of circular through connection zone for reinforced concrete beams and concrete-filled steel tubes. He conducted a cyclic loading test and subsequent axial compression test on six beam-column specimens. The connection area demonstrated high energy absorption capacity under cyclic loading, as well as excellent post-seismic performance. A finite element model is also developed and validated by a comparison with the experimental results and a parametric study was conducted. They were able to observe the influence of the frame beam and ring beam reinforcement ratios, as well as the axial compressive force in the column, on the seismic behavior of the connection. In the study, they developed a formula for calculating the compressive axial load capacity of this type of connection, as well as conducting experiments to verify the formula's accuracy(Q. Chen, Cai, Bradford, Liu, & Wu, 2015; Q. J. Chen, Cai, Bradford, Liu, & Zuo, 2014). The details of tested joints are shown in Figure 2-7.

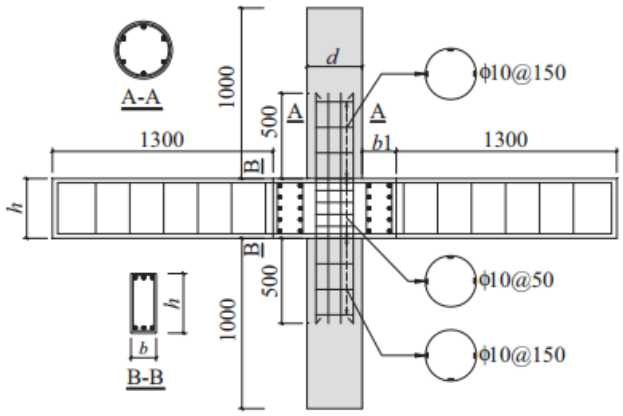

(a) Elevation view

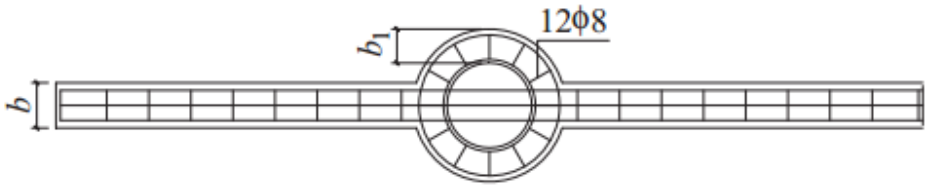

(b) Plan view

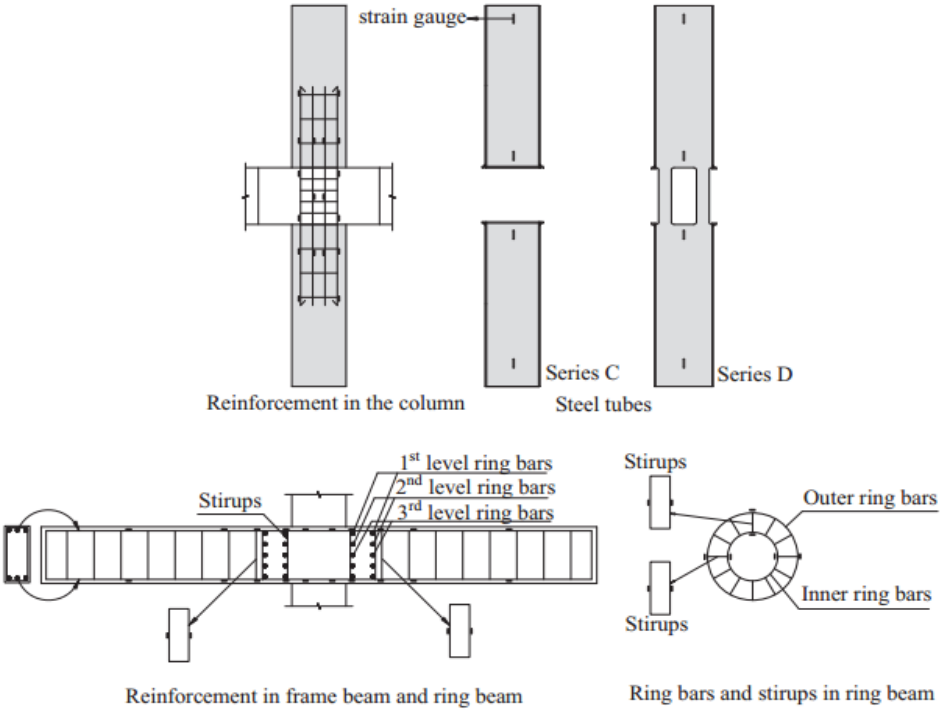

(c) Location of strain gauge

Figure 2-7 Details of specimens (Q. J. Chen, Cai, Bradford, Liu, & Zuo, 2014)

Zhang et al.(2012) studied the behavior of ring beam joints between concrete-filled twin steel tube columns and reinforced concrete beams experimentally. For the longitudinal rebar of the reinforced concrete beam to not be stopped at the junction, the outer steel tube was interrupted. To compensate for the reduced stiffness of the composite column caused by the interruption of the steel tube, confinement of the steel cage anchored inside the joint zone and octagonal ring beam located outside the column was introduced. Four beam-column specimens were tested under cyclic load and their seismic behavior was studied and discussed the load-deflection performance, typical failure modes, stress and strain distributions, and energy dissipation capacity. According to the test result, joints with good aseismic behavior may readily achieve the antiseismic design concepts of "strong column-

weak beam" and "strong joint-weak member." Parametric evaluations were also carried out using finite element modeling (Zhang, Zhao, & Cai, 2012).

Ding et al.(2017) studied the seismic behavior of a new type of non-through core connection between CFST column and SRC beams. A cyclic loading test was conducted on several non through – core connections. The hysteretic response, the skeleton curve, ductility, strain curve, stiffness degradation, and energy dissipation curve were all discussed after he developed a finite element model for analysis. He concluded that the proposed connection works well with concrete-filled steel tubular - steel reinforced concrete joints and had a good seismic performance (Ding, Yin, Wang, Hu, & Chen, 2017).

A cyclic loading test was conducted on four concrete-encased CFST columns to RC beam joints, and three concrete-encased CFST columns to steel beam joints (Liao, Han, & Tao, 2014). The test parameters included the presence of the RC slab or not, axial load level on the composite column, and joint type. The strength, ductility, deterioration of the stiffness, and dissipated energy of the specimens are examined based on the test findings. Based on the test results, the authors concluded that the composite joints demonstrated good seismic performance and may be used in high seismic regions. Figure 2-8 depicts the details of the tested joints.

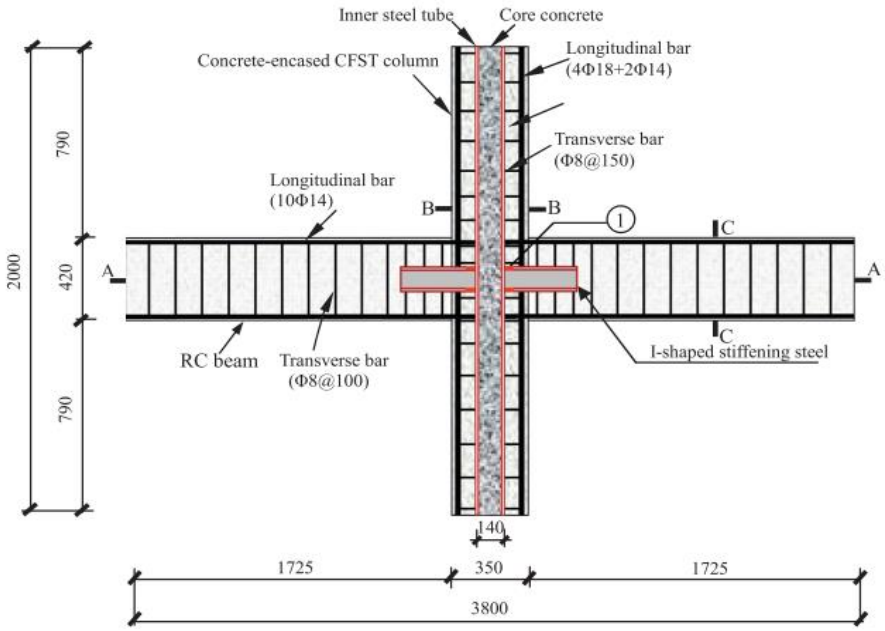

(a) Elevation view

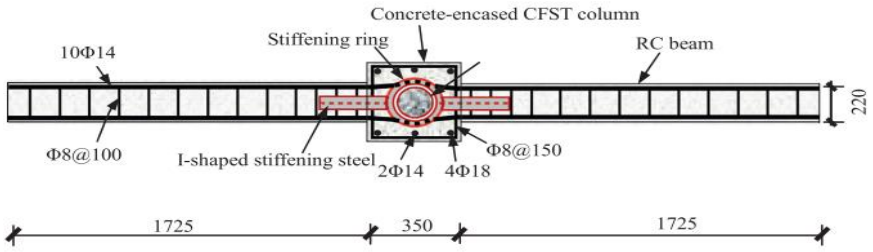

(b) Plan view

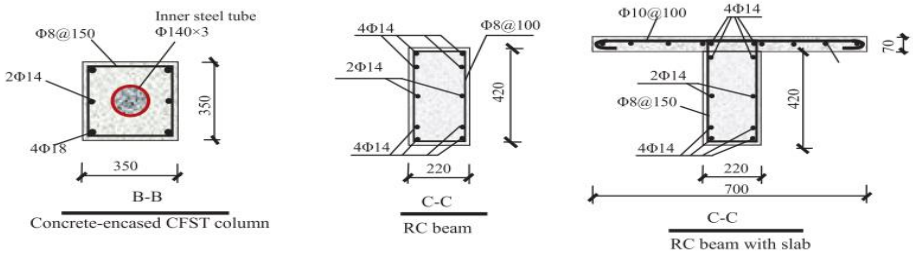

(c) Section of beam and column

Figure 2-8 Details of concrete-encased CFST column to RC beam joints (unit: mm) (Liao et al., 2014)

The existing research's on SRC structures is mainly concentrated on the performance of SRC columns which demonstrated the fact that SRC columns have generally good performance and have the potential of being used in engineering practice. However, one of the most important and problematic components of a moment-resisting frame structure is the connection between the beams and columns, which plays a vital role in the resilience of a building during an earthquake and there is still no sufficient information on beam-column joints of SRC column system particularly on the seismic design of composite connection with SRC column and RC beam joint.

Research on this particular topic is currently limited and almost no discussion is being made regarding the specific performance and adequacy of these joints for frame structures in areas susceptible to earthquakes.

The prominent work by Young-Kyu Ju has significantly put a shade of light on this topic with regards to the application of these joints for underground structures. The work by Young-Kyu Ju concluded that the passing through type and the wing type connections are

the better alternatives over the H-beam type connection(Ju & Chun, 2005). He also proposed a modification to the H-beam bracket type, with a satisfactory structural performance and economically viable solution. But his work did not cover the integral use of these connections at one joint. The details of the specimens are shown in Figure 2-9.

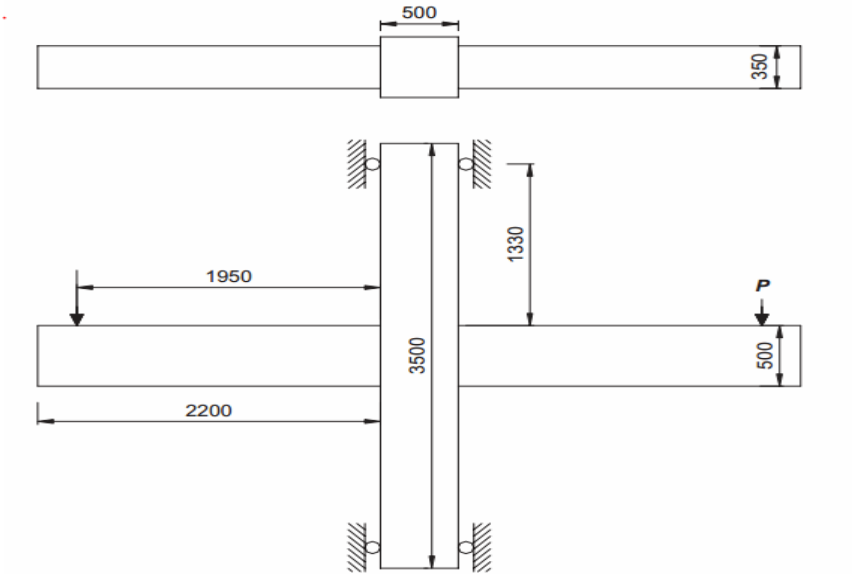

(a) Elevation view

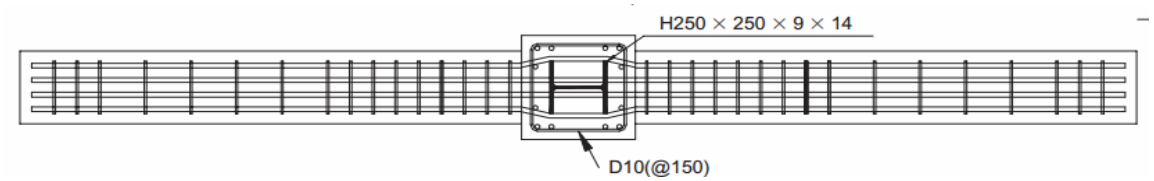

(b) Plan of Passing through type

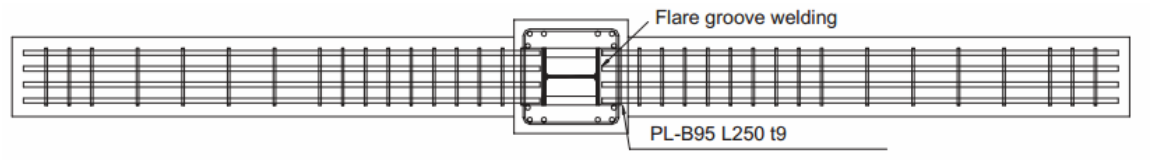

(c) Plan of wing plate type

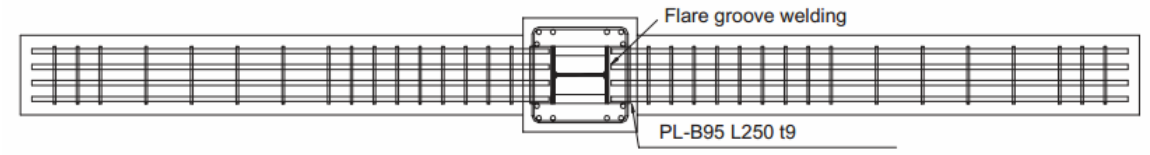

(d) Plan of H-beam bracket type

Figure 2-9 Details of specimens for cyclic loading tests (dimensions in mm) (Ju & Chun, 2005)

This paper is thus an attempt to study the seismic performance of steel-reinforced concrete (SRC) column to reinforced concrete (RC) beam joints where two types of connections are integrated or used together on one joint. The connections are passing-through and wing plate type connections. The non-linear finite element analysis of steel-reinforced concrete (SRC) column to reinforced concrete (RC) beam joints were carried out using the nonlinear analysis software DuCOM-COM3.

CHAPTER 3 METHODOLOGY

3.1 General

The behavior of steel-reinforced concrete (SRC) composite column to reinforced concrete (RC) beam joint is investigated through numerical analysis in DuCOM-COM3. DuCOM-COM3 is non-linear finite element software and this program was developed at the University of Tokyo. The program is an integral of the two simulation tools, DuCOM and COM3. DuCOM stands for Durability Models of Concrete and traces the development of concrete hardening (hydration), structure formation, and several associated phenomena, from casting of concrete to a period of several months or even years while COM3 is a three-dimensional finite element simulating tool.

In this chapter, the experimental specimens for model validation are described and their geometry and reinforcement details are presented. The specimens for the current numerical study are also presented. Following that, finite element modeling, which includes modeling in DuCOM-COM3, modeling of geometry, creating mesh, material properties, bond element, and restraint condition used to simulate the SRC column and RC beam joints under cyclic loading are discussed. Finally, the validation of the nonlinear finite element model using the available experimental results is thoroughly discussed.

3.2 Experimental Specimens for Model Validation

3.2.1 Description of Specimens

An interior steel reinforced concrete (SRC) composite column to reinforced concrete (RC) beam joint connected using the passing through type and the wing plate type which are experimentally tested by Young-Kyu Ju (Ju & Chun, 2005) under reversed cyclic loading are selected and these specimens are numerical modeled using nonlinear finite element procedure in DuCOM-COM3 for validation. These beam-column joint specimens are also used as control specimens.

3.2.1.1 Passing through type

As it can be seen from Figure 3-1 two reinforcing bars of the reinforced concrete beam passed through a hole in the steel column and the remaining reinforcing bars passed

through the width of the steel-reinforced concrete (SRC) composite column. A structural loss is caused by the hole in the steel flange, created by the reinforcing bars of the beam, due to the reduction of the steel section area. Because of this reason, the number of reinforcing bars passing through the columns is limited. In Japanese code, the number of holes in the steel flange is limited to three, and the diameter of each hole is less than 40mm. The column had a cross-sectional dimension of 500 mm × 500 mm, with a height of 3500 mm. The beam had a cross-sectional dimension of 350 mm × 500 mm, with lengths of 2200 mm up to the contra flexure point.

Table 3-1 Cross-sections and number of reinforcement bars of the passing through specimen used in the experimental study by Young-Kyu Ju (2005).

Specimen Type	Beam				Column		
	Cross-section (mmxmm)	Top Bars (mm)	Bottom Bars (mm)	Stirrups (mm)	Cross-section (mmxmm)	Bars (mm)	Stirrups (mm)
	Bxh				Bxh		
Passing Through	350x500	4ø22	2ø22	ø10@100	500x500	12ø22	ø10@150

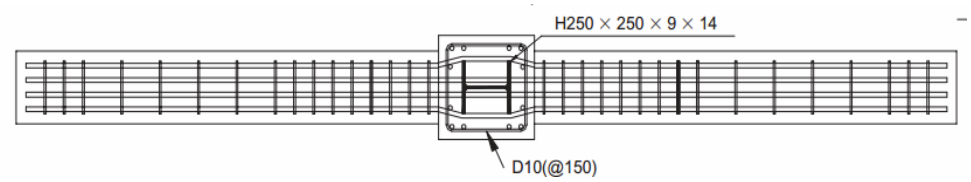

(a)

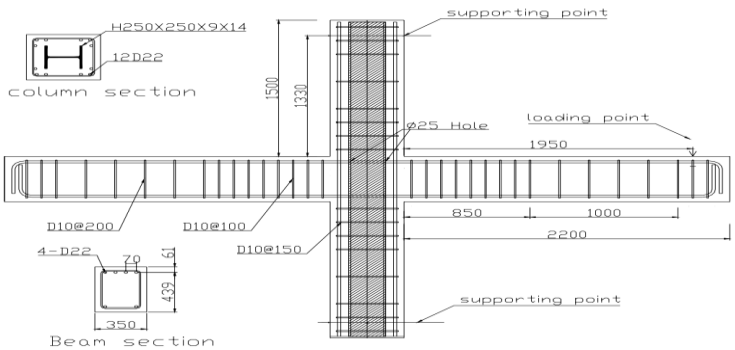

(b)

Figure 3-1 Detail of the specimen tested by Young-Kyu Ju (2005) (a) plan of passing through type;(b) dimensions of the specimen (units: mm)(Ju & Chun, 2005)

3.2.1.2 Wing plate type

Figure 3-2 shows the wing plate type connection in which the wing plate is welded to both sides of the steel column flange and the reinforcing bar of the beam is flare welded in situ to the wing plate. The wing plate also behaves as the shear connector.

Table 3-2 Cross-sections and number of reinforcement bars of the wing plate specimen used in the experimental study by Young-Kyu Ju (2005).

Specimen Type	Beam				Column		
	Cross-section (mmxmm)	Top Bars (mm)	Bottom Bars (mm)	Stirrups (mm)	Cross-section (mmxmm)	Bars (mm)	Stirrups (mm)
	Bxh				Bxh		
Wing plate	350x500	4ø22	2ø22	ø10@100	500x500	12ø22	ø10@150

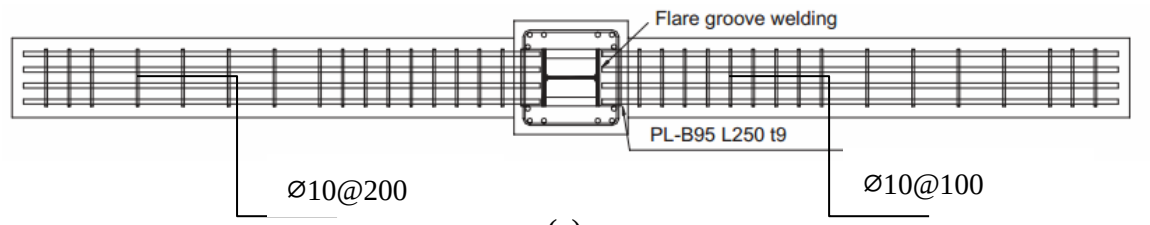

(a)

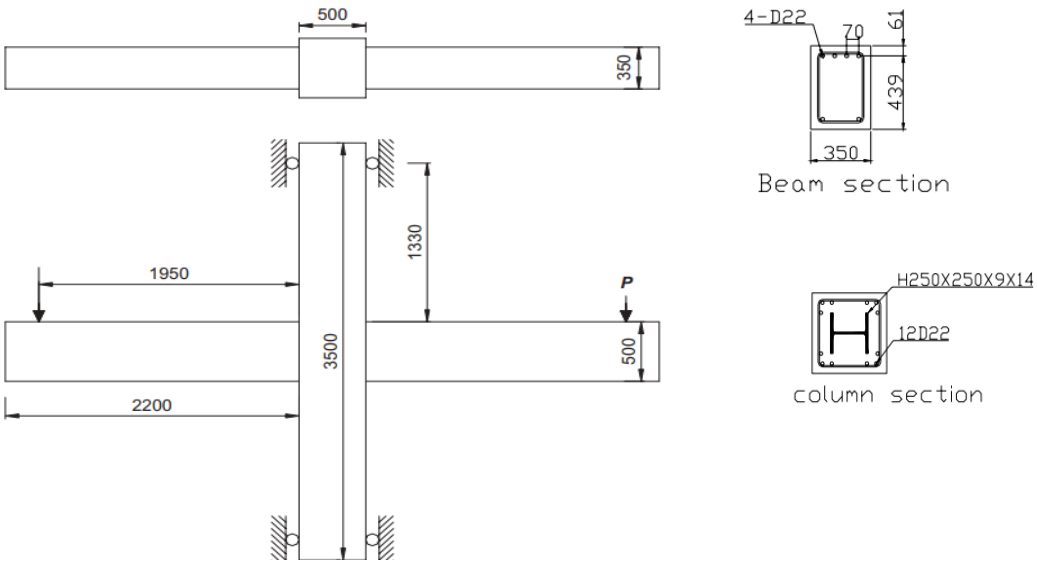

(b)

Figure 3-2 Detail of the specimen tested by Young-Kyu Ju(2005) (a) plan of wing plate type;(b)dimensions of specimen (units: mm) (Ju & Chun, 2005)

The uniaxial 28-day compressive strength of the concrete was 24.9 N/mm2 in the research by Young-Kyu Ju (Ju & Chun, 2005), which employed identical materials for all specimens. The average uniaxial tensile strengths of the reinforcing bars were 406 N/mm2 (⌀10) and 392 N/mm2 (⌀22). The wide flange form steel beam and plate had average uniaxial tensile strengths of 374 N/mm2 and 296 N/mm2, respectively.

The specimens were evaluated under reversed cyclic loading with a sinusoidal displacement control wave consisting of fully reversed cycles at amplitudes of 1δ,2δ, 4δ, 6δ, 8δ (δ was the displacement when the tensile reinforcing bar began to yield) was applied. The column was attached to the reaction frame and could only rotate. During the test, the top of the column was subjected to a continuous axial force of 1470 kN (about 25% of the column's design axial strength). The test configuration, as well as the positions of the transducers and measuring equipment used to detect the displacements of the loading points and the rotation of the beam against the column, is shown in Figure 3-3.

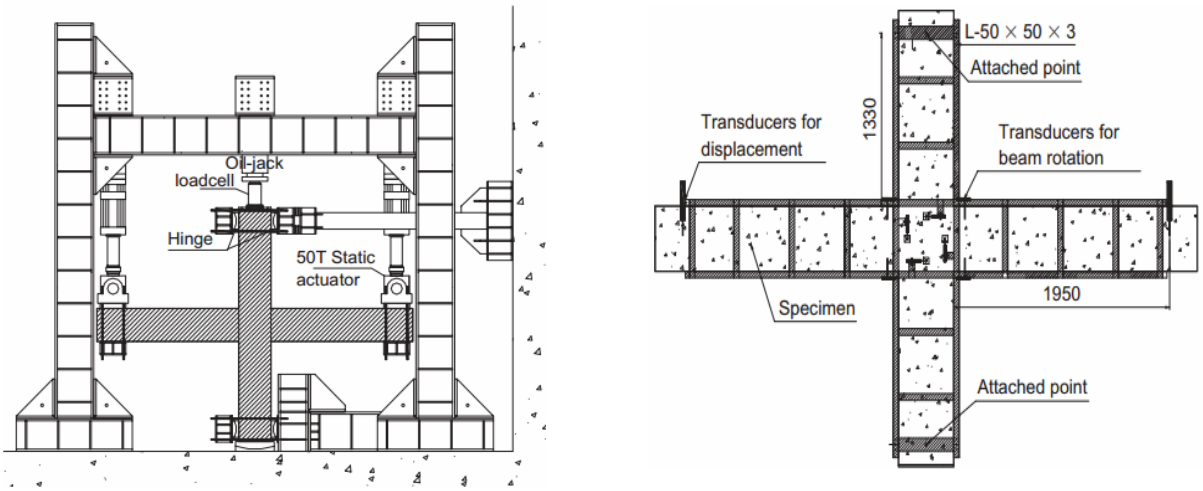

(a) **(b)**

Figure 3-3 (a) Test set-up; (b) location of transducers and measuring instruments (dimensions in mm) (Ju & Chun, 2005)

3.3 Specimens for the current numerical study

As mentioned above, both the passing through type and wing plate type connections of an interior steel reinforced concrete (SRC) composite column to reinforced concrete (RC)

beam joint is selected as the control specimens for the present study. The other specimen is developed by integrating the two connection types, passing through and wing plate type, at one joint in an interior steel reinforced concrete (SRC) composite column to reinforced concrete (RC) beam joint, where only 50% of the longitudinal reinforcement bars of the reinforced concrete beam passed through the joint and the remaining longitudinal reinforcement are flare welded to the wing plate which is welded to the steel column flange as depicted in Figure 3-4.

The behavior of this integrated type specimen is investigated and compared to the control specimens under cyclic loading. Furthermore, a parametric analysis was carried out to understand the behavior of the above-mentioned connection types by varying axial load ratios. The specimen's dimension and materials used in the experimental study conducted by (Ju & Chun, 2005) were used in this study for modeling the integrated connection type.

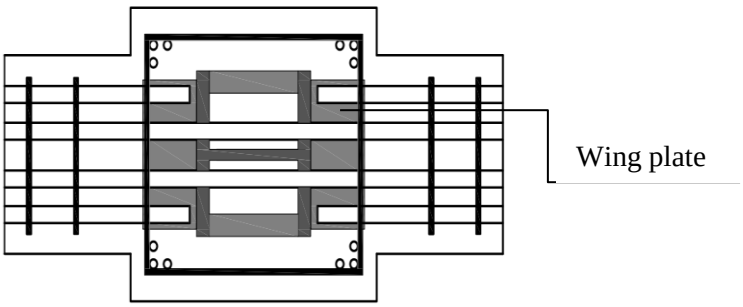

Figure 3-4 Detail of the integrated connection type

3.4 Finite element modeling

3.4.1 Modeling in DuCOM-COM3

In this study, the simulation and analysis are done using a finite element analysis platform called DuCOM-COM3. This platform was developed at the University of Tokyo and it is a multi-scale analysis platform that integrates DuCOM and COM3, where DuCOM (Durability Model of Concrete) is a micro- durability platform that simulates cement hydration, micro-pore structure, and mass transport in concrete. While COM3 (Concrete Model for 3 Dimensional Problems) is a three-dimensional finite element analysis that uses a multi-directional fixed crack model with uncracked and cracked concrete constitutive laws and hardening or matured concrete (Maekawa et al.,2003). It also

undertakes simulation and nonlinear FEM analysis of concrete structures comprising short and long-term time-dependent high nonlinear mechanics under static and dynamic loads. The multi-scale and multi-physical model depicted in Figure 3-6 is implemented in the software to simulate the time-dependent deformation and cracking behavior of concrete structures.

Mix proportions, structural geometry, and boundary condition in terms of environmental exposure of the structure over the time-space domain are the basic input data for DuCOM-COM3. Kinematic, chemo-physical, and mechanical events on elements would be solved at the same time step for both material and structure (Ishida et al., 2018). The software integrates the actual phenomena which are shown in Figure 3-5.

For rationally simulating largely deformed elements, plastic localization of reinforcement and averaging of local stress and strain along the reinforcement are essential. Steel and concrete local stress and strain are modeled. To simulate actual behavior, tension softening and stiffening were included in the software. Equation 3.1 describes the relationship between average stress and average strain for concrete under tension.

$$\sigma_t = f_t \left(\frac{\varepsilon_{tu}}{\varepsilon_t} \right)^c \qquad \textbf{(3.1)}$$

Where ε_{tu} is the cracking strain and c is the parameter describing the inclination of the descending branch, σ is the average tensile stress, ε is the average tensile strain, f_t is uniaxial tensile strength

In the reinforced concrete region (RC) and plain concrete region (PL Zones), this coefficient C is varied to describe the gradual release of normal stress and the sharp release of normal stress after cracking, respectively. As a result, C is 0.4 in the RC zone for tension stiffening and 2.0 in the PL zone for tension softening (Maekawa et al.,2003).

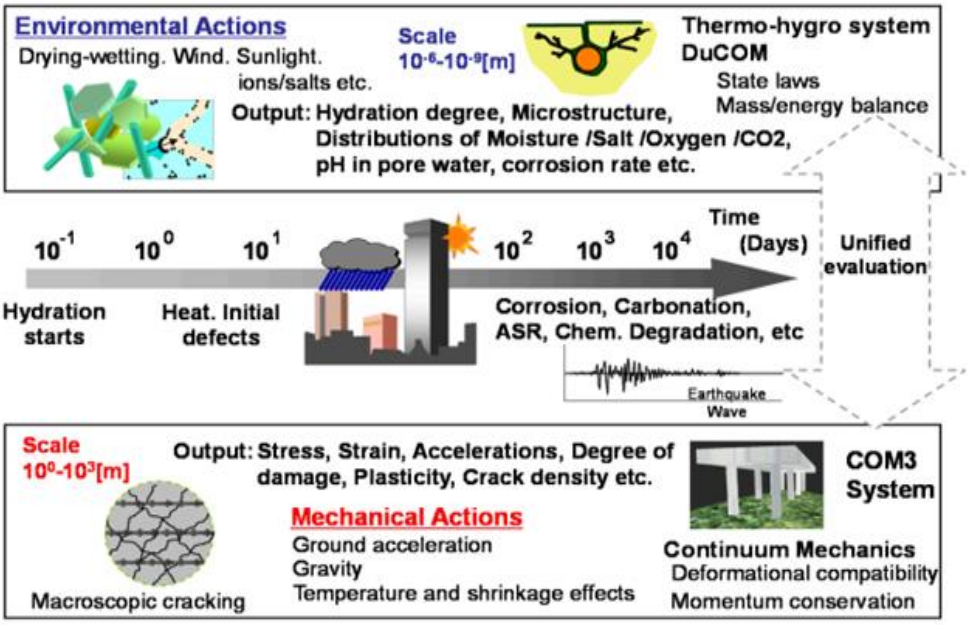

Figure 3-5 Multiscale and multi-physical modeling to simulate time-dependent concrete (Ishida et al., 2018) and (Maekawa et al., 2003)

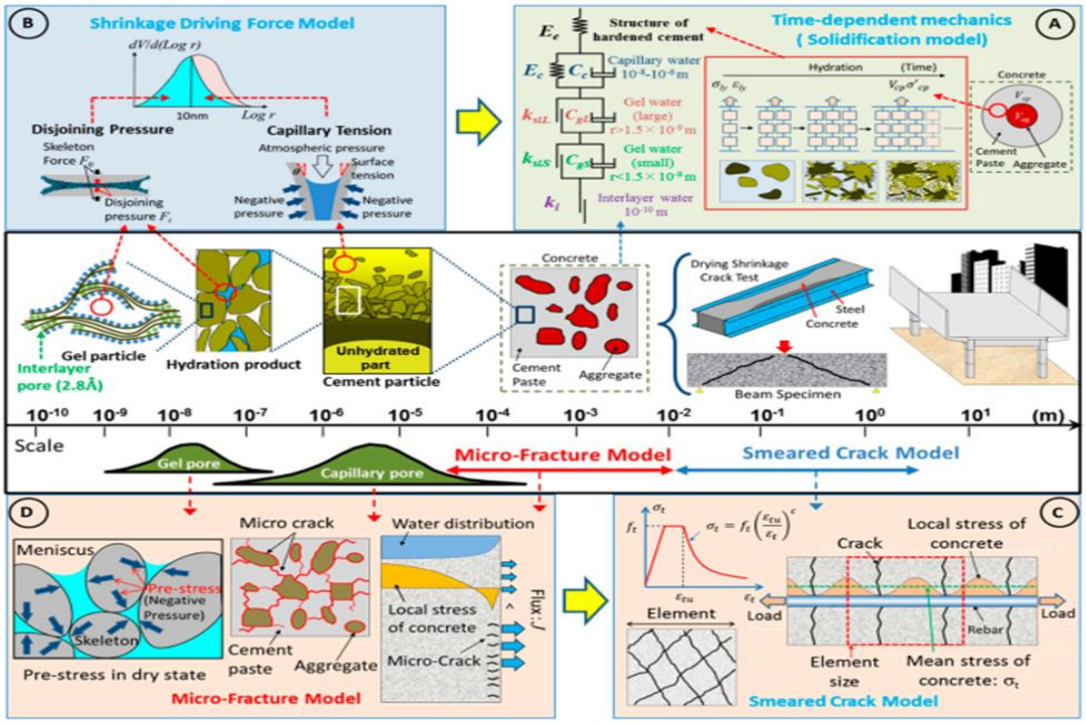

Figure 3-6 Multiscale and multi-physical modeling to simulate time-dependent deformation and cracking. (Ishida et al., 2018) and (Maekawa et al., 2003)

3.4.2 Modeling of Geometry

The interior steel reinforced concrete (SRC) composite column to reinforced concrete (RC) beam joint is modeled using the detail and dimension that is shown in Figure 3-1. A three-dimensional cube geometry provided in the software is used to create parts of the specimen. The geometry of the interior beam-column joint is shown in Figure 3-7. For the simulation time to be lesser, half of the three-dimensional geometry is taken along the longitudinal direction of the specimen due to symmetry.

Units used in DuCOM-COM3 finite element software should be consistent throughout the modeling process on material definition, modeling of geometry, and when applying load. The output result will also have the same unit as the input. The units used in this model are second, cm and kN.

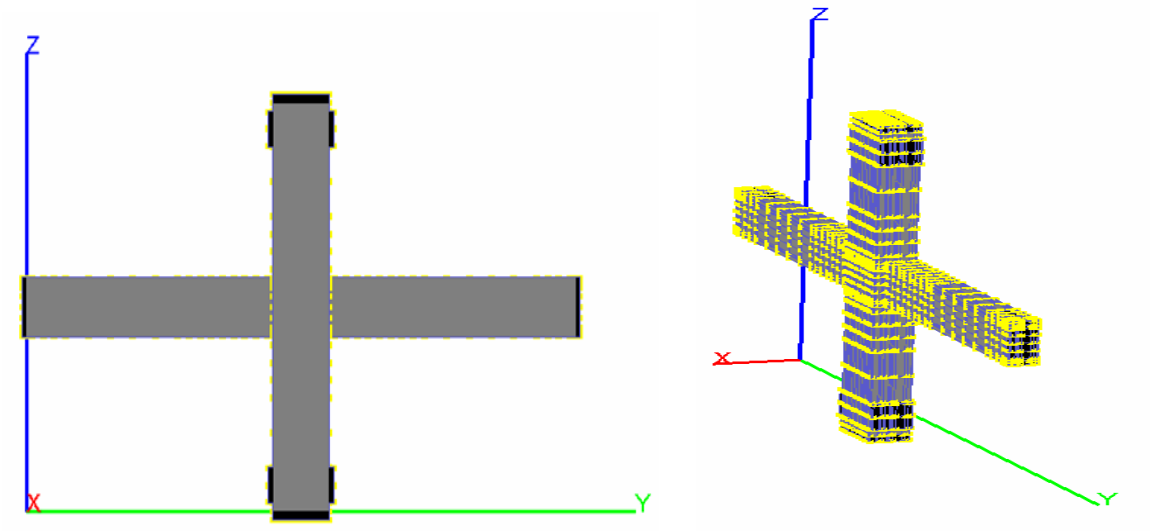

Figure 3-7 Geometry of the specimen

3.4.3 Creating mesh

The mesh in DuCOM-COM3 is created during modeling and it can be created automatically or manually where the number of finite elements can be created in the X, Y, and Z direction as shown in Figure 3-8.

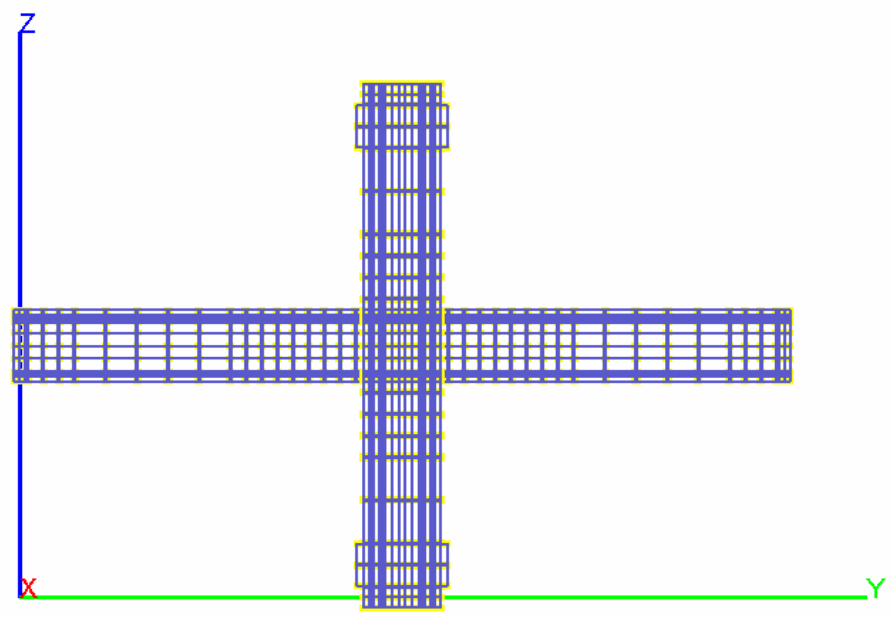

Figure 3-8 Finite element mesh

3.4.4 Defining Material Properties

There is a material definition database in DuCOM-COM3 software where user material properties can be defined. The concrete, structural steel section, steel reinforcement, and plate material properties used in the experimental test are defined. For the loading plate, the elastic material property is defined to distribute stress without crushing. After defining material properties, materials defined are assigned for the respective elements that are present in the model.

3.4.4.1 Concrete

The uniaxial 28-day compressive strength of the concrete used in the experiment was taken. The tensile strength and modulus of elasticity were calculated using the formula stated in (Eurocode 2, 2004).

Table 3-3 Concrete properties used in the model

Initial Stiffness (MPa)	31475.8
Compressive Strength (MPa)	24.9
Tensile Strength (MPa)	2.56
Poisson's Ratio	0.2
Unit Weight (Kg/m^3)	2500

3.4.4.2 Reinforcement and Structural Steel section

The reinforcement is modeled as smeared reinforcement by providing a reinforcement ratio in the concrete element. The properties used in the experiment are assigned in the model.

Table 3-4 Reinforcement properties used in the model

Diameter 10	
Initial Stiffness (MPa)	200000
Yield Strength (MPa)	406
Tensile Strength (MPa)	466.9
Poisson's Ratio	0.3
Unit Weight (Kg/m^3)	7800

Diameter 12	
Initial Stiffness (MPa)	200000
Yield Strength (MPa)	392
Tensile Strength (MPa)	450.8
Poisson's Ratio	0.3
Unit Weight (Kg/m^3)	7800

Table 3-5 Structural H- Steel and plate properties used in the model

Structural H-Steel	
Initial Stiffness (MPa)	200000
Yield Strength (MPa)	374
Tensile Strength (MPa)	430.1
Poisson's Ratio	0.3
Unit Weight (Kg/m^3)	7800

Plates	
Initial Stiffness (MPa)	200000
Yield Strength (MPa)	296
Tensile Strength (MPa)	340.4
Poisson's Ratio	0.3
Unit Weight (Kg/m^3)	7800

3.4.5 Bond element

A bi-linear open-closure response with contact density is used to model the bond element. The model has been used to represent the behavior of the beam-column joint interface. The input parameters for the model are shear stiffness, gap limit value, tension opening stiffness, and maximum roughness size. The bond element parameters are shown in Table 3-6

Table 3-6 Parameters of bond element

Shear stiffness (Mpa)	13115
Gap limit value (cm)	0
Tension opening stiffness (Mpa)	157079.6
Maximum roughness size (cm)	1

3.4.6 Restraint condition

Once the interior beam-column joint is modeled in DuCOM-COM3, the restraint condition is assigned to the model following the experimental boundary condition used during the test and it is shown in Figure 3-9. The longitudinal length of the model is in the Y direction

whereas the transverse length of the model is in the X direction and the height of the beam and column is modeled in the Z direction.

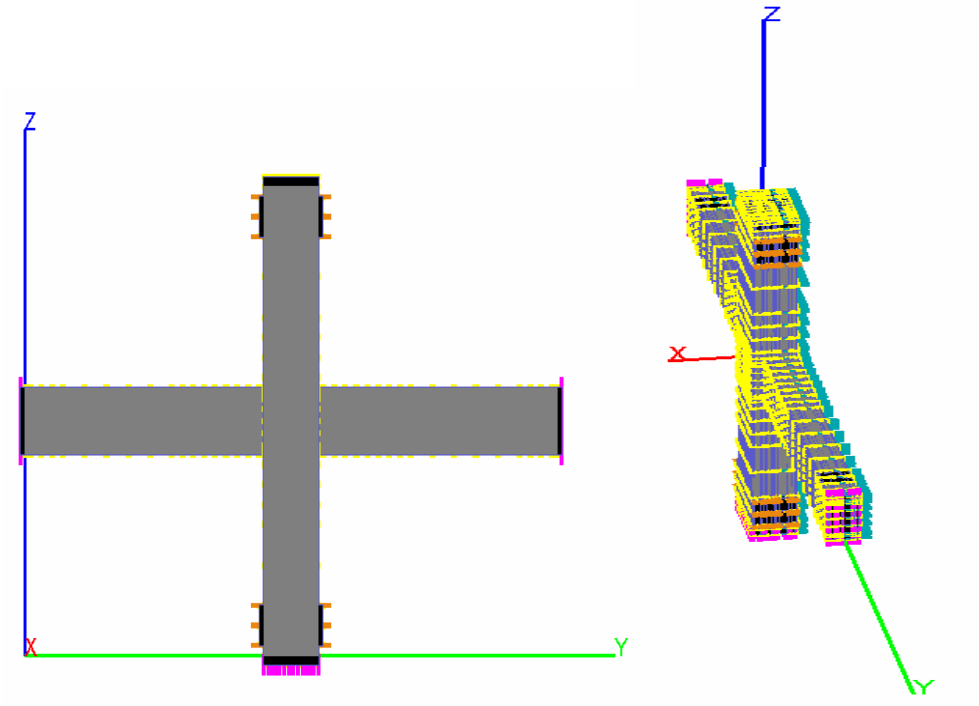

Figure 3-9 Boundary conditions

3.5 Validation of the Nonlinear Finite Element Model

To idealize the real behavior of the actual tested specimens and predict the behavior of other specimens that cannot be tested experimentally, finite element analysis and their comparison with experimental test results are highly crucial. This verification could provide proof that the finite element model can be used to investigate structural behavior.

An interior steel reinforced concrete (SRC) composite column to reinforced concrete (RC) beam joint connected using the passing through type and wing plate type, which were experimentally tested by (Ju & Chun, 2005), are selected to validate the nonlinear finite element model. The accuracy of the nonlinear finite element model is evaluated by comparing the analytical result of the specimens with experimental results in terms of load-displacement response and failure pattern.

3.5.1 Load – Displacement Response

The comparison of the load-displacement response of the specimen obtained from the finite element software and reported from the experimental test results are discussed in the following subsection.

3.5.1.1 Passing through type specimen

The comparison of the load-displacement hysteretic curve obtained from DuCOM-COM3 compared with the experimental results of the passing through type specimen is displayed in Figure 3-10.

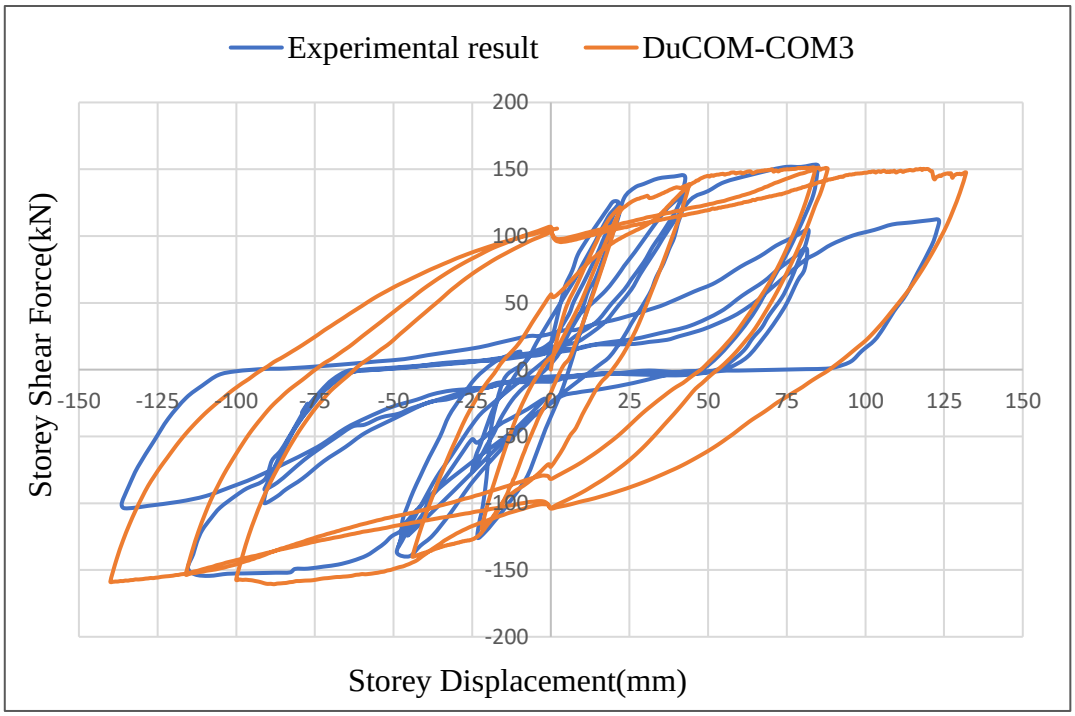

Figure 3-10 Analytical and experimental hysteretic response comparison of passing through type specimen

As shown in Figure 3-10 the load-displacement response of the passing through type specimen predicted by DuCOM-COM3 shows good agreement with the experimental result for the first two cycles and it captures the ultimate storey shear force capacity well. But due to lack of experimental data that was essential for the joint element, the pinching behavior in the hysteresis curve was not captured.

The maximum load obtained from DuCOM-COM3 of this specimen is 0.60% higher than the load reported from the experimental study in the positive loading on the other hand in the negative loading it is 5.89% higher than the maximum load reported from the experimental study as shown in Table 3-7 and Table 3-8.

The error and overall model accuracy of the two specimens are predicted analytically and compared with the test result and presented in Table 3-7 and Table 3-8. To describe the overall model accuracy, and associated average underestimation or overestimation of the finite element software, the error (%) and mean model accuracy [M (%)] evaluated based on the relation given in (Behnam, Kuang, & Samali, 2018) and is defined as:

$$\text{Error}(\%) = \left| \frac{\text{Analytical result - Test result}}{\text{Test result}} \right| \times 100$$

$$\text{Mean modal accuracy, } M(\%) = \frac{\text{Analytical result}}{\text{Test result}} \times 100$$

Table 3-7 Yield and ultimate storey shear force comparisons of DuCOM-COM3 and test result of passing through type specimen (positive loading).

Specimen Type	Yield storey shear force(kN)				Ultimate storey shear force(kN)			
	DuCOM-COM3	Experiment	Error (%)	M (%)	DuCOM-COM3	Experiment	Error (%)	M (%)
Passing Through	121.49	124.30	-2.26	97.74	150.20	149.30	0.60	100.60

Table 3-8 Yield and ultimate storey shear force comparisons of DuCOM-COM3 and test result of passing through type specimen (negative loading).

Specimen Type	Yield storey shear force(kN)				Ultimate storey shear force(kN)			
	DuCOM-COM3	Experiment	Error (%)	M (%)	DuCOM-COM3	Experiment	Error (%)	M (%)
Passing Through	-119.09	-128.10	-7.03	92.97	-160.64	-151.70	5.89	105.89

3.5.1.2 Wing plate type specimen

The comparison of the load-displacement hysteretic curve obtained from DuCOM-COM3 compared with the experimental results of the wing plate type specimen is shown in Figure 3-11.

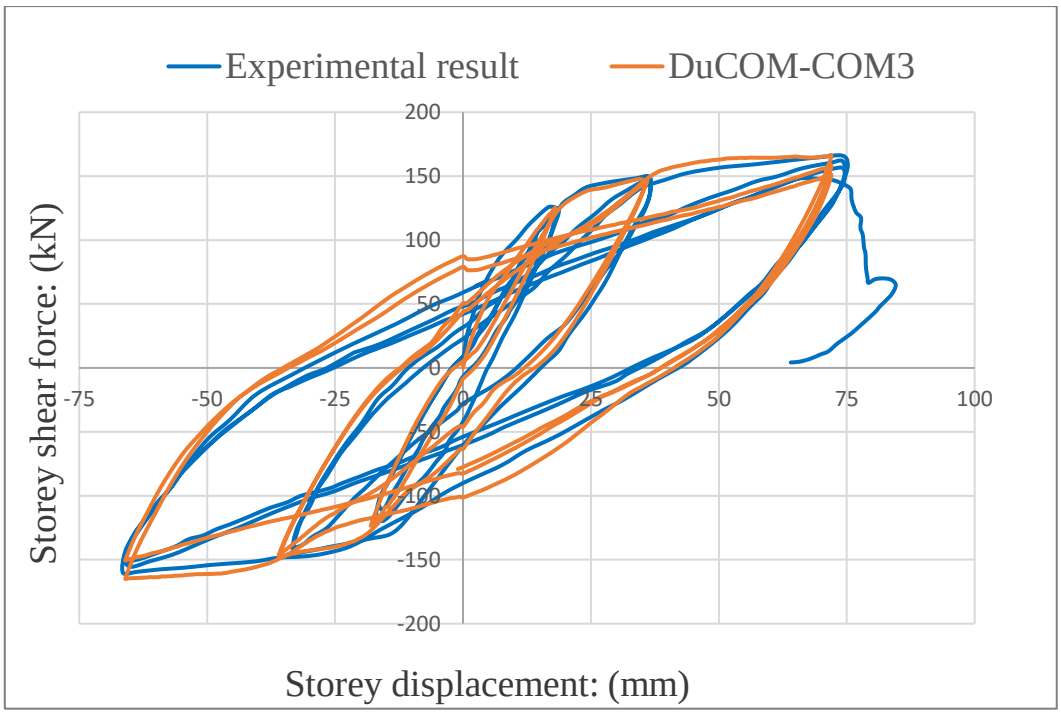

Figure 3-11 Analytical and experimental hysteretic response comparison of wing plate type specimen

The load-displacement response of the wing plate type specimen obtained by the DuCOM-COM3 shows good agreement with the experimental result as displayed in Figure 3-11. The average maximum load obtained from the DuCOM-COM3 of this specimen is 0.65% lower than the maximum load reported from the experimental study in the positive loading. On the other hand, the negative loading is 1.68% lower than the maximum load reported from the experimental study as shown in Table 3-9 and Table 3-10.

Table 3-9 Yield and ultimate storey shear force comparisons of DuCOM-COM3 and test result of wing plate type specimen. (positive loading).

Specimen Type	Yield storey shear force(kN)				Ultimate storey shear force(kN)			
	DuCOM-COM3	Experiment	Error (%)	M (%)	DuCOM-COM3	Experiment	Error (%)	M (%)
Wing Plate	124.99	127.00	-1.58	98.42	165.92	167.00	-0.65	99.35

Table 3-10 Yield and ultimate storey shear force comparisons of DuCOM-COM3 and test result of wing plate type specimen. (negative loading).

Specimen Type	Yield storey shear force(kN)				Ultimate storey shear force(kN)			
	DuCOM-COM3	Experiment	Error (%)	M (%)	DuCOM-COM3	Experiment	Error (%)	M (%)
Wing Plate	-123.19	-127.80	-3.61	96.39	-164.58	-167.40	-1.68	98.32

3.5.2 Failure Patterns

The cracking patterns of the specimen obtained from the finite element software were compared to the experimental test results and discussed in the following subsection. However, the experimental study did not report the crack patterns of the passing through type specimen. As a result, the finite element software crack patterns of the wing plate type specimen were only compared to the experimental crack pattern. Figure 3-12 shows the comparison of crack patterns of the wing plate type specimens obtained by DuCOM-COM3 and the crack patterns of the experimental study.

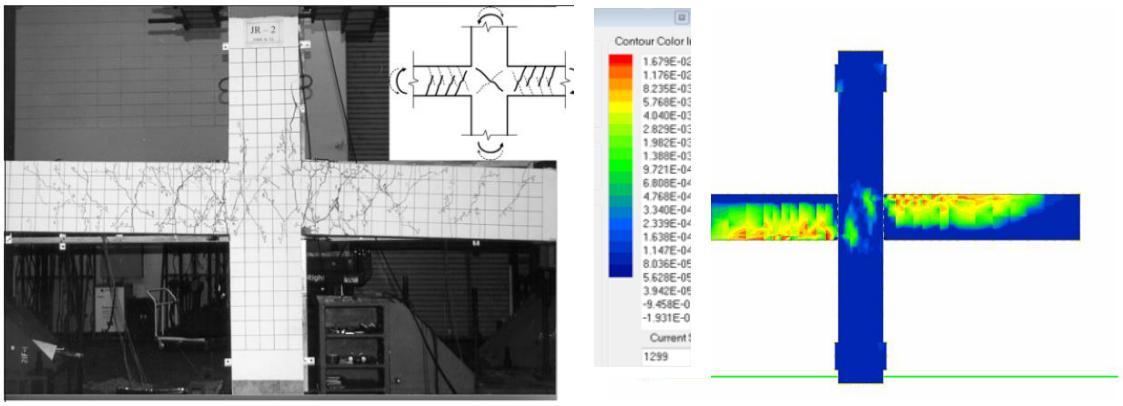

(a) Experimental crack pattern (Ju & Chun, 2005) (b) DuCOM-COM3

Figure 3-12 Comparison of crack patterns of wing plate type specimen

As shown in Figure 3-12, the crack pattern obtained from the numerical model shows good agreement with the cracking patterns reported in the experimental study. The predicted cracking patterns of the wing plate type specimen occurred in an inclined direction from the transverse axis of the beam to the beam-column joint panel zone which correlates to the test crack pattern. The accuracy of the finite element model is further approved by this numerical result and shows its strong capability in predicting the failure patterns of the specimens.

CHAPTER 4 RESULTS AND DISCUSSIONS

4.1 General

This chapter presents the results and discussion for all simulated specimens. This paper sets two goals to study. The first objective of the thesis is to compare the structural performance of the integrated connection type over the passing through and wing plate connection types on the seismic performance of steel-reinforced composite columns to RC beam joints. The second objective is to observe the effect of the axial load ratios on the seismic performance of the three connection types.

The results and discussion of the analytical investigations are presented in two parts. Part one deals with the structural response under reverse cyclic loading of the integrated type joints and the two control joint specimens that are previously validated. The details of the connection types are shown in Figure 4-1. Part two focuses on the investigations and analysis results of the effects of axial load ratios for all of the three connection types. The types of the different connections with varying axial load ratios are summarized in Table 4-1.

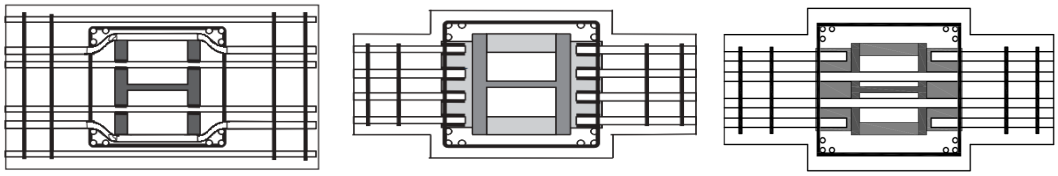

(a) Passing through type (b) Wing plate type (c) Integrated type

Figure 4-1 Details of the connection types

Table 4-1Summary of simulated specimens

No	Specimen name	Connection type	Axial load ratio (ALR)
1	PTT-ALR0	Passing through type	0
2	PTT-ALR0.1	Passing through type	0.1
3	PTT-ALR0.2	Passing through type	0.2
4	PTT-ALR0.4	Passing through type	0.4
5	PTT-ALR0.6	Passing through type	0.6
6	PTT-ALR0.7	Passing through type	0.7
7	WPT-ALR0	Wing plate type	0

8	WPT-ALR0.1	Wing plate type	0.1
9	WPT-ALR0.2	Wing plate type	0.2
10	WPT-ALR0.4	Wing plate type	0.4
11	WPT-ALR0.6	Wing plate type	0.6
12	WPT-ALR0.7	Wing plate type	0.7
13	IT-ALR0	Integrated type	0
14	IT-ALR0.1	Integrated type	0.1
15	IT-ALR0.2	Integrated type	0.2
16	IT-ALR0.4	Integrated type	0.4
17	IT-ALR0.6	Integrated type	0.6
18	IT-ALR0.7	Integrated type	0.7

4.2 Analytical result

4.2.1 Part I – Results of Non-linear FE analysis of the three types of connections

The three connection types as shown in Figure 4-1 were modeled using the finite element software and subjected to reverse cyclic loading with a sinusoidal displacement control wave. The two specimens, the passing through type and the wing plate type, experimentally tested by Young-Kyu Ju (Ju & Chun, 2005) which are numerically modeled and validated against the experimental result in section 3.5 are the control specimens for the present study. Similar to the experimental study a constant axial load was applied to the top of the column for the integrated type specimen.

A comparative study was conducted on the seismic performance of these three connection types based on storey shear strength and ductility. The seismic performance of these connection types of an interior steel-reinforced composite column to RC beam joint was evaluated using the storey shear force vs storey displacement hysteretic response. Where the storey shear force is the lateral reaction at the tip of the beam and the storey displacement is equal to the lateral displacement history applied at the tip of the beam. The hysteresis response of the three connection types is shown in Figure 4-2, Figure 4-3, and Figure 4-4. The load-displacement envelope curve of the three connection types is depicted in Figure 4-5.

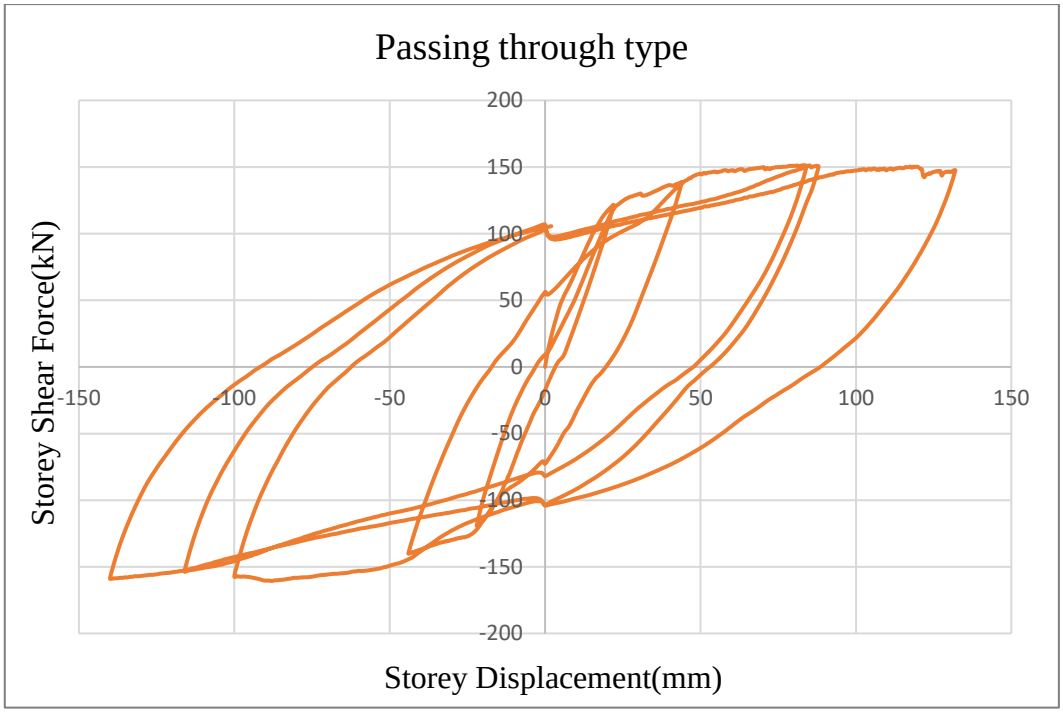

Figure 4-2 Hysteresis response of the passing through type specimen

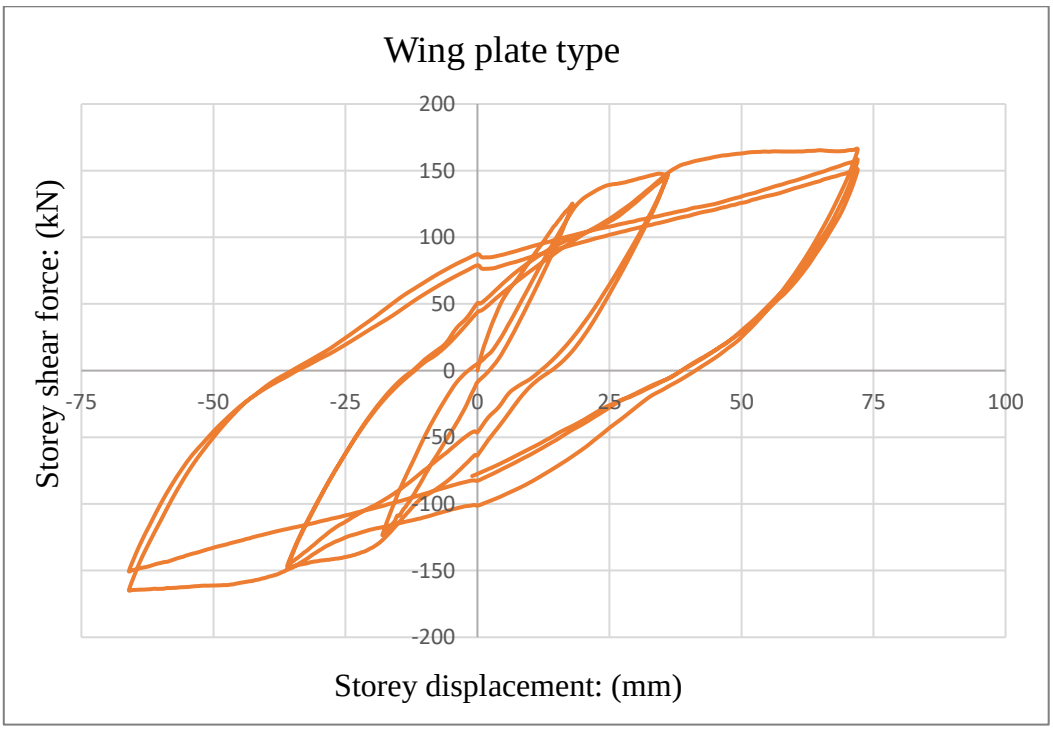

Figure 4-3 Hysteresis response of the wing plate type specimen

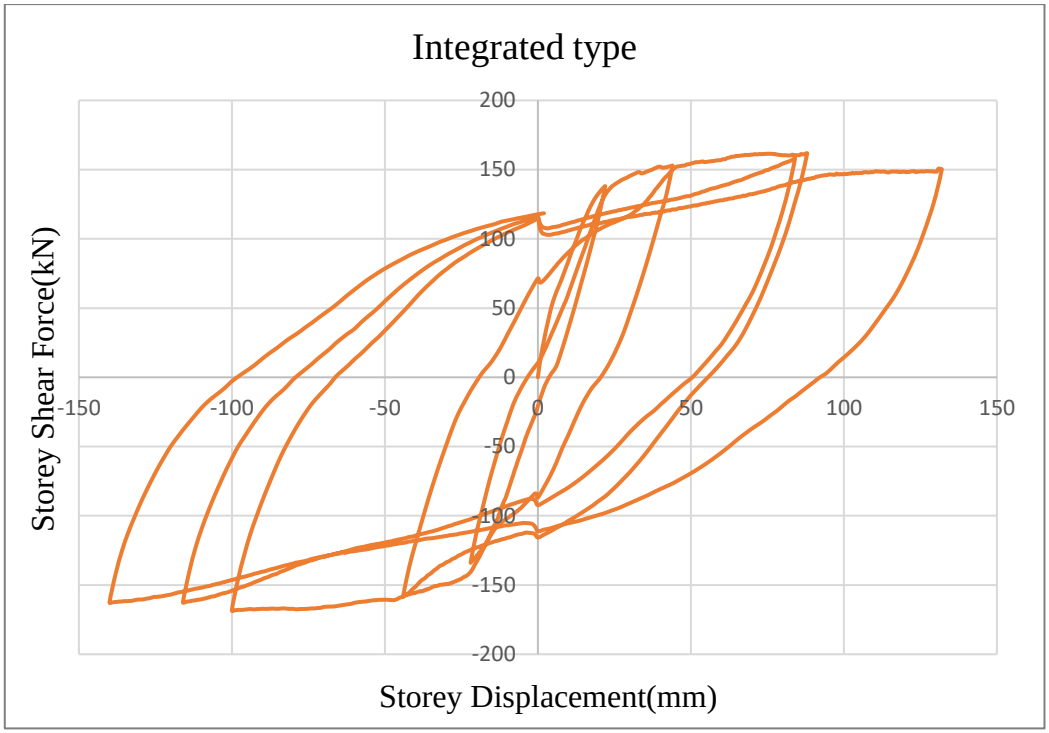

Figure 4-4 Hysteresis response of the integrated type specimen

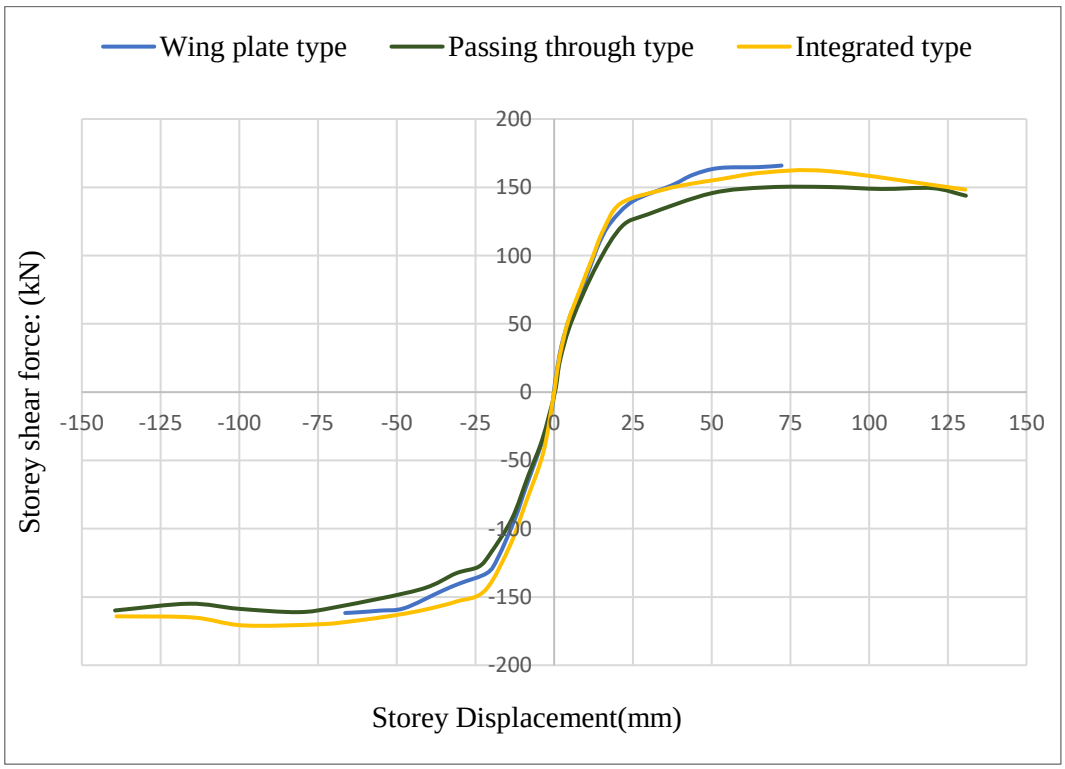

Figure 4-5 Comparison of envelope curves

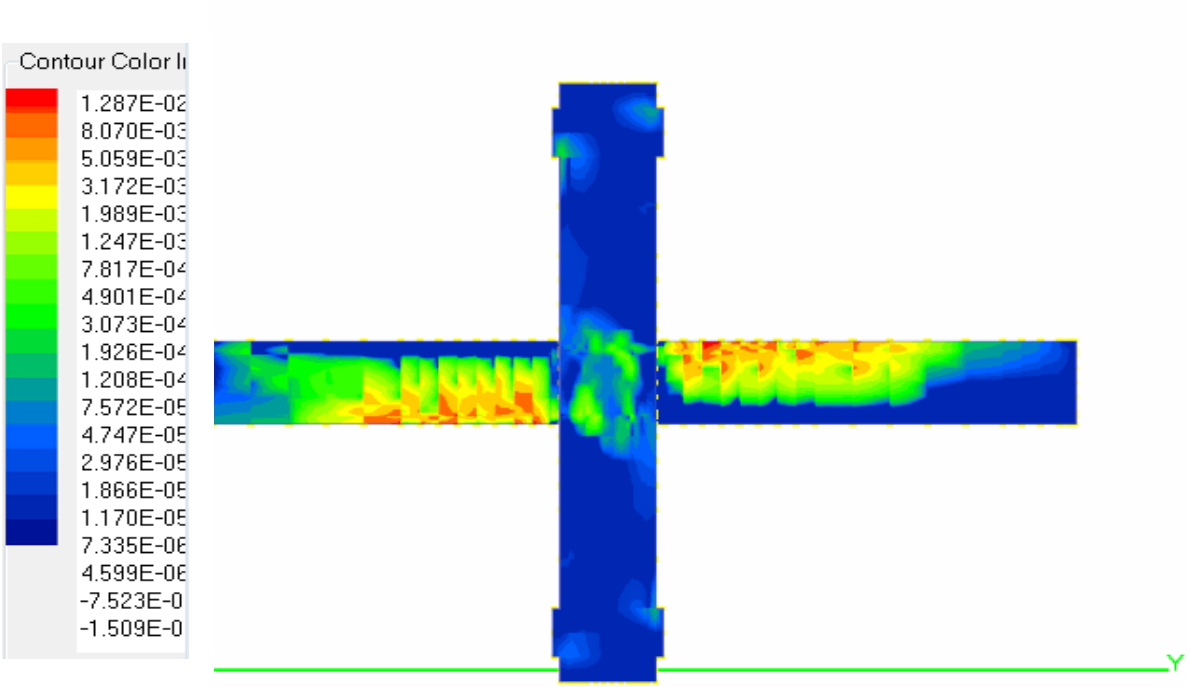

Figure 4-6 Concrete strain of the passing through type specimen at the first cycle

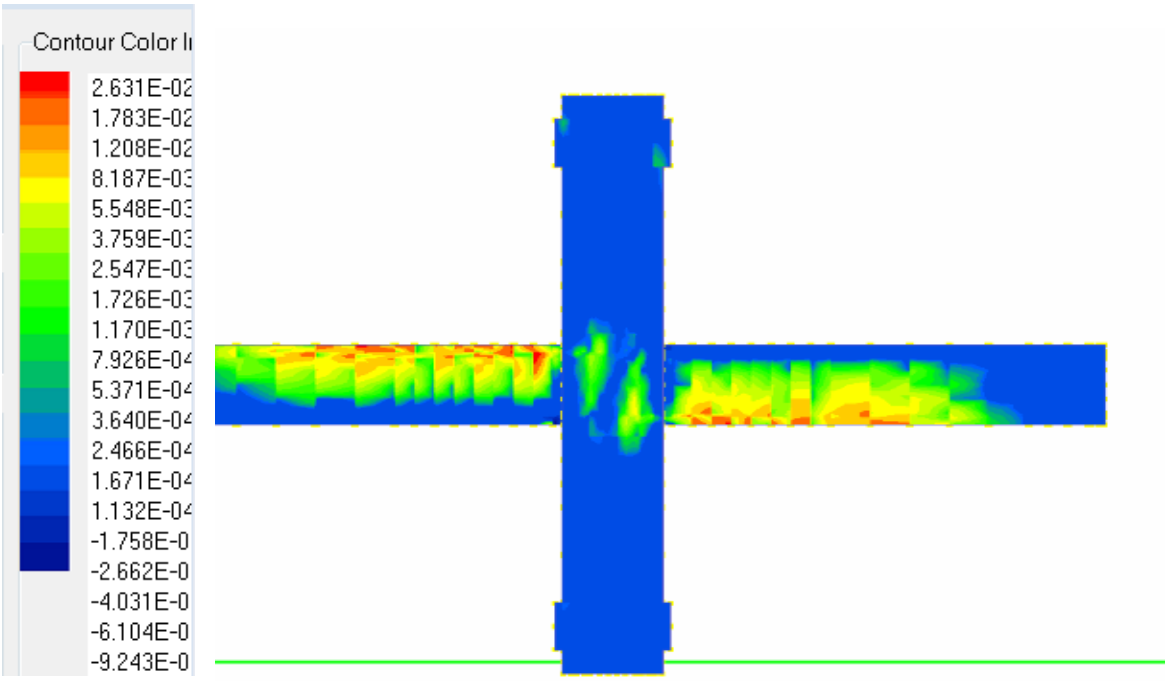

Figure 4-7 Concrete strain of the wing plate type specimen at the first cycle

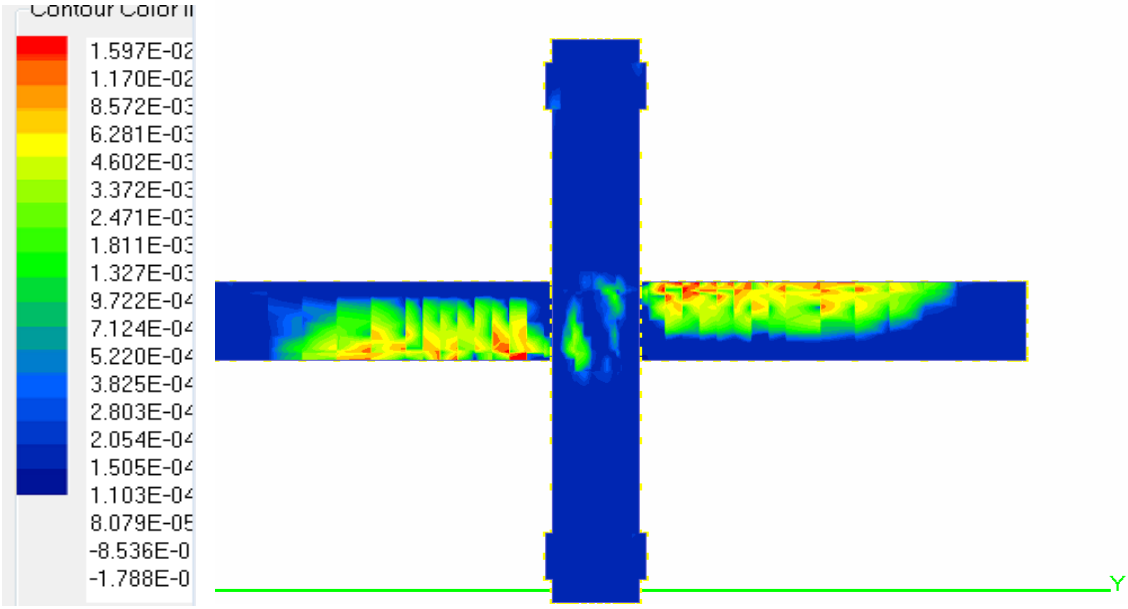

Figure 4-8 Concrete strain of the integrated type specimen at the first cycle

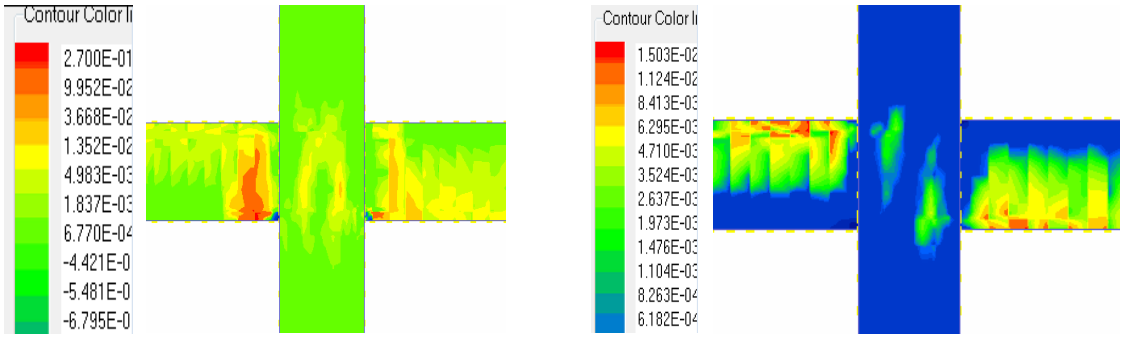

(a) Passing through type (b) Wing plate type

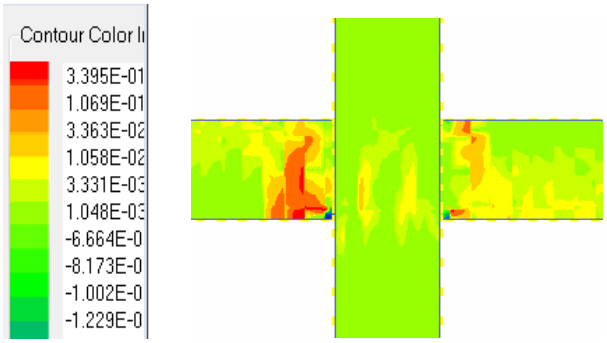

(c) Integrated type

Figure 4-9 Concrete strain of the specimens at final loading

4.2.2 Part II – Non-linear FE analysis results of the effects of varying axial load ratio on the different connections

To study the influence of column axial load variation on an interior SRC-RC beam joint behavior under cyclic loading. A total of 18 interior beam-column joint specimens using the three connection types are modeled as shown in Table 4-1. Six different column axial load levels that is (0, 0.1, 0.2, 0.4, 0.6, 0.7) *($A_c f_{cd} + A_s f_{yd}$) were modeled and simulated. The hysteretic loops obtained from the nonlinear finite element simulation of specimens with different column axial load ratios are shown in APPENDIX A. The concrete strain distribution at final storey displacement for all specimens is shown in APPENDIX B.

The effect of different levels of axial loads on the seismic behavior of the joints is compared in terms of the storey shear strength and ductility for all three connection types. In addition, the influence of column axial load variation on the seismic behavior of the wing plate connection type is further discussed in terms of stiffness degradation and energy dissipation capacity.

4.3 Discussion

4.3.1 Part I – Discussion of Non-linear FE analysis results of the three types of connections

4.3.1.1 Shear strength

From the finite element analysis of the specimens, it was observed that the ultimate shear capacity of the passing through, wing plate, and integrated connection type is 150.2 kN, 165.92 kN, and 161.74 kN respectively in the positive loading as shown in Figure 4-10. The percentage ultimate shear capacity increment of the integrated type specimen over the passing through type is 7.7 % and shows a 2.5% decrement over the wing plate type. Whereas in the negative loading, the ultimate storey shear capacity obtained is 160.64 kN, 164.58kN, and 168.28kN for the passing through, wing plate, and integrated connection type respectively as depicted in Figure 4-11.

As it can be seen, the integrated type specimen shows a percentage ultimate shear capacity increment of 4.8% and 2.2% over the passing through type and the wing plate type

specimen respectively. This result shows that the integrated connection type is better in the strength perspective.

In the integrated connection type, the edge longitudinal reinforcements will not be bent and pass through the beam-column joint. The edge reinforcement bars are rather flare welded to the wing plate. This prevents the cover from spalling at the edge of the column which had a detrimental effect on the ductility and seismic performance of the column. The cover spalling problem usually occurs in the passing through connection type since the edge longitudinal reinforcements create high stress when they are bent to pass through the column.

Under normal circumstances, Cover spalling is a critical problem when the axial force in the column increases. The international building codes restrict the normalized axial force ratio to prevent the adverse effect of cover spalling. For example, for DCM cases, the ES EN 1998 code limits the normalized axial force ratio of primary seismic columns to be less than 0.65. It is even more restrictive in the case of composite columns. These kinds of restrictions are provided to minimize the occurrence of the cover spalling of the column. The cover spalling problem is the main cause for the exposure of the column core which leads to the buckling of longitudinal reinforcement and local buckling of steel flanges in the case of composite columns both of which lead to strength and stiffness degradation. This normal circumstance will be aggravated by the presence of a bent bar at the edge of the column. The presence of the bent reinforcement bars accelerates the cover spalling process by creating high stress in the corner edge of the column. The integrated connection type does not have a bent reinforcement so there is no high stress in the corner edge of the column which makes it favorable over other connection types.

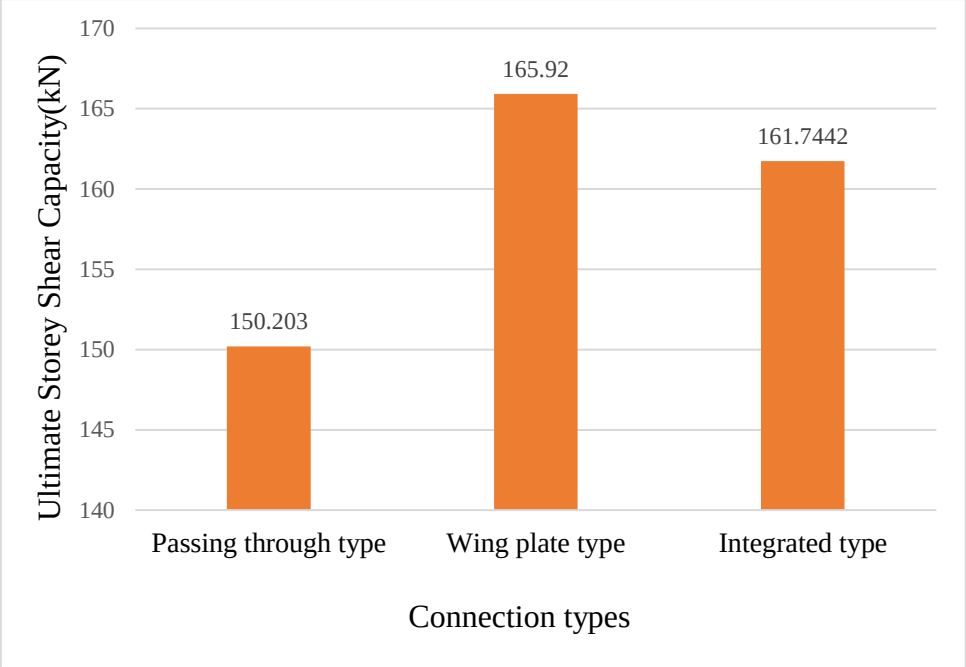

Figure 4-10 Ultimate storey shear capacity of part one specimens (positive loading)

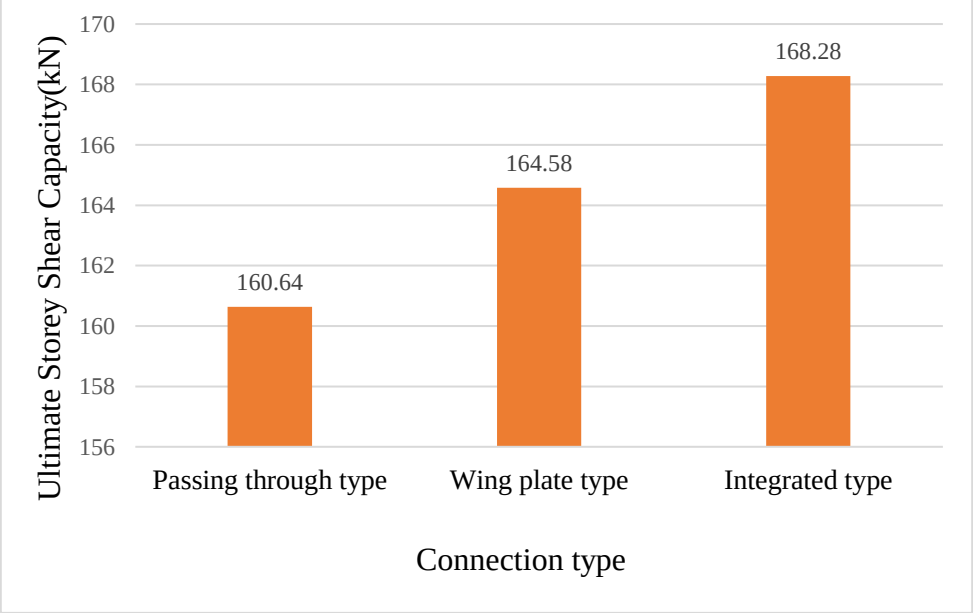

Figure 4-11 Ultimate storey shear capacity of part one specimens (negative loading)

4.3.1.2 Ductility

Ductility refers to a structure's ability to dissipate energy by undergoing large plastic deformations without significantly reducing strength. When it comes to analyzing the cyclic performance of structural members, ductility is crucial. The ductility of structural

members is an important factor to consider when investigating their cyclic performance. Ductile structural components help to dissipate plastic energy by resisting seismic behavior during an earthquake (Paulay & Priestley, 1992).

Ductility is an important parameter to consider when evaluating seismic performance. It is usually expressed in terms of the ductility factor (μ_{Δ}), which is calculated as the ratio of the ultimate displacement (Δ_u) to the yielding displacement(Δ_y), as shown in Equation (4.1) (R Park, 1989).

$$\mu_{\Delta} = \frac{\Delta_u}{\Delta_y} \quad \textbf{(4.1)}$$

Because there is no well-defined yield point on the load-displacement envelope curves, determining yielding displacement in reinforced concrete structural components may be subjective. This is primarily due to the nonlinear behavior of materials and yielding in various parts of structures at different loading levels. To address this issue, an idealized bilinear force-displacement curve has been widely used to define the ductility parameters of reinforced concrete components based on reduced stiffness equivalent elasto-plastic theory, as shown in Figure 4-12. (Li et al., 2019; R Park, 1989)

The yield displacement in this study is determined using an idealized bilinear force-displacement response with reduced stiffness determined as the secant stiffness at 75% of the maximum load (Park and Priestley, 1987). The point connecting the coordinate origin and the point (0.75Pmax, Δ y1) on the envelope curve was used to determine the yielding point (Pmax, Δ y) based on 75% of the peak load of the specimens as shown Figure 4-12.

The ultimate displacement is defined as the displacement that corresponds to a 15% reduction in load from the peak (Hu & Kundu, 2019; Mostofinejad & Akhlaghi, 2017). As a result, the failure load stage of the specimens was determined as the point on the post-peak branch (P = 0.85Pmax), which corresponded to the ultimate displacement (Δu).

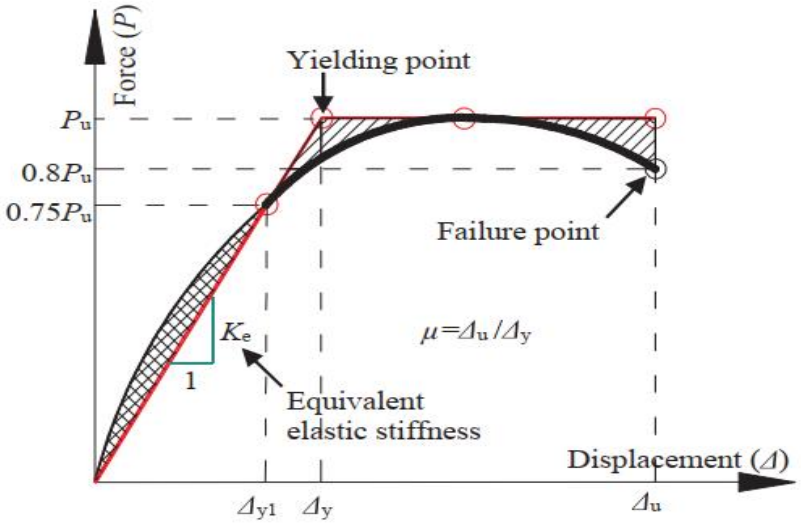

Figure 4-12 Characteristic points on the load-displacement curve (Li et al., 2019)

In terms of ductility performance, the passing through type specimen performs well and has a good ductility behavior, whereas the wing plate type specimen has a limited ductility behavior. The integrated type Specimen is expected to have a better ductility capacity than the Wing plate type specimen. The analytical result also portrays that the integrated model exhibits a good ductility performance than the wing plate type specimen. As shown in Figure 4-13, the displacement ductility factor of the passing through type, wing plate type, and integrated type connection is 5.68, 2.88, and 5.21 respectively.

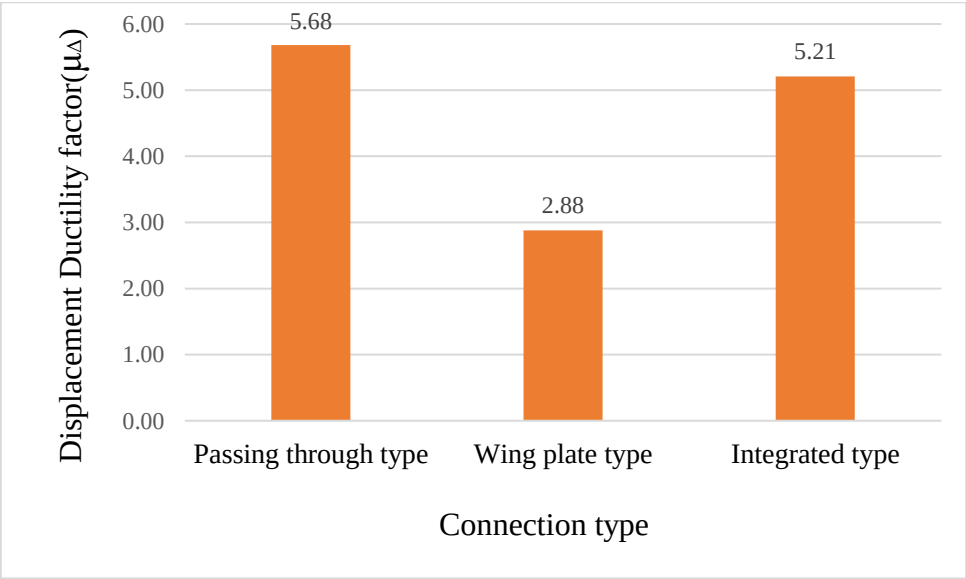

Figure 4-13 Displacement ductility factor of part one specimens

Compared to the passing through type specimen, the integrated type specimen shows a decrease in its displacement ductility by 8.3%. however, the integrated type specimen shows an enhancement in its ductility factor by 80.84% when compared to the wing plate type specimen. The result shows that the displacement ductility factor of the integrated Specimen is a little below than the passing through connection type. It can be deduced that the integrated connection type has an excellent ductility enhancement than the wing plate connection specimen.

As discussed in section 3.2, in the wing plate specimen the longitudinal rebars stopped at the face of the Structural steel section. Whereas in the passing through connection type, the longitudinal reinforcement bars pass through the beam-column joint by getting sufficient anchorage and bond strength. The fact that the passing through type possesses a good anchorage and bond strength gives it a good ductility performance (Paulay & Priestley, 1992). Likewise, the integrated specimen also shows a good ductility behavior since 50% of the longitudinal reinforcement bars of the reinforced concrete beam pass through the beam-column joint. Thus, the beam-column joint gains a good anchorage and bond strength.

4.3.2 Part II – Discussion of Non-linear FE analysis results of the effects of varying axial load ratio on the different connections

4.3.2.1 Shear strength

The effect of varying axial load on ultimate storey shear capacity of the passing through type specimen is shown in Figure 4-14. From the positive and negative loading direction, the average ultimate storey shear capacity for specimen PTT-ALR0, PTT-ALR0.1, PTT-ALR0.2, PTT-ALR0.4, PTT-ALR0.6, and PTT-ALR0.7 is 155.47kN, 161.45kN, 162.51kN, 151.91kN, 145.56kN, and 143.52kN respectively.

As it can be observed the average ultimate storey shear capacity of the passing through type specimen increased by around 3.85 and 4.53%, as the axial load was enhanced to $0.1*(A_c f_{cd} + A_s f_{yd})$ and $0.2*(A_c f_{cd} + A_s f_{yd})$, respectively, when compared to the specimen with no column axial load i.e PTT-ALR0. However, any increase in the axial load further reduced the ultimate storey shear capacity with a percentage of 2.28%, 6.37%, and 7.68% for specimens PTT-ALR0.4, PTT-ALR0.6, and PTT-ALR0.7, respectively, when

compared to specimen PTT-ALR0. This degradation of lateral strength is due to the formation of higher compressive shear stress in the joint panel zone.

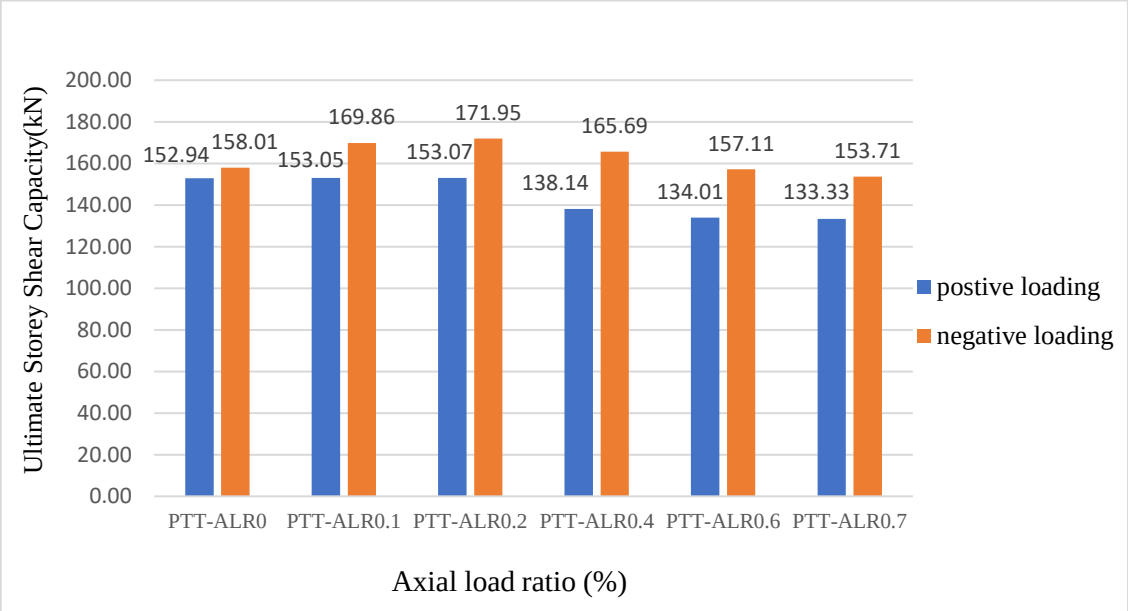

Figure 4-14 Effect of column axial load on ultimate storey shear capacity of passing through type specimens

Figure 4-15 depicts the effect of varying axial load on the ultimate storey shear capacity of the wing plate type specimen. The average ultimate storey shear capacity for specimens WPT-ALR0, WPT-ALR0.1, WPT-ALR0.2, WPT-ALR0.4, WPT-ALR0.6, and WPT-ALR0.7 is 162.75kN, 167.71kN, 162.43kN, 148.50kN, 141.35kN, and 137.95kN, respectively, when compared to the specimen with no column axial load, i.e. WPT-ALR0, the wing plate type specimen's average ultimate storey shear capacity increased by around 3.05% as the axial load was increased to 0.1*(Acfcd + Asfyd). However, further enhancement of axial load led to the reduction in the ultimate storey shear capacity with a percentage of 0.20%, 8.75%, 13.15%, and 15.24% for specimens WPT-ALR0.2, WPT-ALR0.4, WPT-ALR0.6, and WPT-ALR0.7, respectively, when compared to specimen WPT-ALR0.

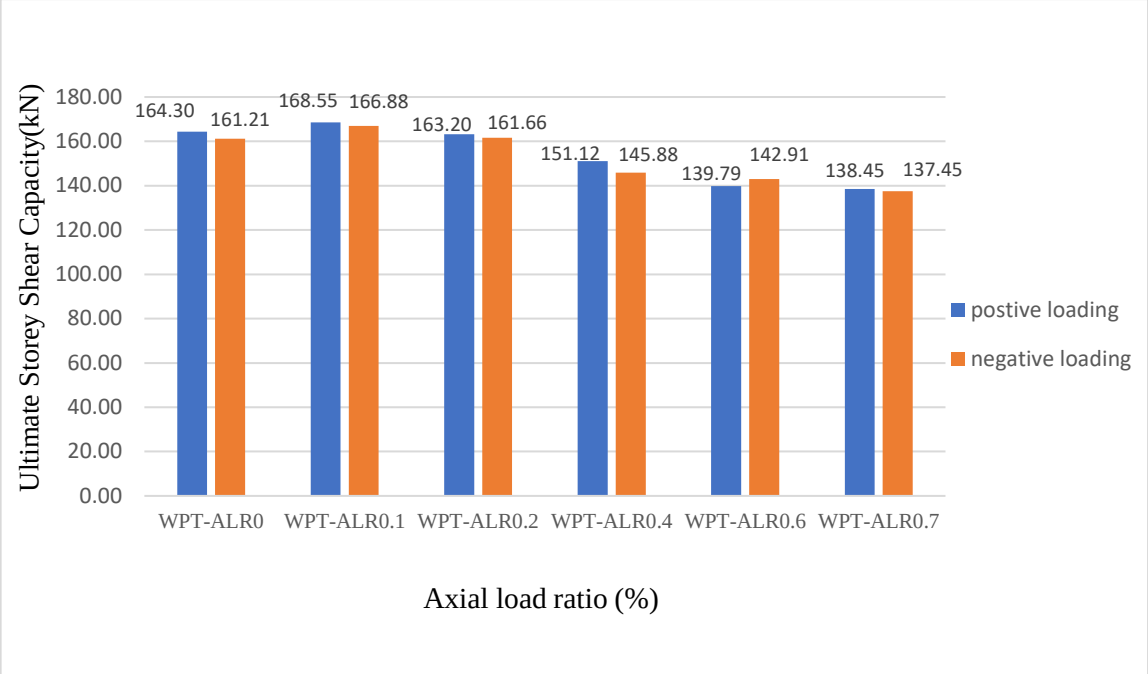

Figure 4-15 Effect of column axial load on ultimate storey shear capacity of wing plate type specimens

The effect of varying axial load on the ultimate storey shear capacity of the integrated type specimen is shown in Figure 4-16. IT-ALR0, IT-ALR0.1, IT-ALR0.2, IT-ALR0.4, IT-ALR0.6, and IT-ALR0.7 have an average ultimate storey shear capacity of 167.28kN, 174.23kN, 171.98kN, 162.72kN, 154.73kN, and 151.24kN, respectively. The integrated type specimen's average ultimate storey shear capacity increased by about 4.27% and 2.81% when the axial load was increased to 0.1*(Acfcd + Asfyd) and 0.2*(Acfcd + Asfyd), respectively, as compared to the specimen with no column axial load, i.e. IT-ALR0. However, when the axial load was increased further, the ultimate storey shear capacity decreased by 2.72%, 7.50%, and 9.58% for specimens IT-ALR0.4, IT-ALR0.6, and IT-ALR0.7, respectively, when compared to specimen IT-ALR0.

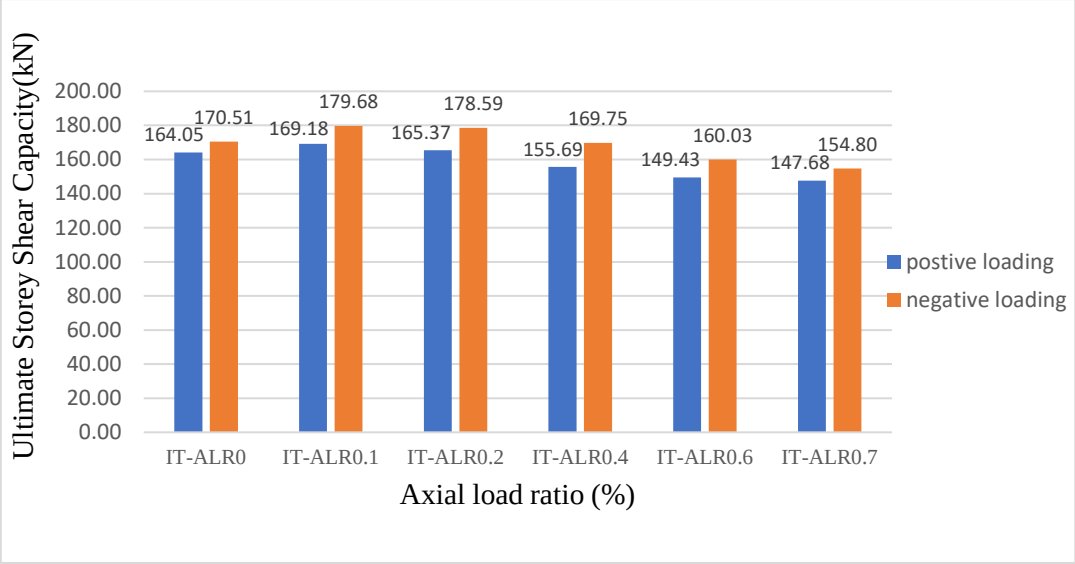

Figure 4-16 Effect of column axial load on ultimate storey shear capacity of integrated type specimens

4.3.2.2 Ductility

The displacement ductility factor is computed as discussed in section 4.3.1.2. The influence of the column axial load on the ductility performance of the passing through connection type is shown in Figure 4-17. Compared to the specimen with no axial load (PTT-ALR0), specimens PTT-ALR0.1, PTT-ALR0.2, PTT-ALR0.4, PTT-ALR0.6 and PTT-ALR0.7 exhibited a decrease in displacement ductility by 4.2%, 8.2%, 15.3%, 38.3% and 43.2% respectively.

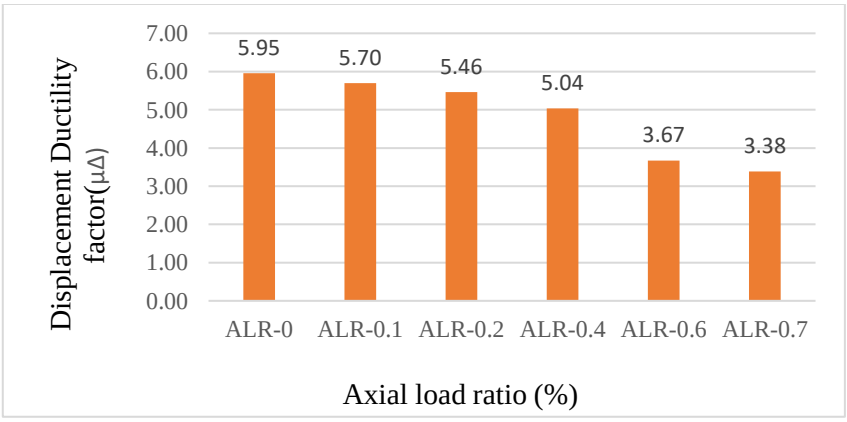

Figure 4-17 Effect of column axial load on displacement ductility factor of passing through type specimens

Figure 4-18 depicts the effect of the column axial load on the ductility of the wing plate connection type. The displacement ductility of specimens WPT-ALR0.1, WPT-ALR0.2, WPT-ALR0.4, WPT-ALR0.6, and WPT-ALR0.7 was reduced by 7.9%, 11.5%, 20.7%, 32.3%, and 39.6%, respectively, as compared to the specimen with no axial load (WPT-ALR0).

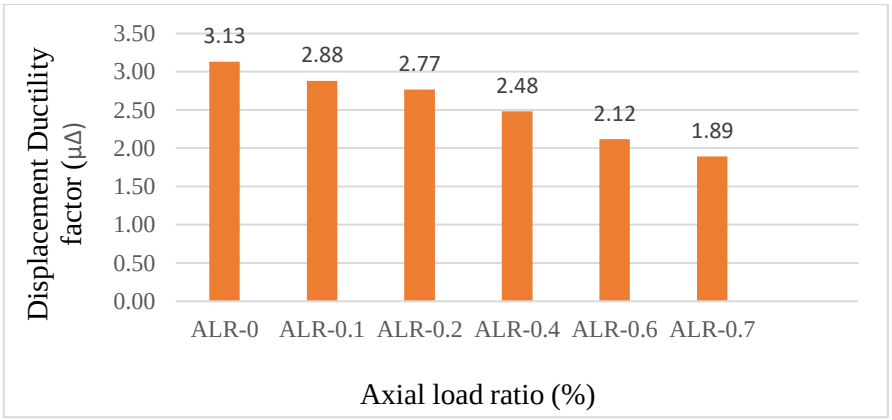

Figure 4-18 Effect of column axial load on displacement ductility factor of wing plate type specimens

The effect of column axial load on the ductility performance of the integrated connection type is shown in Figure 4-19. In comparison to the specimen with no axial load (PTT-ALR0), the displacement ductility of specimens IT-ALR0.1, IT-ALR0.2, IT-ALR0.4, IT-ALR0.6, and IT-ALR0.7 decreased by 7.7%, 11.2%, 25.1%, 32.1%, and 47.6%, respectively.

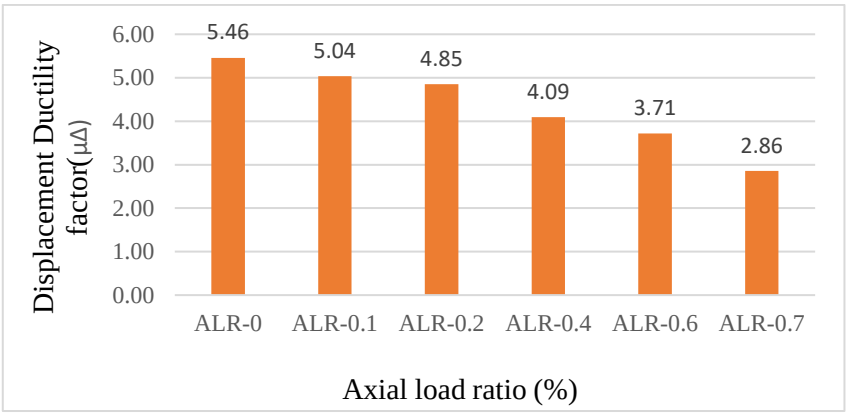

Figure 4-19Effect of column axial load on displacement ductility factor of integrated type specimens

4.3.2.3 Stiffness

The accumulation of structural damage is reflected in stiffness degradation, which is an important part of assessing structural seismic performance. Because of flexural and shear cracks, shear deformation of the joint core, yielding of longitudinal rebar, nonlinear behavior, and concrete crushing, the stiffness of reinforced concrete structural components is gradually reduced. As shown in Equation (4.2) the calculated stiffness was expressed in terms of secant stiffness in this study, which is the most common method for evaluating the response of inelastic structures (A. S. Elnashai and L. D iSarno, 2008). The stiffness was calculated using the positive loading section of the hysteretic curve. Since the ultimate loading capacity did not differ considerably in the positive and negative loading directions.

$$K_i = \frac{P_{\max,i}}{\Delta_{\max,i}} \quad \textbf{(4.2)}$$

Where K_i is the cyclic secant stiffness, $P_{max,i}$ is the maximum storey shear capacity per cycle, i, and $\Delta_{max,i}$ is the maximum storey displacement per cycle, i.

The cyclic stiffness degradation of the wing plate type specimen is shown in Figure 4-20. As it can be seen from Table 4-2, the cyclic stiffness of all specimens exhibited similar stiffness in the first loading cycle. However, the cyclic stiffness decreased with the increase of the loading cycle.

Table 4-2 Secant stiffness of wing plate type specimen

Loading cycle	WPT-ALR0	WPT-ALR0.1	WPT-ALR0.2	WPT-ALR0.4	WPT-ALR0.6	WPT-ALR0.7
	Stiffness(kN/mm)					
1	6.88	6.95	6.95	6.96	6.97	6.96
2	4.15	4.09	4.08	3.97	3.88	3.85
3	2.28	2.34	2.267	2.10	1.93	1.80

Compared to the specimen with no column axial load (WPT-ALR0) the specimens WPT-ALR0.1, WPT-ALR0.2, WPT-ALR0.4, WPT-ALR0.6, and WPT-ALR0.7 resulted 1.52%, -1.78%, -4.33%, -6.49% and -7.39%, respectively in the second loading cycle and exhibited 2.58%, -0.67%, -8.02%, -15.56% and -20.99% respectively in the third loading cycle. As it can be seen from the result, with increasing column axial load level the cyclic secant stiffness decreased.

Table 4-3 Percentage variation of stiffness about WPT-ALR0

Loading cycle	WPT-ALR0	WPT-ALR0.1	WPT-ALR0.2	WPT-ALR0.4	WPT-ALR0.6	WPT-ALR0.7
	Stiffness variation about WPT-ALR0 (%)					
1	0.00	+0.97	+0.95	+1.11	+1.34	+1.06
2	0.00	-1.52	-1.78	-4.33	-6.49	-7.39
3	0.00	+2.58	-0.67	-8.02	-15.56	-20.99

N.B: A positive value represents a percentage increase, while a negative value represents a decrease in percentage about specimen WPT-ALR0.

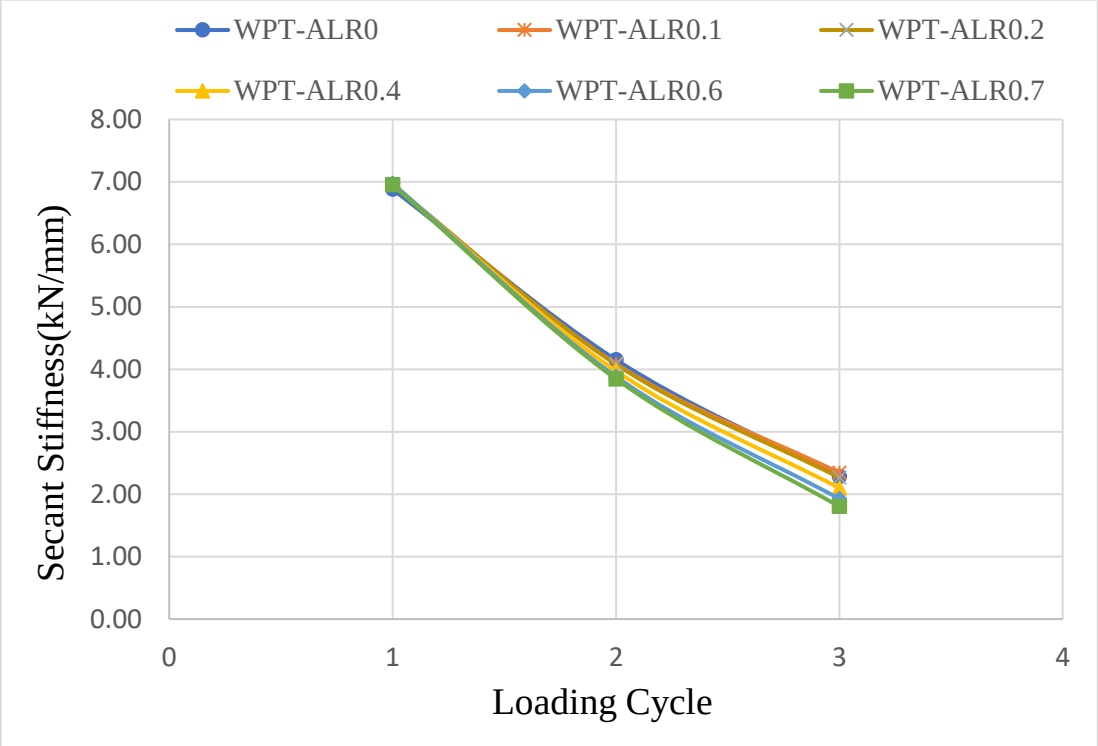

Figure 4-20 Effect of column axial load on stiffness degradation of wing plate type specimens

4.3.2.4 Energy dissipation capacity

One of the most important parameters to consider when evaluating a structure's seismic performance is its energy dissipation capacity. It refers to a structure's ability to absorb seismic energy through its own plastic deformation during an earthquake. According to previous experimental findings, the plastic energy dissipated by reinforced concrete structural components comprises of the energy dissipated by reinforcing bars, the friction of concrete fractures, and during the development of new cracks (Al-Salloum, Almusallam, Alsayed, & Siddiqui, 2011). Structural members capable of dissipating more

plastic energy reduce the effects of seismic forces on the structure. The area enclosed inside the corresponding load-displacement hysteretic loop determines the energy dissipation.

The accumulated dissipated energy (ADE) was calculated in this study by adding the product of the storey shear force and storey displacement for each loading cycle, as shown in Equation (4.3) (Tawfik Essa, Kotp Badr, & El-Zanaty, 2014).

$$\text{ADE} = \sum_{LS_i}^{LS_f} |V_{ED} * d| \quad \textbf{(4.3)}$$

Where "ADE" is the accumulated dissipated energy; "LS_i" is the initial loading stage; "LS_f" is the final loading stage; "V_{ED}" is the storey shear force and "d" is the storey displacement.

The effect of column axial load on accumulated dissipated energy is shown in Figure 4-21 for the wing plate specimen. As presented in Table 4-4, in the first loading cycle the energy dissipation was enhanced with a slight extent following the increment of column axial load ratio. However, for the final loading cycle the specimens WPT-ALR0.2, WPT-ALR0.4, WPT-ALR0.6, and WPT-ALR0.7 showed a decrease in the plastic energy dissipation than that of the specimen WPT-ALR0.1 with column axial load of 0.1*(Acfcd + Asfyd). Therefore, this investigation indicated that the increase of column axial load ratio has a detrimental effect on the energy dissipation capacity due to axial failure and local crushing of concrete.

Table 4-4 Accumulated energy dissipation for wing plate type specimen

Loading cycle	Accumulated energy dissipation(kN.mm)					
	WPT-ALR0	WPT-ALR0.1	WPT-ALR0.2	WPT-ALR0.4	WPT-ALR0.6	WPT-ALR0.7
0	0	0	0	0	0	0
1	4370.26	4390.95	4382.72	4405.15	4424.30	4415.46
2	26177.05	26541.09	26337.16	25869.45	25217.43	24685.52
3	85510.96	89395.64	86298.776	80108.16	75192.42	71901.45

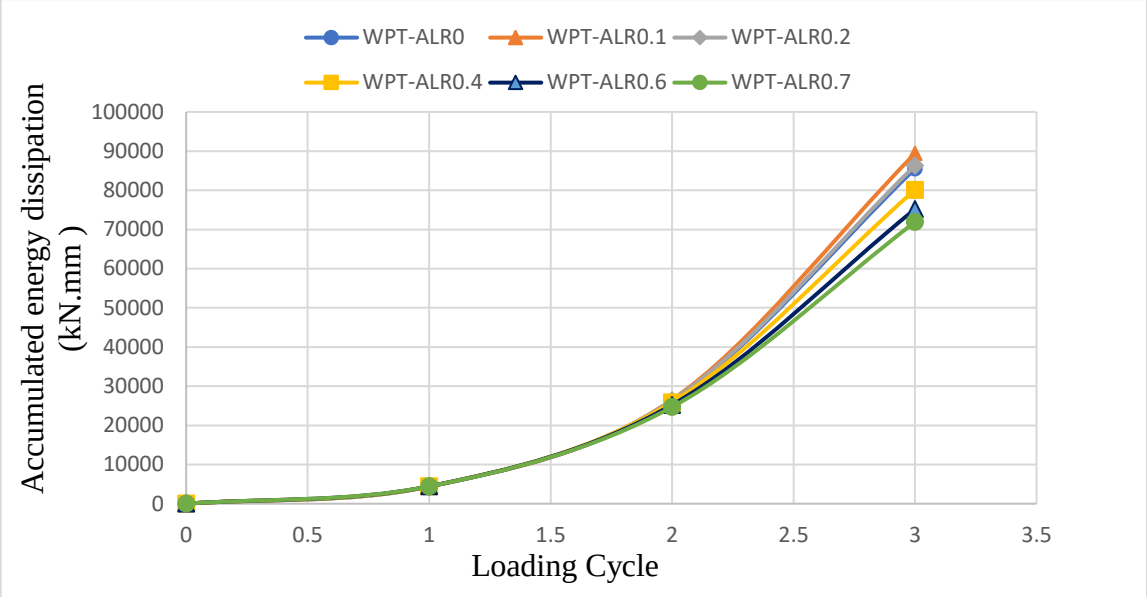

Figure 4-21 Effect of column axial load on accumulated energy dissipation of wing plate type specimens

CHAPTER 5 CONCLUSIONS AND RECOMMENDATIONS

5.1 Conclusion

In this study, the behavior of steel-reinforced composite column and reinforced concrete beam joints for selected connection types have been investigated analytically under reversed cyclic loading. The strength and ductility structural performance of the two connections types, passing through and wing plate was thoroughly investigated separately and their structural performance was compared with the integrated connection type. The improvement of the integrated connection type over the two separated connection types was investigated from the perspective of ductility and strength performance. The specimen's dimension and materials used in the experimental study conducted by (Ju & Chun, 2005) were used in this study for modeling the integrated connection type. The influence of axial load variation on the response of interior steel-reinforced composite column and reinforced concrete beam joints using the three connection types under cyclic loading were also examined.

According to the analytical result, the ultimate strength of the wing plate type exceeds the ultimate strength of the passing through type. On the other hand, from the perspective of ductility, the passing through type possesses a good ductility behavior. Whereas the integrated type exhibits improved structural performance from the separated connection types. The integrated connection type obtains a good ductility behavior from passing through type since the reinforcement bars of the reinforced concrete beam directly pass through the beam-column joint which gives it adequate anchorage and sufficient bond strength.

The integrated type acquires good strength performance from the wing plate connection type because the stress induced in the corner of the column due to the bent reinforcement bar of the reinforced concrete beam is avoided. This was because the edge reinforcement bars of the reinforced concrete beam of the integrated connection type are flare welded to the wing plate. This in turn prevents the cover spalling problem observed in the passing through type. The elimination of the corner column cover spalling contributes to the ultimate strength performance of the integrated type. Hence, the integrated connection type demonstrates increased ductility and strength behavior, that it gets from the two individual

connection types which make it a preferable connection type over the other connection types.

Based on the finite element analysis result, the variation of column axial load on the integrated type specimen and the two control specimens, passing through type and wing pate type, exhibited a slight increment in the ultimate storey shear capacity when the column axial load level was 20%, 20% and 10% of the column capacity, respectively. However, increasing the column axial load further reduces the ultimate storey shear because of the adverse effect of axial forces on the lateral stiffness of columns. Furthermore, increasing the column axial load ratio resulted in a decrease in the ductility performance of the joints.

For the wing plate type connection, increasing column axial load levels improves the energy dissipation capacity of joints at the first stage of loading, but has a negative impact as the loading stages progress owing to axial failure and local crushing of concrete. Similarly, when the axial load level increased, the cyclic stiffness decreased due to the degradation induced by the local crushing of concrete in the column.

5.2 Recommendation

This research is not enough to fully comprehend the structural performance of steel-reinforced concrete composite column and reinforced concrete beam joint under reverse cyclic loading. The author suggests that more research be done on the following points:

I. This research is carried out on an interior beam-column joint, further studies can be expanded to other joints such as the knee, exterior, and corner joints.
II. The effect of reinforcement ratio (transverse and longitudinal), concrete compressive strength, column cross-sectional type, the shape of structural steel section, and the presence of transverse slab on the performance of steel-reinforced concrete composite column and reinforced concrete beam joint should be investigated.
III. Numerical models that predict the pinching behavior of steel-reinforced concrete composite columns and reinforced concrete beam joints under cyclic loading are highly recommended.

IV. Stiffness degradation and energy dissipation capacity with increasing axial load ratio were done only for the wing plate type connection in this study. Further investigation is needed for the hysteretic response of the passing through and integrated connection type to be evaluated based on stiffness degradation and energy dissipation capacity.

V. Further experimental investigation is recommended for the integrated type connection due to its accuracy compared to the finite element model.

REFERENCES

A. S. Elnashai and L. D iSarno. (2008). Fundamentals of earthquake engineering. In *Bulletin of the New Zealand Society for Earthquake Engineering* (First Edit, Vol. 5). https://doi.org/10.5459/bnzsee.5.1.36

AISC, A. I. of S. (2010). *Specification for Structural Steel Buildings*. 1–612.

Al-Salloum, Y. A., Almusallam, T. H., Alsayed, S. H., & Siddiqui, N. A. (2011). Seismic Behavior of As-Built, ACI-Complying, and CFRP-Repaired Exterior RC Beam-Column Joints. *Journal of Composites for Construction*, *15*(4), 522–534. https://doi.org/10.1061/(asce)cc.1943-5614.0000186

Bai, Y., Nie, J., & Cai, C. S. (2008). New Connection System for Confined Concrete Columns and Beams. II: Theoretical Modeling. *Journal of Structural Engineering*, *134*(12), 1800–1809. https://doi.org/10.1061/(asce)0733-9445(2008)134:12(1800)

Behnam, H., Kuang, J. S., & Samali, B. (2018). Parametric finite element analysis of RC wide beam-column connections. *Computers and Structures*, *205*, 28–44. https://doi.org/10.1016/j.compstruc.2018.04.004

Chen, Q., Cai, J., Bradford, M. A., Liu, X., & Wu, Y. (2015). Axial Compressive Behavior of Through-Beam Connections between Concrete-Filled Steel Tubular Columns and Reinforced Concrete Beams. *Journal of Structural Engineering*, *141*(10), 04015016. https://doi.org/10.1061/(asce)st.1943-541x.0001249

Chen, Q. J., Cai, J., Bradford, M. A., Liu, X., & Zuo, Z. L. (2014). Seismic behaviour of a through-beam connection between concrete-filled steel tubular columns and reinforced concrete beams. *Engineering Structures*, *80*, 24–39. https://doi.org/10.1016/j.engstruct.2014.08.036

Ding, F. xing, Yin, G. an, Wang, L. ping, Hu, D., & Chen, G. qiang. (2017). Seismic performance of a non-through-core concrete between concrete-filled steel tubular columns and reinforced concrete beams. *Thin-Walled Structures*, *110*(October 2016), 14–26. https://doi.org/10.1016/j.tws.2016.10.014

EBCS EN- 8 Part. (2014). *EBCS- 8 Design of Structures for Earthquake Resistance* Part 1: General Rules, Seismic Actions and Rules for Buildings. (December).

El-Ghazaly, H. A., & Al-Zamel, H. S. (1991). Innovative detail for precast concrete beam-column moment connections. *Canadian Journal of Civil Engineering*, *18*(4), 690–710. https://doi.org/10.1139/l91-084

Eurocode 2. (2004). Design of Concrete Structures: Part 1-1: General Rules and Rules for Buildings, *CEN, London*.

Eurocode 8. (2003).Design of Structures for Earthquake Resistance Part 1: General Rules, Seismic Actions, and Rules for Buildings, *European Committee for Standardization, Brussels, Belgium*, p. 121. doi: 10.1680/cien.144.6.55.40618.

Han, L. H., Qu, H., Tao, Z., & Wang, Z. F. (2009). Experimental behaviour of thin-walled steel tube confined concrete column to RC beam joints under cyclic loading. *Thin-Walled Structures*, *47*(8–9), 847–857. https://doi.org/10.1016/j.tws.2009.03.001

Hu, B., & Kundu, T. (2019). Seismic Performance of Interior and Exterior Beam-Column Joints in Recycled Aggregate Concrete Frames. *Journal of Structural Engineering*, *145*(3), 04018262. https://doi.org/10.1061/(asce)st.1943-541x.0002261

Hung-Jen Lee and Jen-wen ko. (2007). Eccentric Reinforced Concrete Beam-Column Connections Subjected to Cyclic Loading in Principal Directions. *ACI Structural Journal*, *104*(4), 459–467. https://doi.org/10.14359/18776

Ishida, T., Pen, K., Tanaka, Y., Kashimura, K., & Iwaki, I. (2018). Numerical simulation of early age cracking of reinforced concrete bridge decks with a full-3D multiscale and multi-chemo-physical integrated analysis. *Applied Sciences (Switzerland)*, *8*(3), 1–18. https://doi.org/10.3390/app8030394

Jia, J., Zhu, W., Meng, G., & Yao, D. (2011). Study on shear strength of SRC beam-column connections. *Advanced Materials Research*, *255–260*, 25–29. https://doi.org/10.4028/www.scientific.net/AMR.255-260.25

Ju, Y., & Chun, S. (2005). *Assessment of composite column and RC beam joints*. (June), 201–215.

Kaliluthin, A. K., Kothandaraman, S., & Ahamed, T. S. S. (2015). A Review on Behavior of Reinforced Concrete Beam-Column Joint. *International Journal of Innovative Research in Science, Engineering and Technology*, *2014*(4), 11299–11312.

Li, L. Z., Liu, X., Yu, J. T., Lu, Z. D., Su, M. N., Liao, J. H., & Xia, M. (2019). Experimental study on seismic performance of post-fire reinforced concrete frames. *Engineering Structures*, *179*(April 2018), 161–173. https://doi.org/10.1016/j.engstruct.2018.10.080

Liao, F. Y., Han, L. H., & Tao, Z. (2014). Behaviour of composite joints with concrete encased CFST columns under cyclic loading: Experiments. *Engineering Structures*, *59*, 745–764. https://doi.org/10.1016/j.engstruct.2013.11.030

Maekawa, K., Okamura, H., & Pimanmas, A. (2003). (2003). *Non-linear mechanics of reinforced concrete* (Vol. 148).

Mostofinejad, D., & Akhlaghi, A. (2017). Experimental Investigation of the Efficacy of EBROG Method in Seismic Rehabilitation of Deficient Reinforced Concrete Beam–Column Joints Using CFRP Sheets. *Journal of Composites for Construction*, *21*(4), 04016116. https://doi.org/10.1061/(asce)cc.1943-5614.0000781

Park and Priestley. (1987). Strength and Ductility of Concrete Bridge Columns Under Seismic Loading. *ACI Structural Journal*, *84*(1), 285–336. https://doi.org/10.14359/2800

Paulay, T., & Priestley, M. J. N. (1992). *Seismic Design Of Reinforced Concrete* (p. 744). p. 744.

Pinkham, C. W., Hanson, N. W., Aristizibal, J. D., Wight, J. K., Bertero, V. V., Criswell, M. E., … Park, R. (1985). Recommendations for Design of Beam-Column Joints in Monolithic Reinforced Concrete Structures. *Journal of the American Concrete Institute*, *82*(3), 266–283. https://doi.org/10.14359/11078

R Park. (1989). Evaluation of Ductility of Structures And Structural Assemblages From Laboratory Testing. *Bulletin of the New Zealand National Society for Earthquake Engineering*, *22*(3), 155–166.

Raffaelle, G.S. and Wight, J. K. (1992). Reinforced Concrete Eccentric Beam-Column Connections Subjected to Earthquake-Type Loading. *ACI Structural Journal*, *92*(1). https://doi.org/10.14359/1474

Tawfik Essa, A. S. A., Kotp Badr, M. R., & El-Zanaty, A. H. (2014). Effect of infill wall on the ductility and behavior of high strength reinforced concrete frames. *HBRC Journal*, *10*(3), 258–264. https://doi.org/10.1016/j.hbrcj.2013.12.005

Zhang, Y. F., Zhao, J. H., & Cai, C. S. (2012). Seismic behavior of ring beam joints between concrete-filled twin steel tubes columns and reinforced concrete beams. *Engineering Structures*, *39*, 1–10. https://doi.org/10.1016/j.engstruct.2012.01.014

APPENDIX A

A.1 Hysteretic response of the three connection types with varying axial load ratio

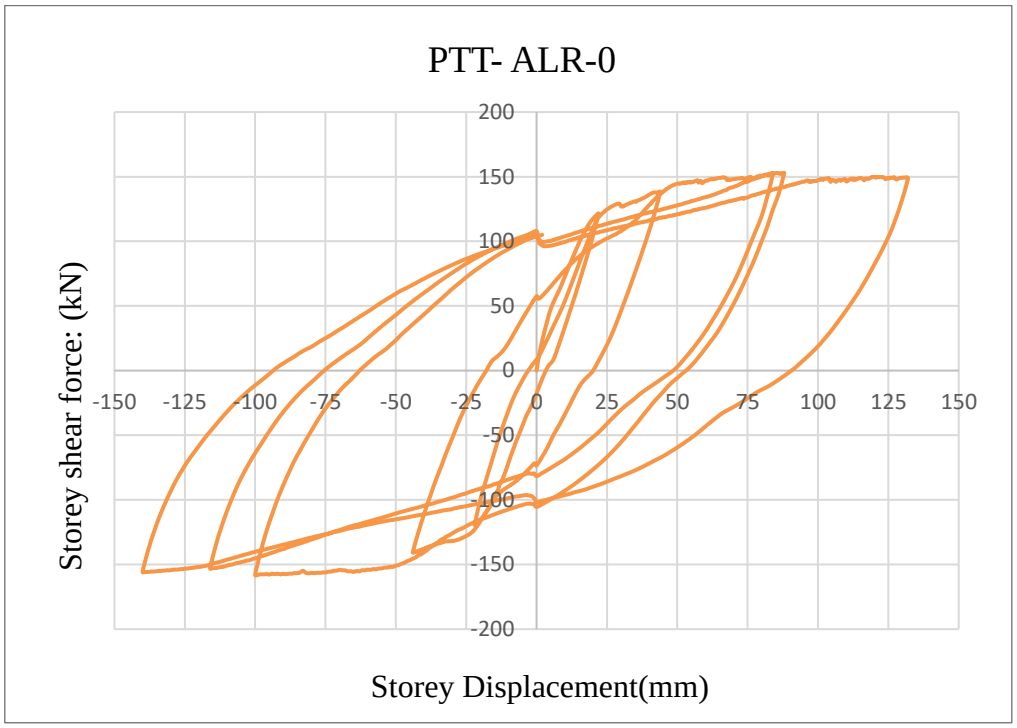

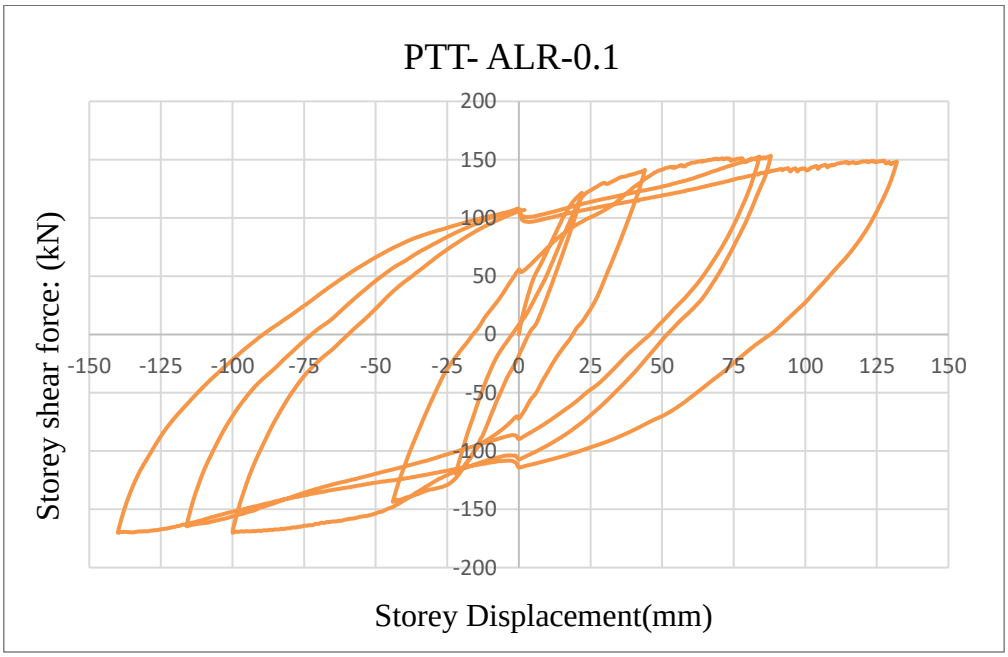

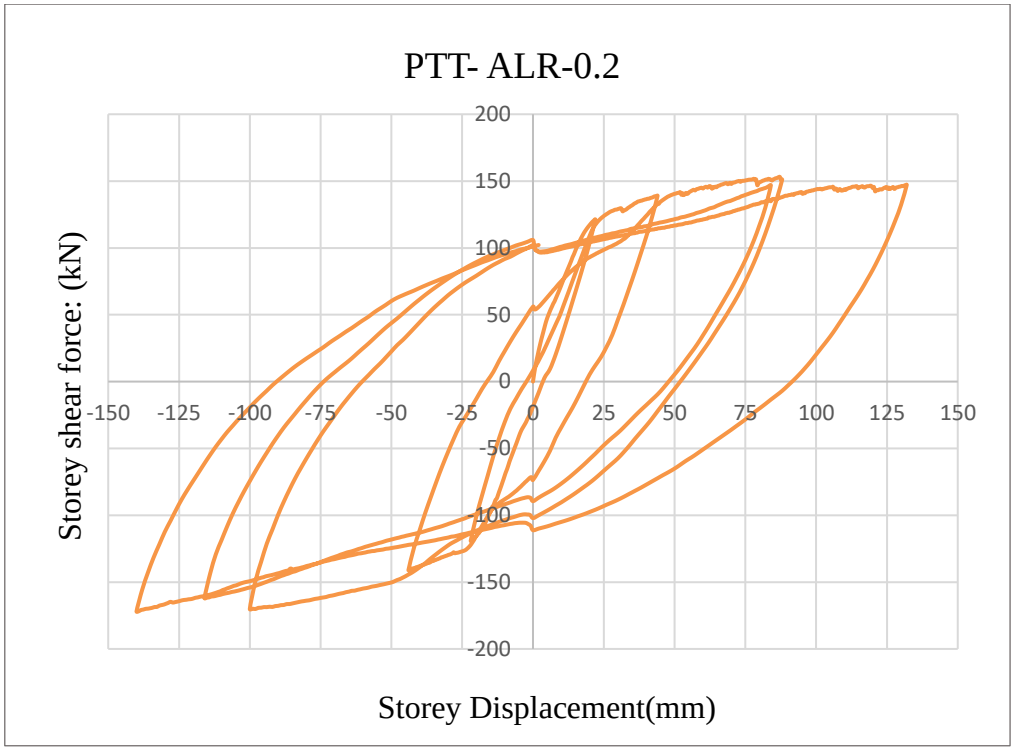
PTT- ALR-0.2
Storey shear force: (kN)
200
150
100
50
0
-50
-100
-150
-200
-150 -125 -100 -75 -50 -25 0 25 50 75 100 125 150
Storey Displacement(mm)

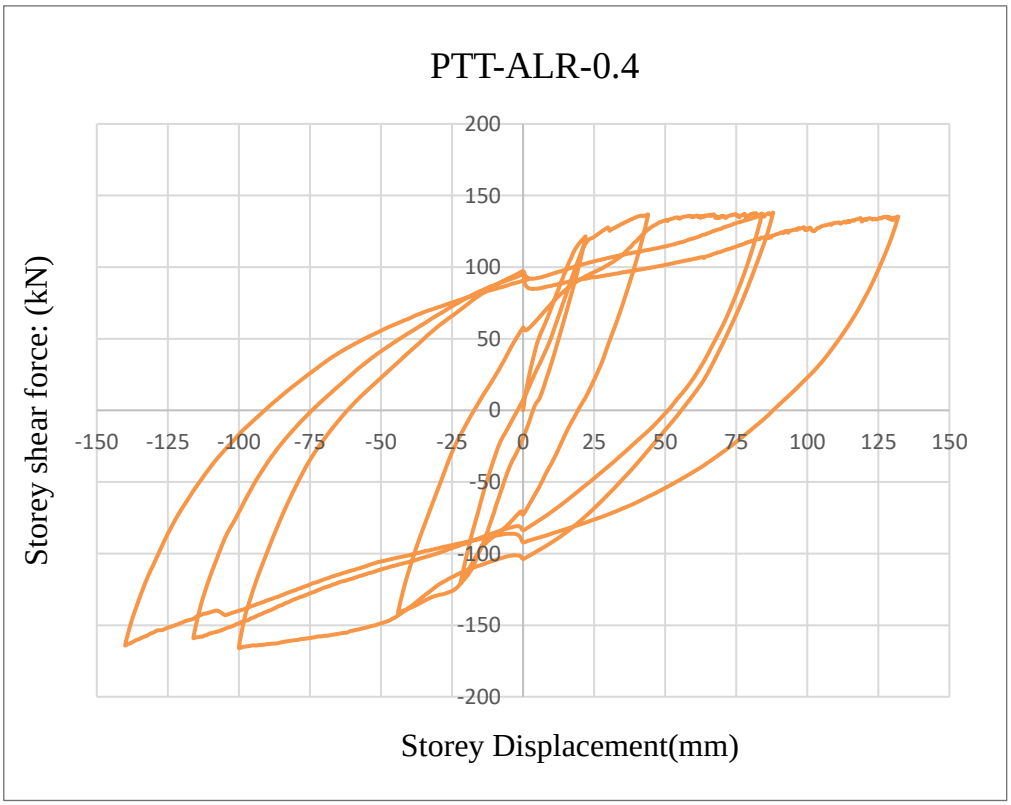
PTT-ALR-0.4
Storey shear force: (kN)
200
150
100
50
0
-50
-100
-150
-200
-150 -125 -100 -75 -50 -25 0 25 50 75 100 125 150
Storey Displacement(mm)

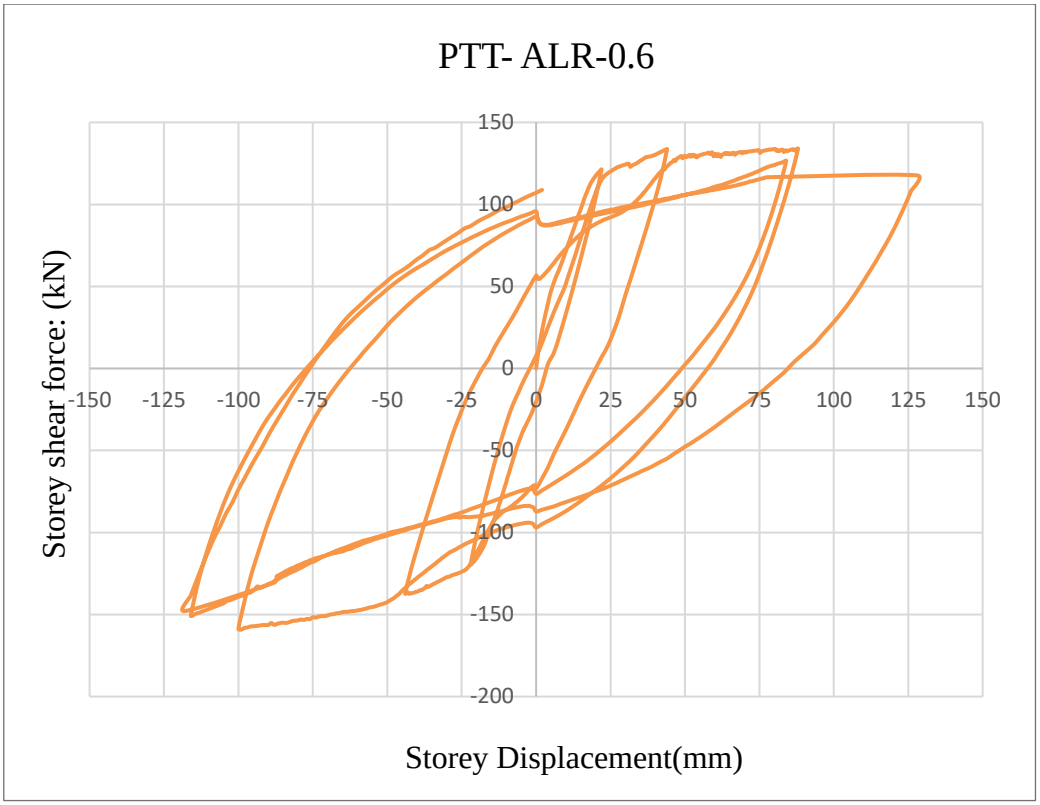
PTT- ALR-0.6
Storey shear force: (kN)
150
100
50
0
-50
-100
-150
-200
-150 -125 -100 -75 -50 -25 0 25 50 75 100 125 150
Storey Displacement(mm)

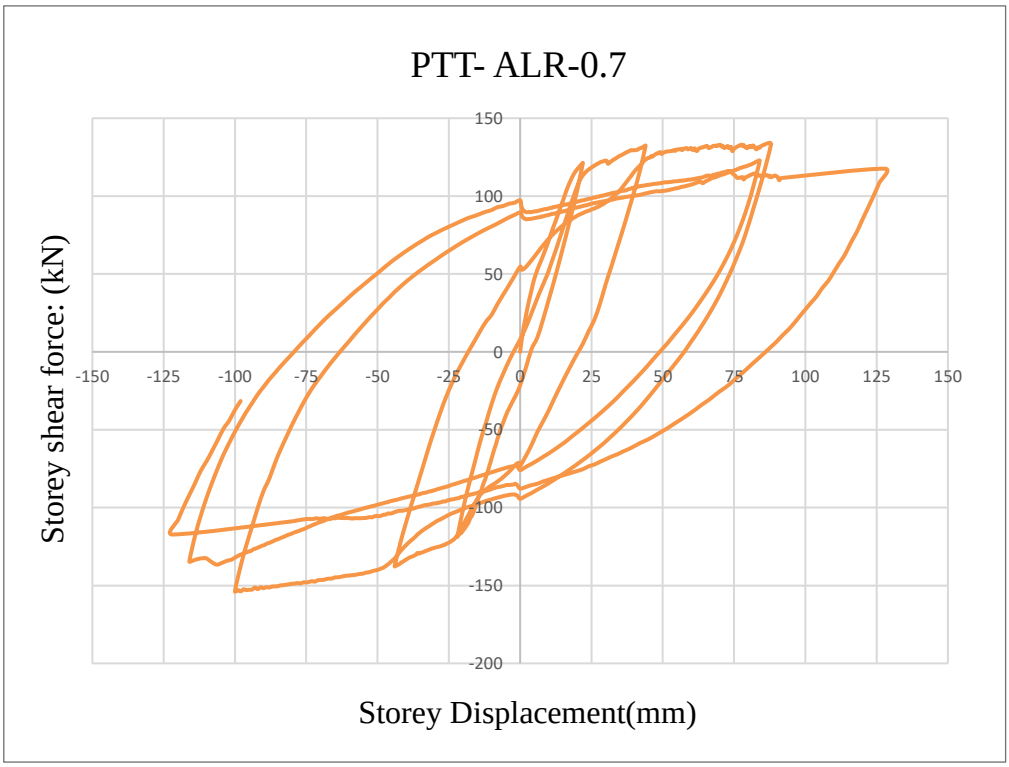
PTT- ALR-0.7
Storey shear force: (kN)
150
100
50
0
-50
-100
-150
-200
-150 -125 -100 -75 -50 -25 0 25 50 75 100 125 150
Storey Displacement(mm)

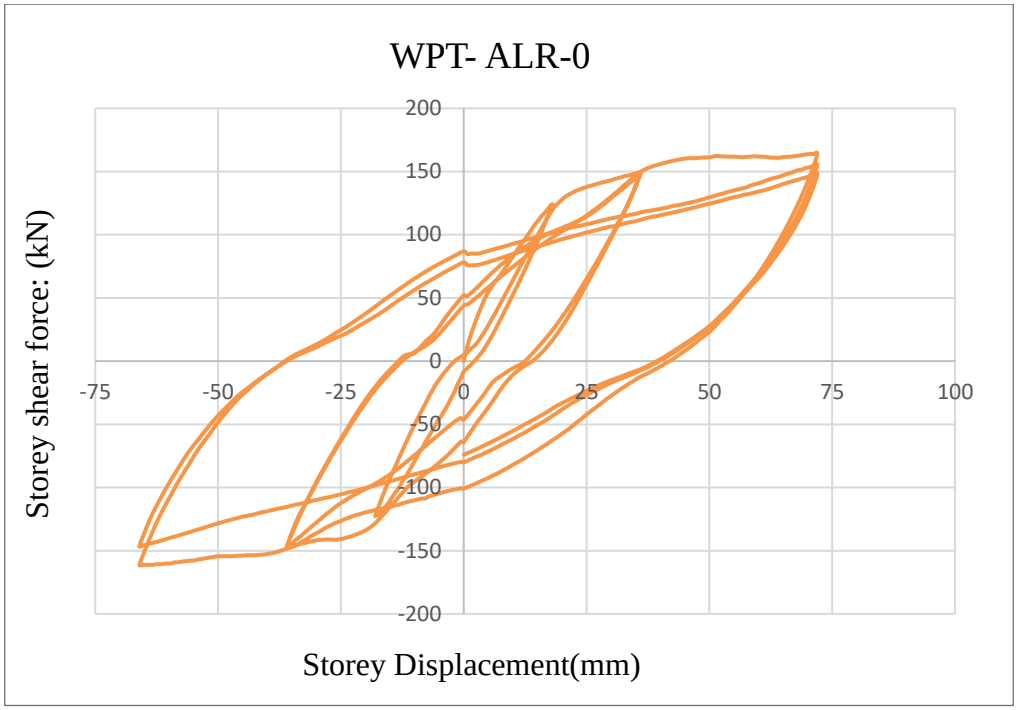
WPT- ALR-0
Storey shear force: (kN)
200
150
100
50
0
-50
-100
-150
-200
-75
-50
-25
0
25
50
75
100
Storey Displacement(mm)

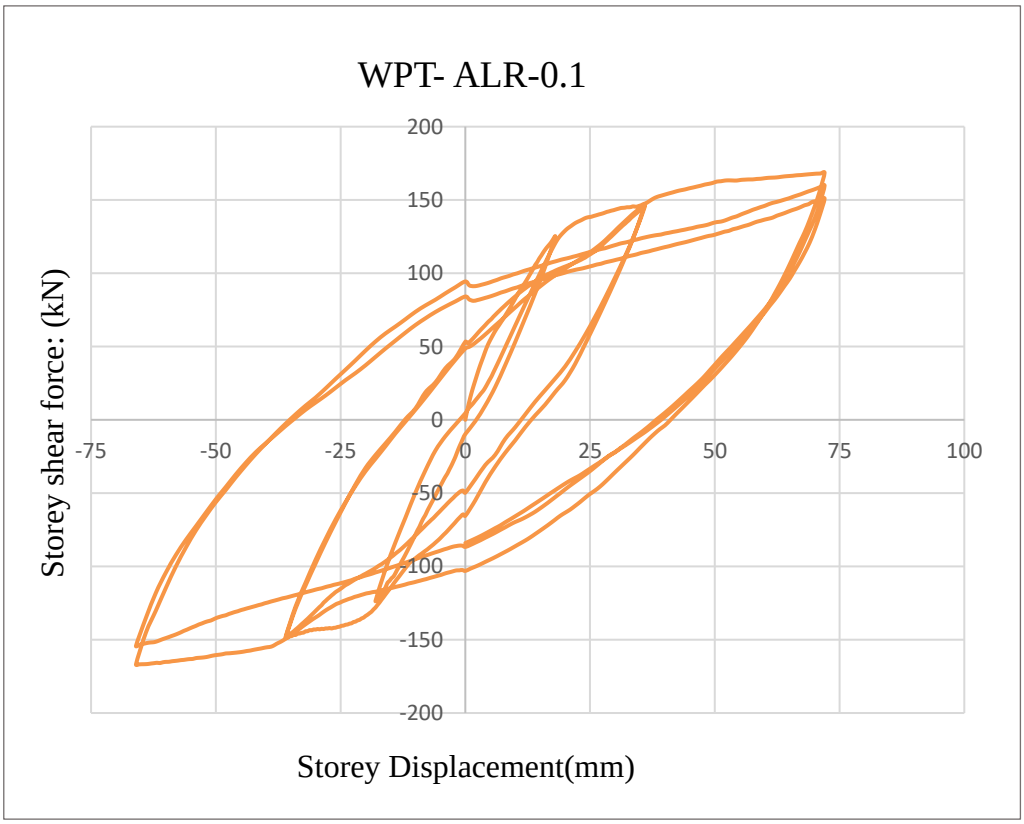
WPT- ALR-0.1
Storey shear force: (kN)
200
150
100
50
0
-50
-100
-150
-200
-75
-50
-25
0
25
50
75
100
Storey Displacement(mm)

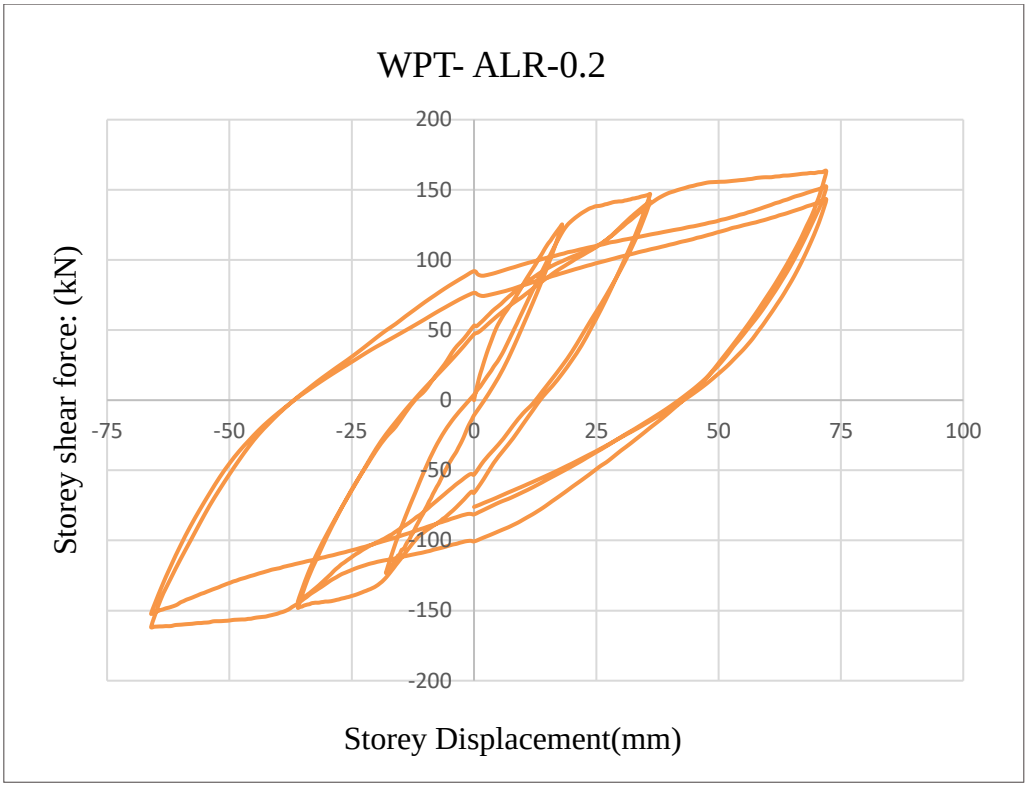
WPT- ALR-0.2
Storey shear force: (kN)
200
150
100
50
0
-50
-100
-150
-200
-75
-50
-25
0
25
50
75
100
Storey Displacement(mm)

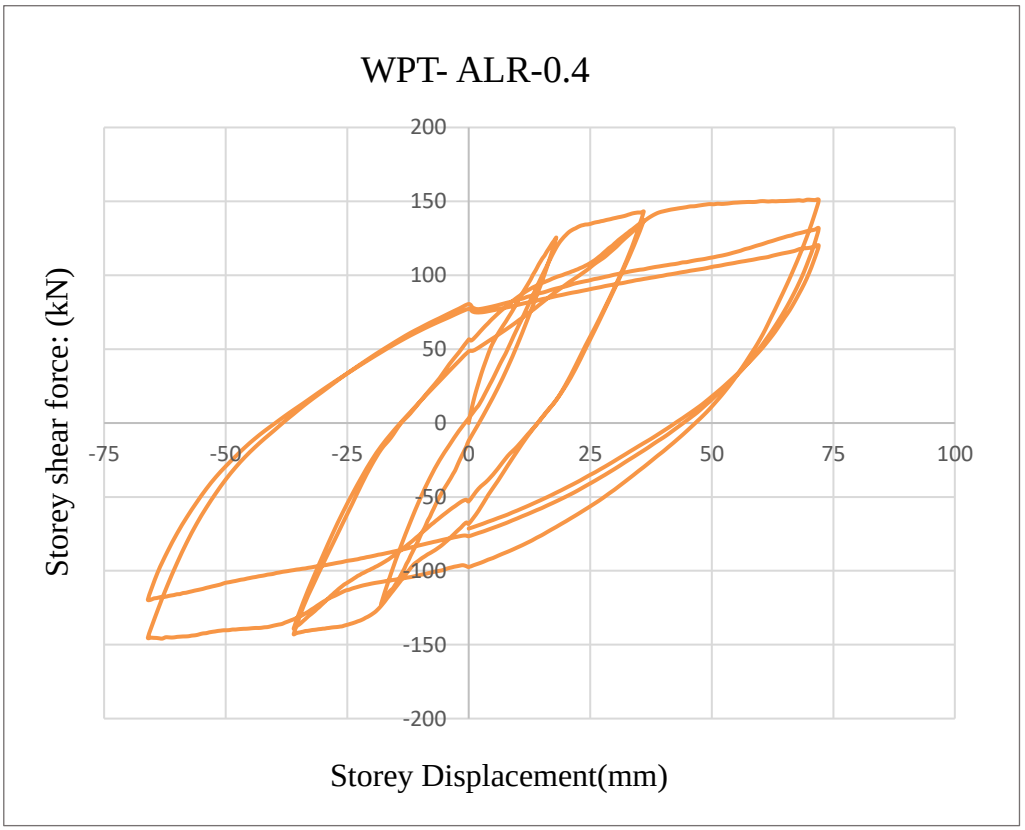
WPT- ALR-0.4
Storey shear force: (kN)
200
150
100
50
0
-50
-100
-150
-200
-75
-50
-25
0
25
50
75
100
Storey Displacement(mm)

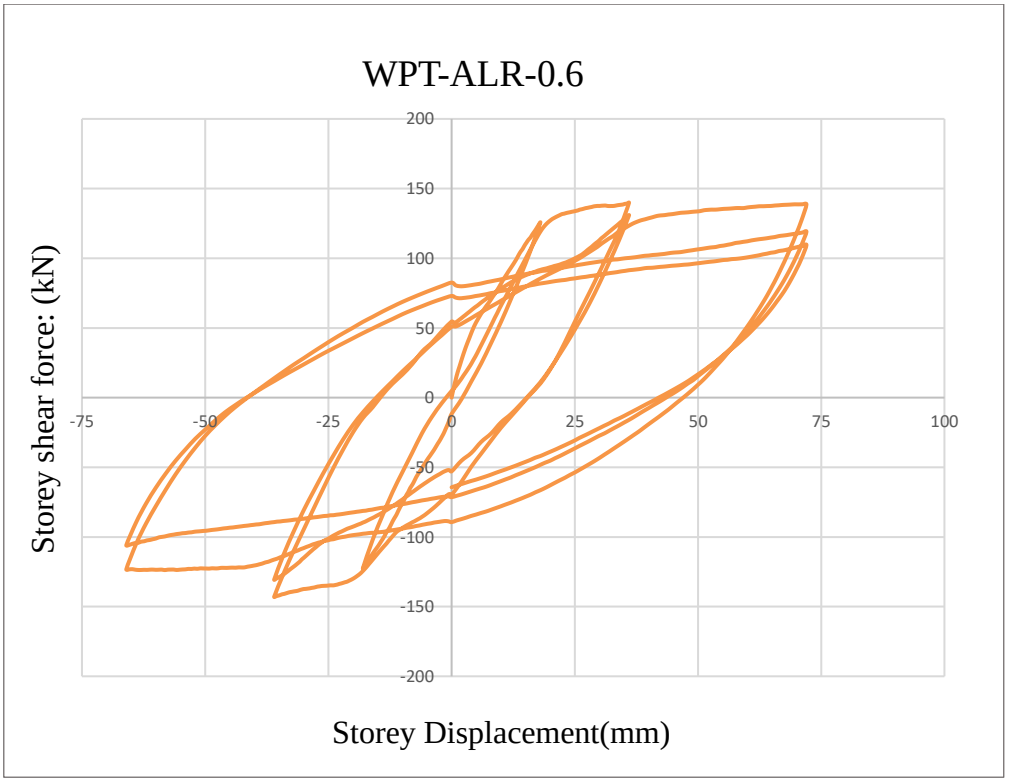
WPT-ALR-0.6
Storey shear force: (kN)
200
150
100
50
0
-50
-100
-150
-200
-75
-50
-25
0
25
50
75
100
Storey Displacement(mm)

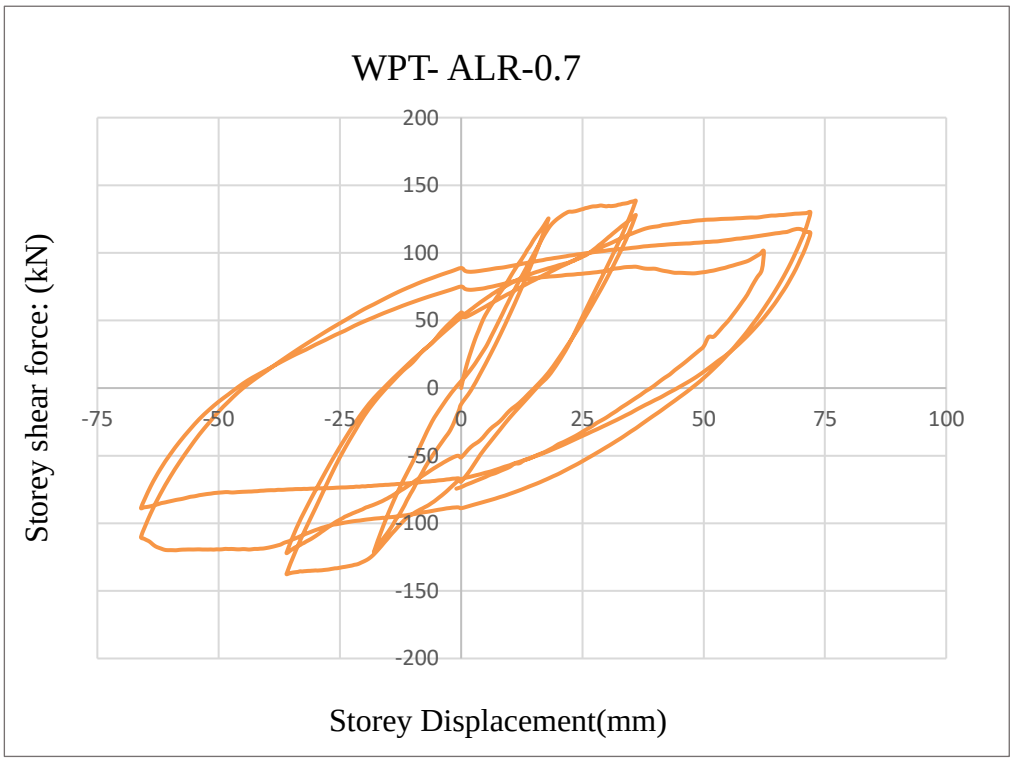
WPT- ALR-0.7
Storey shear force: (kN)
200
150
100
50
0
-50
-100
-150
-200
-75
-50
-25
0
25
50
75
100
Storey Displacement(mm)

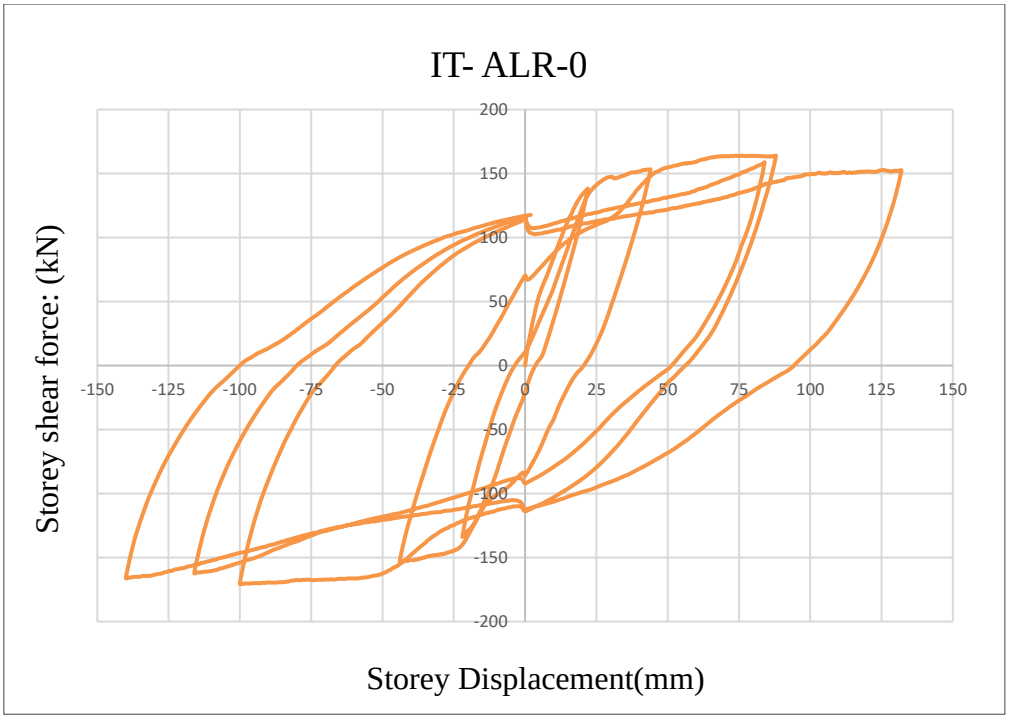
IT- ALR-0
Storey shear force: (kN)
200
150
100
50
0
-50
-100
-150
-200
-150 -125 -100 -75 -50 -25 0 25 50 75 100 125 150
Storey Displacement(mm)

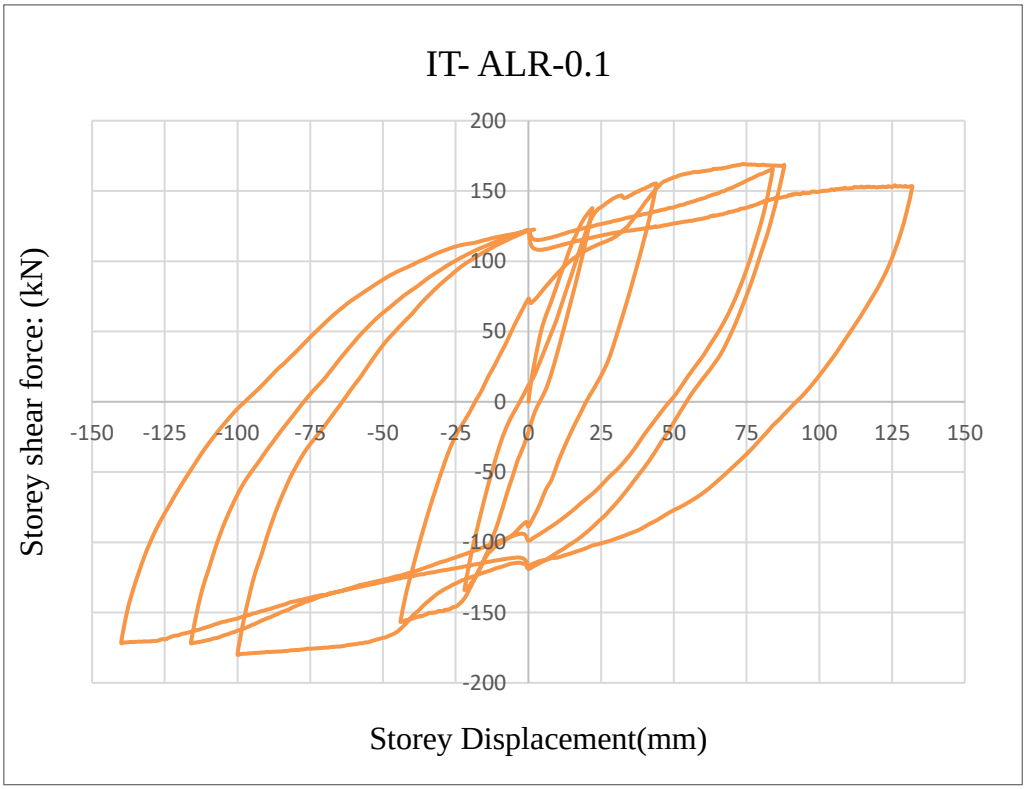
IT- ALR-0.1
Storey shear force: (kN)
200
150
100
50
0
-50
-100
-150
-200
-150 -125 -100 -75 -50 -25 0 25 50 75 100 125 150
Storey Displacement(mm)


IT- ALR-0.2
Storey shear force: (kN)
200
150
100
50
0
-50
-100
-150
-200
-150 -125 -100 -75 -50 -25 0 25 50 75 100 125 150
Storey Displacement(mm)


IT- ALR-0.4
Storey shear force: (kN)
200
150
100
50
0
-50
-100
-150
-200
-150 -125 -100 -75 -50 -25 0 25 50 75 100 125 150
Storey Displacement(mm)

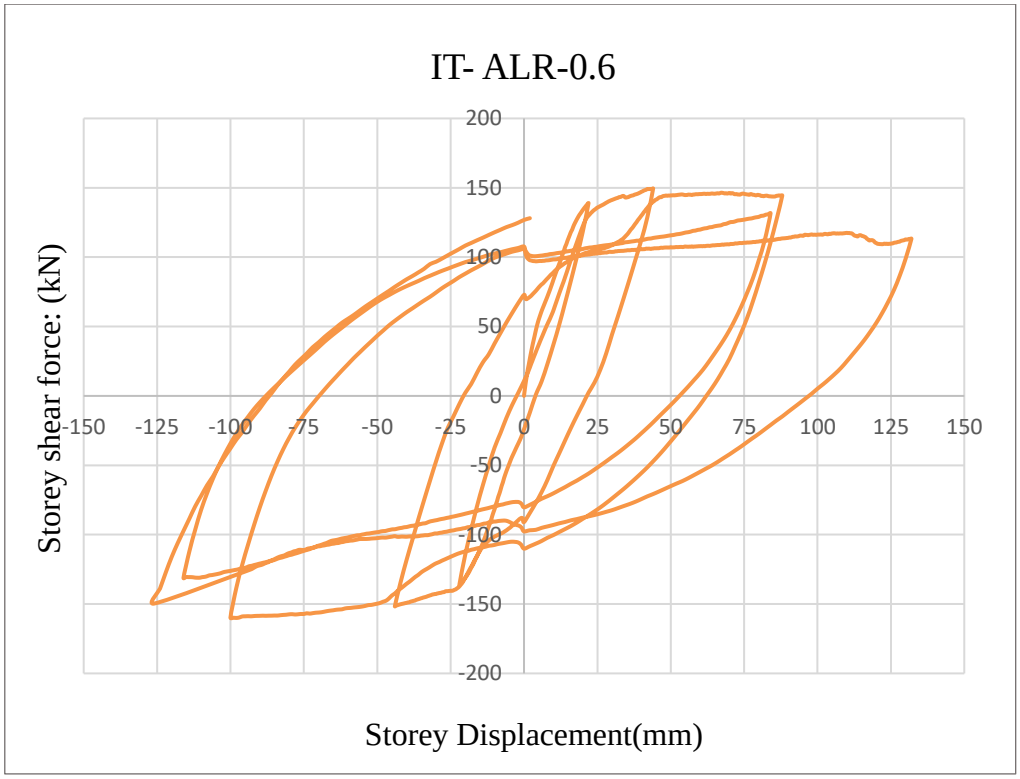
IT- ALR-0.6
Storey shear force: (kN)
200
150
100
50
0
-50
-100
-150
-200
-150 -125 -100 -75 -50 -25 0 25 50 75 100 125 150
Storey Displacement(mm)

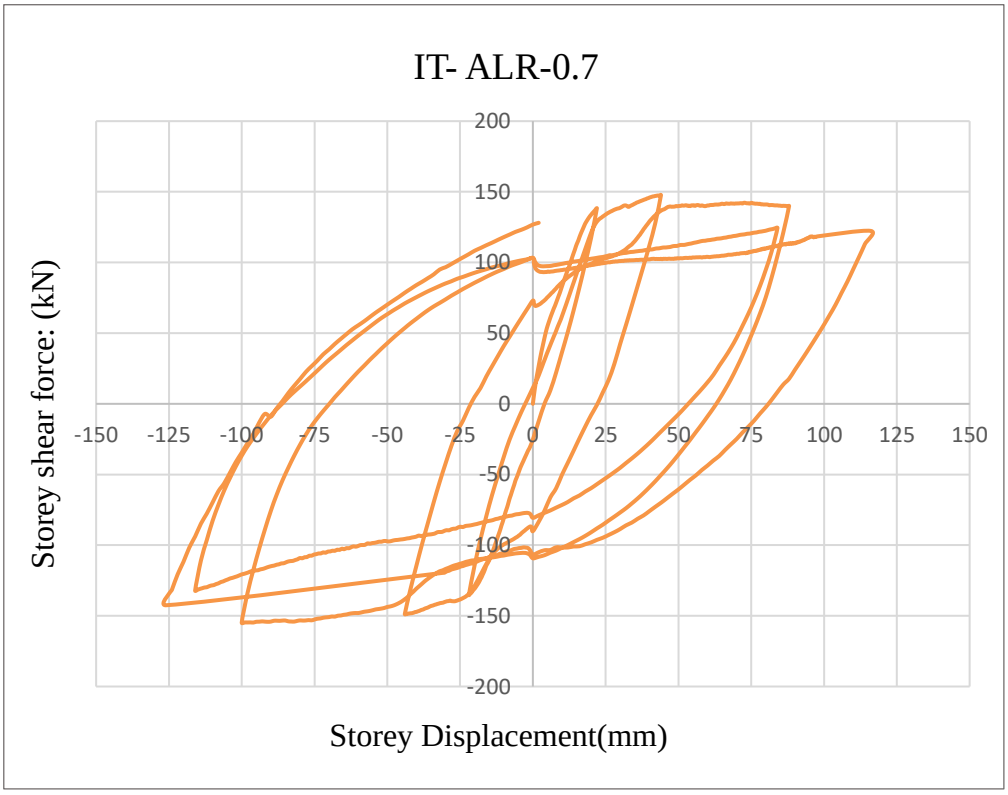
IT- ALR-0.7
Storey shear force: (kN)
200
150
100
50
0
-50
-100
-150
-200
-150 -125 -100 -75 -50 -25 0 25 50 75 100 125 150
Storey Displacement(mm)

APPENDIX B

B.1 Concrete strain of the three connection types at final loading

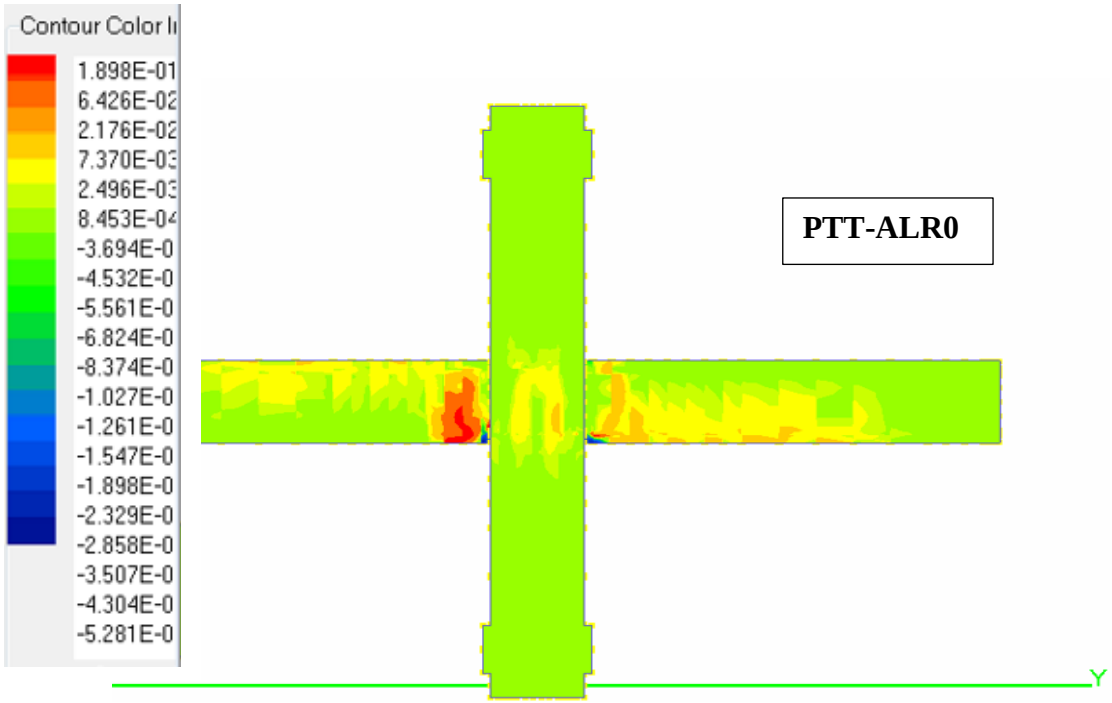

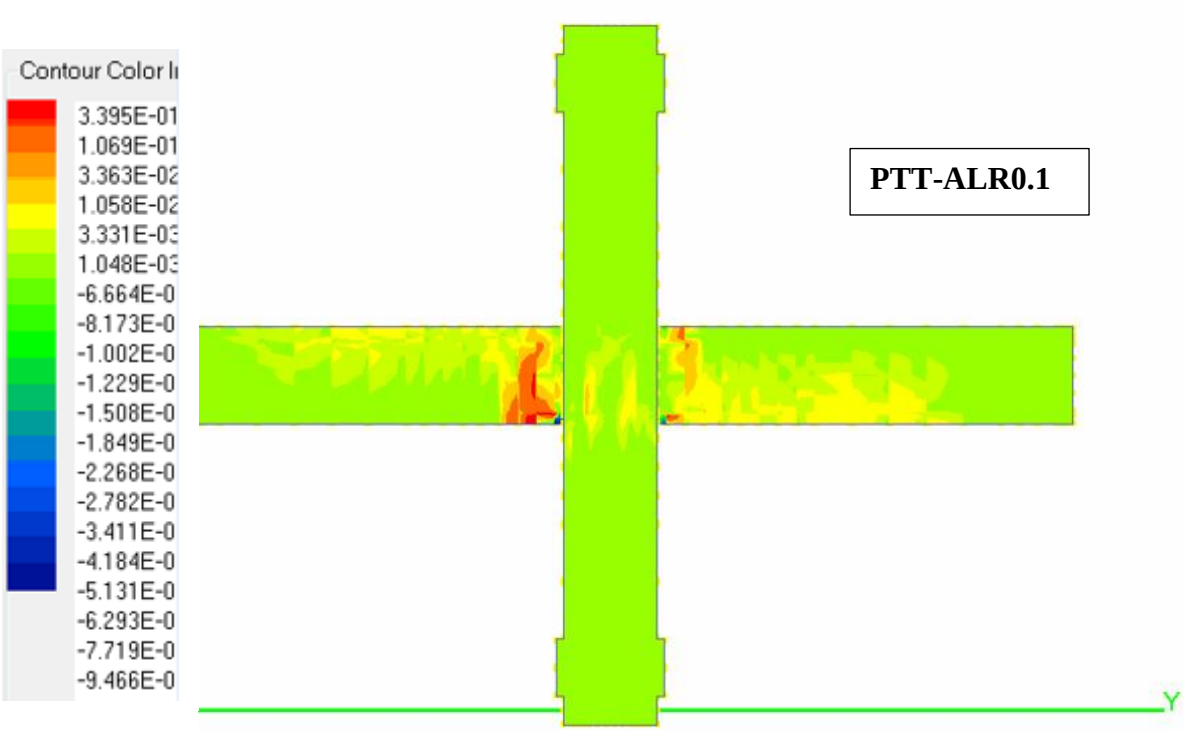

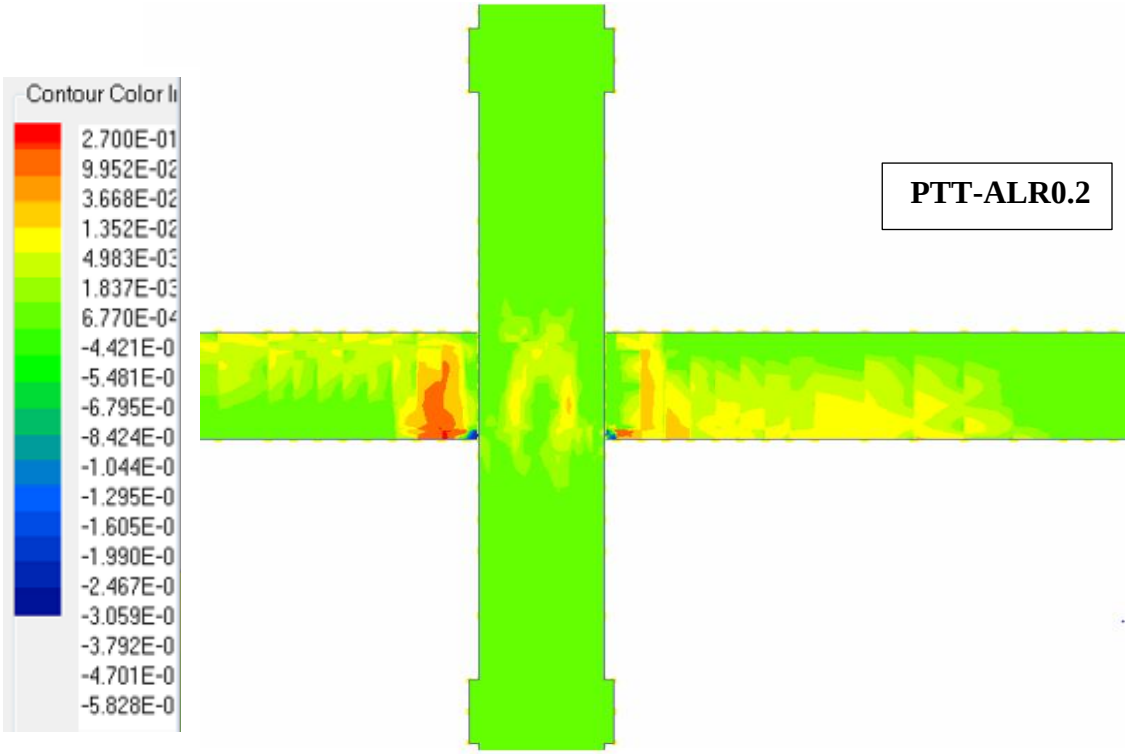
Contour Color li
2.700E-01
9.952E-02
3.668E-02
1.352E-02
4.983E-03
1.837E-03
6.770E-04
-4.421E-0
-5.481E-0
-6.795E-0
-8.424E-0
-1.044E-0
-1.295E-0
-1.605E-0
-1.990E-0
-2.467E-0
-3.059E-0
-3.792E-0
-4.701E-0
-5.828E-0
PTT-ALR0.2

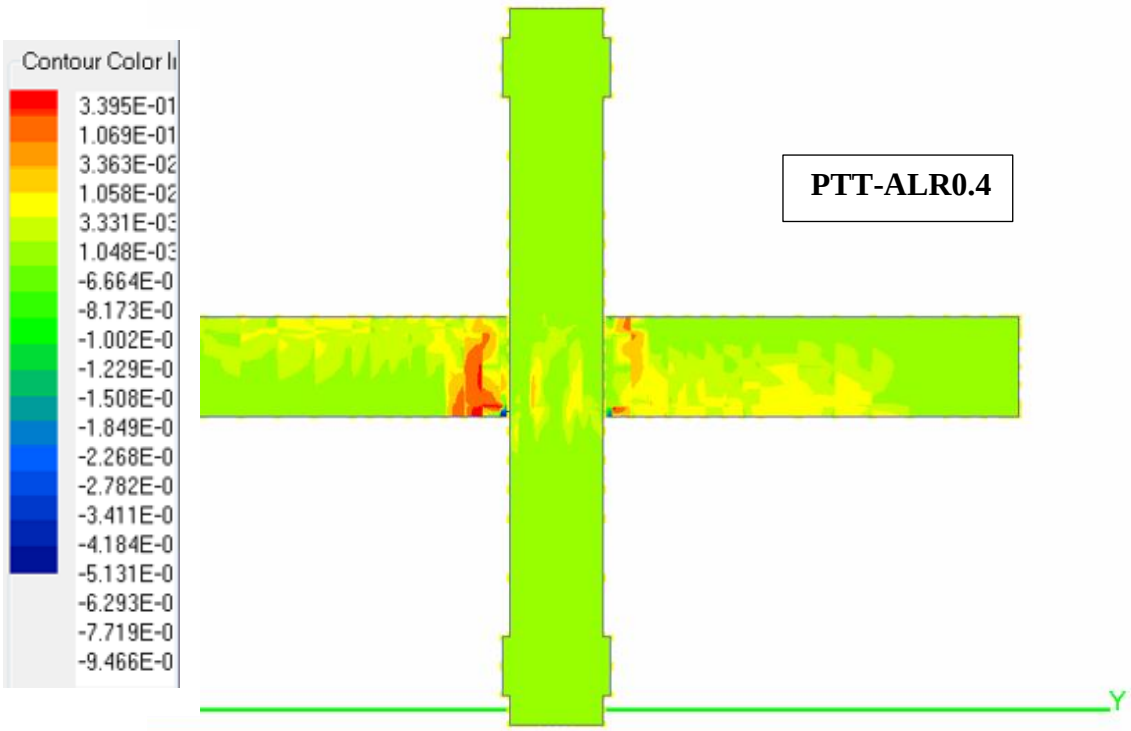
Contour Color li
3.395E-01
1.069E-01
3.363E-02
1.058E-02
3.331E-03
1.048E-03
-6.664E-0
-8.173E-0
-1.002E-0
-1.229E-0
-1.508E-0
-1.849E-0
-2.268E-0
-2.782E-0
-3.411E-0
-4.184E-0
-5.131E-0
-6.293E-0
-7.719E-0
-9.466E-0
PTT-ALR0.4
Y

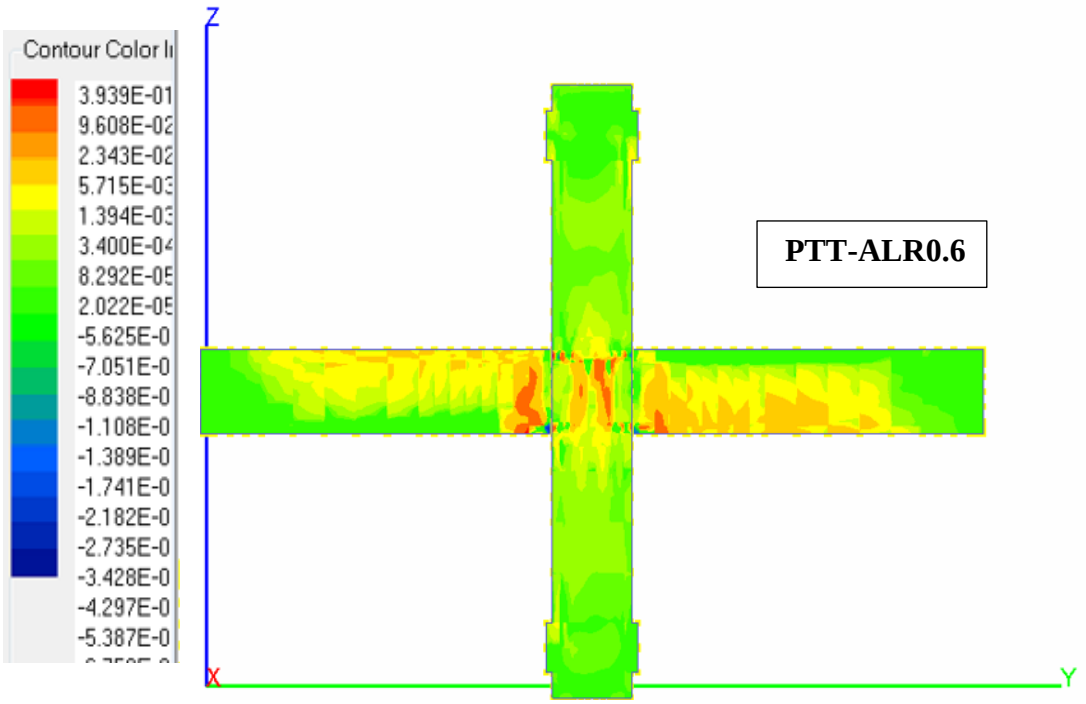

PTT-ALR0.6

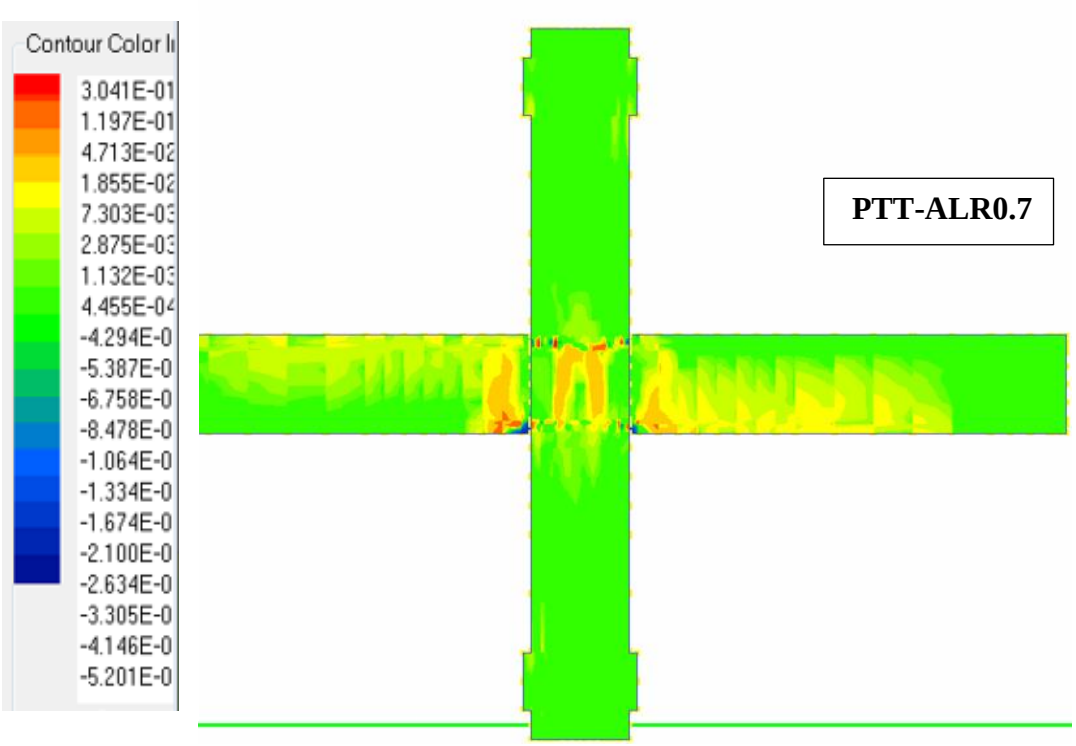

PTT-ALR0.7

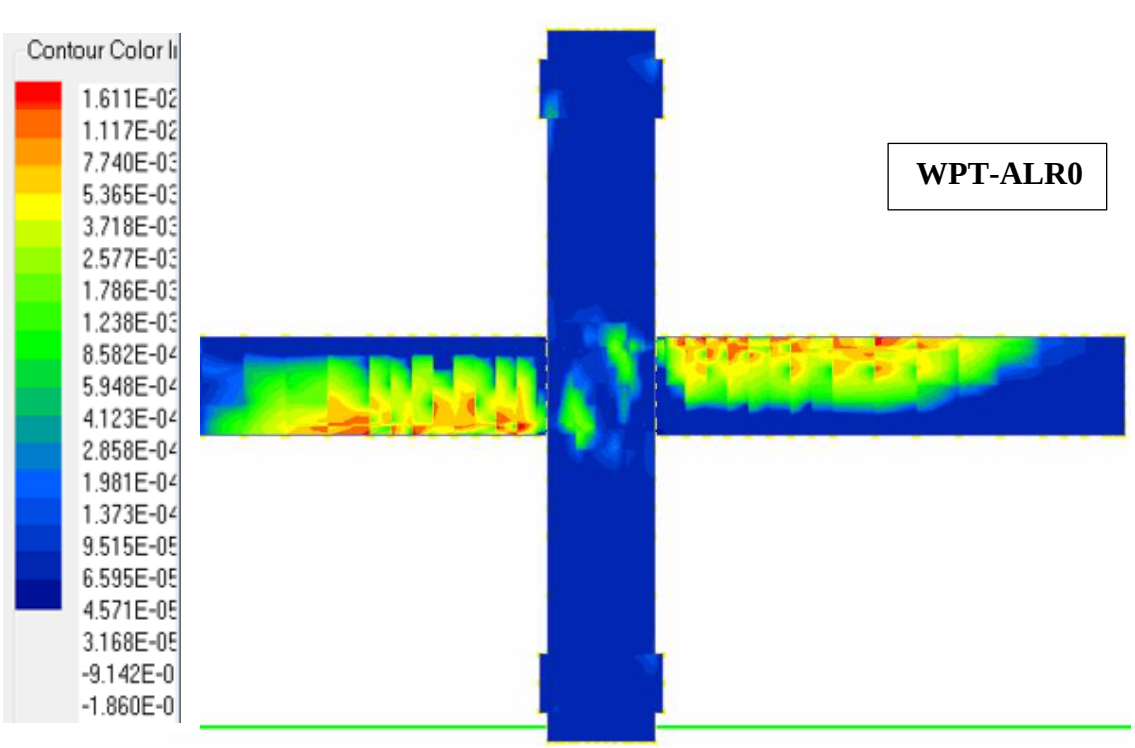
Contour Color li
1.611E-02
1.117E-02
7.740E-03
5.365E-03
3.718E-03
2.577E-03
1.786E-03
1.238E-03
8.582E-04
5.948E-04
4.123E-04
2.858E-04
1.981E-04
1.373E-04
9.515E-05
6.595E-05
4.571E-05
3.168E-05
-9.142E-0
-1.860E-0
WPT-ALR0

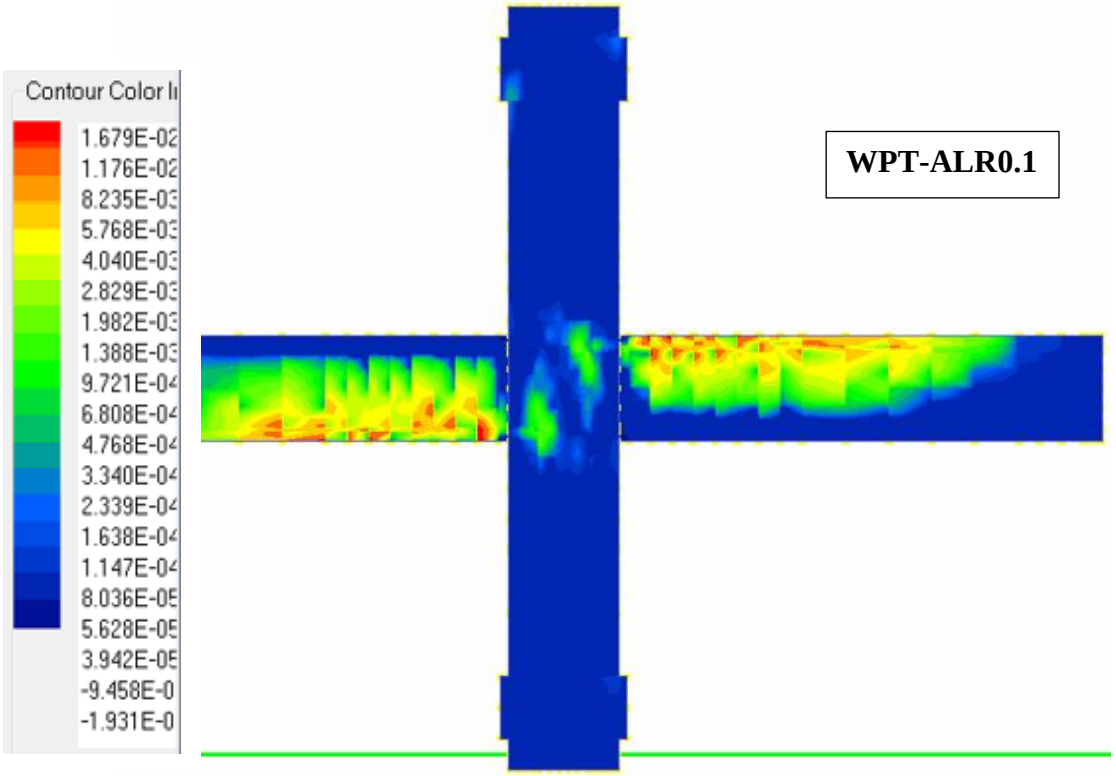
Contour Color li
1.679E-02
1.176E-02
8.235E-03
5.768E-03
4.040E-03
2.829E-03
1.982E-03
1.388E-03
9.721E-04
6.808E-04
4.768E-04
3.340E-04
2.339E-04
1.638E-04
1.147E-04
8.036E-05
5.628E-05
3.942E-05
-9.458E-0
-1.931E-0
WPT-ALR0.1

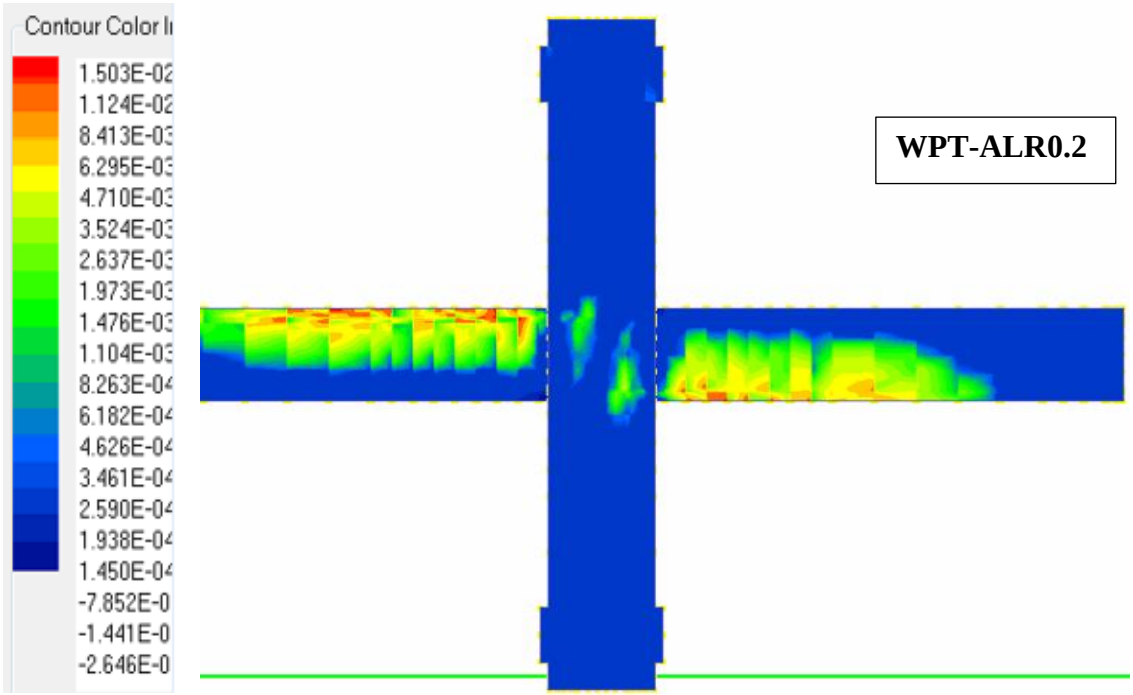
Contour Color li
1.503E-02
1.124E-02
8.413E-03
6.295E-03
4.710E-03
3.524E-03
2.637E-03
1.973E-03
1.476E-03
1.104E-03
8.263E-04
6.182E-04
4.626E-04
3.461E-04
2.590E-04
1.938E-04
1.450E-04
-7.852E-0
-1.441E-0
-2.646E-0
WPT-ALR0.2

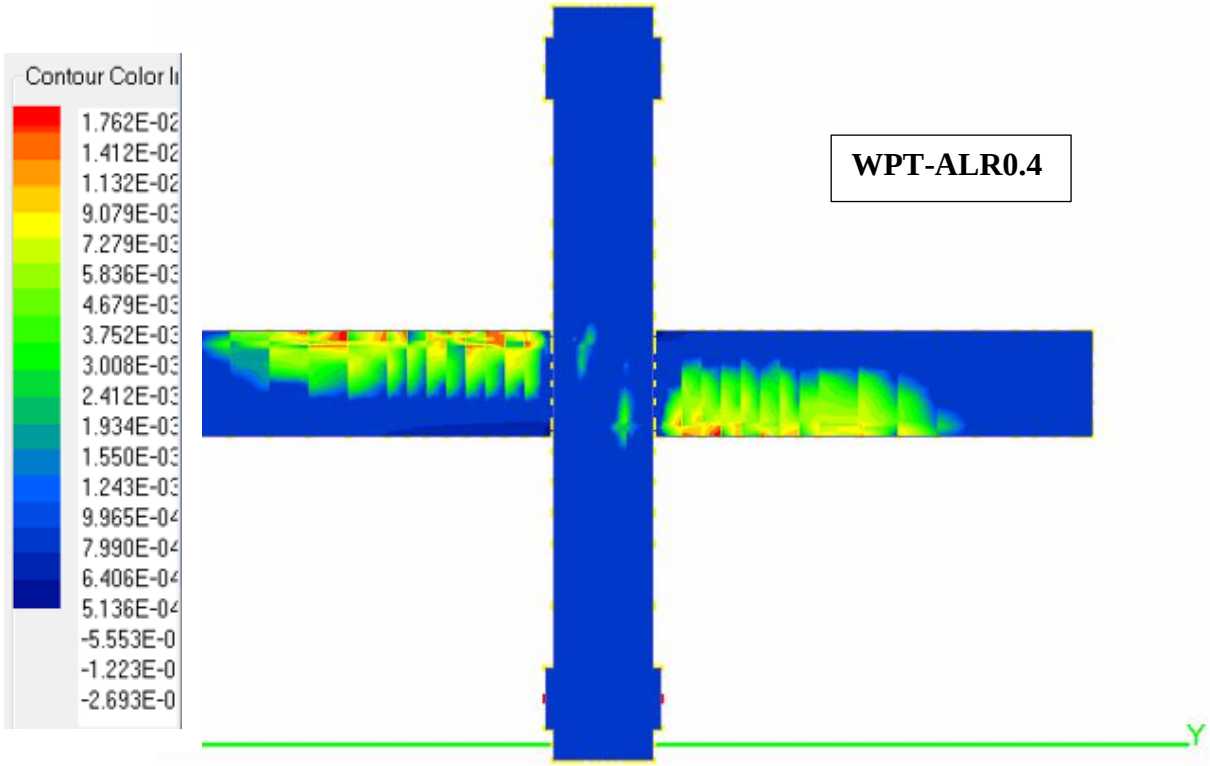
Contour Color li
1.762E-02
1.412E-02
1.132E-02
9.079E-03
7.279E-03
5.836E-03
4.679E-03
3.752E-03
3.008E-03
2.412E-03
1.934E-03
1.550E-03
1.243E-03
9.965E-04
7.990E-04
6.406E-04
5.136E-04
-5.553E-0
-1.223E-0
-2.693E-0
WPT-ALR0.4
Y

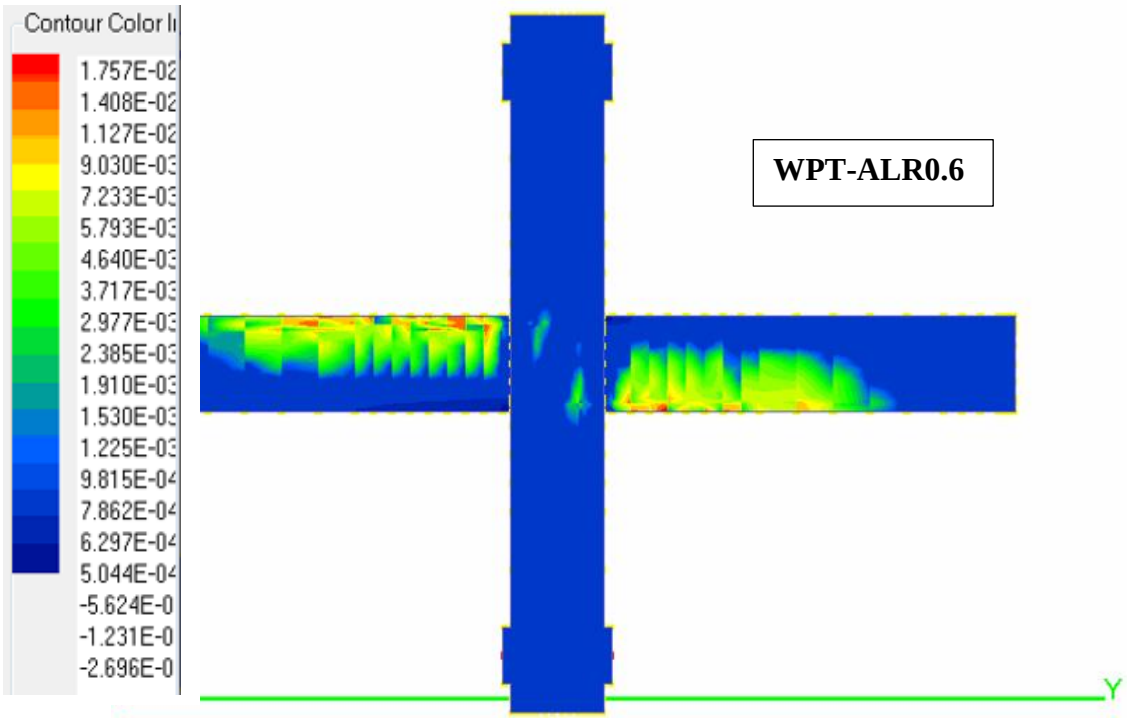
Contour Color li
1.757E-02
1.408E-02
1.127E-02
9.030E-03
7.233E-03
5.793E-03
4.640E-03
3.717E-03
2.977E-03
2.385E-03
1.910E-03
1.530E-03
1.225E-03
9.815E-04
7.862E-04
6.297E-04
5.044E-04
-5.624E-0
-1.231E-0
-2.696E-0
WPT-ALR0.6
Y

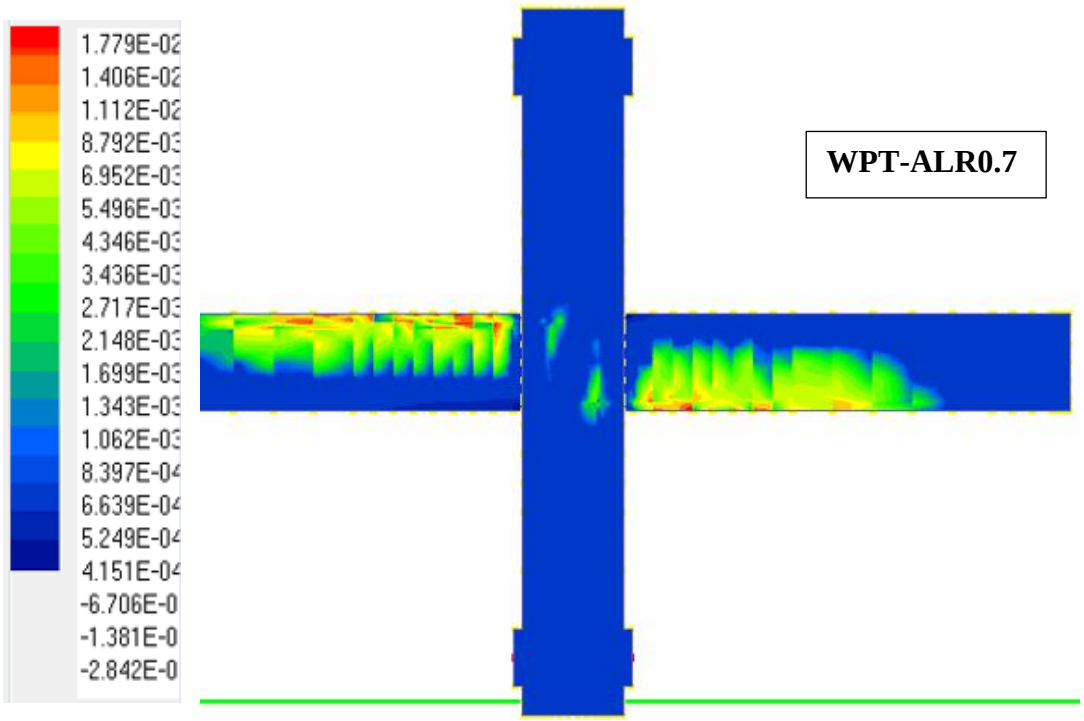
1.779E-02
1.406E-02
1.112E-02
8.792E-03
6.952E-03
5.496E-03
4.346E-03
3.436E-03
2.717E-03
2.148E-03
1.699E-03
1.343E-03
1.062E-03
8.397E-04
6.639E-04
5.249E-04
4.151E-04
-6.706E-0
-1.381E-0
-2.842E-0
WPT-ALR0.7

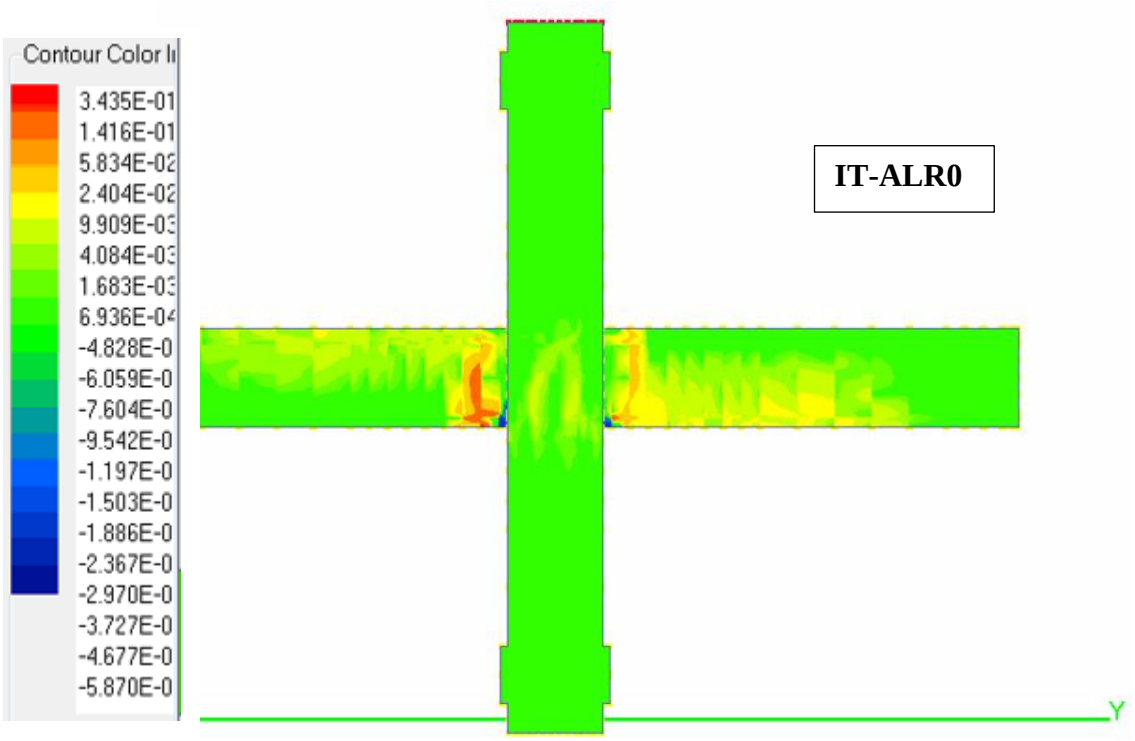
Contour Color Ii
3.435E-01
1.416E-01
5.834E-02
2.404E-02
9.909E-03
4.084E-03
1.683E-03
6.936E-04
-4.828E-0
-6.059E-0
-7.604E-0
-9.542E-0
-1.197E-0
-1.503E-0
-1.886E-0
-2.367E-0
-2.970E-0
-3.727E-0
-4.677E-0
-5.870E-0
IT-ALR0
Y

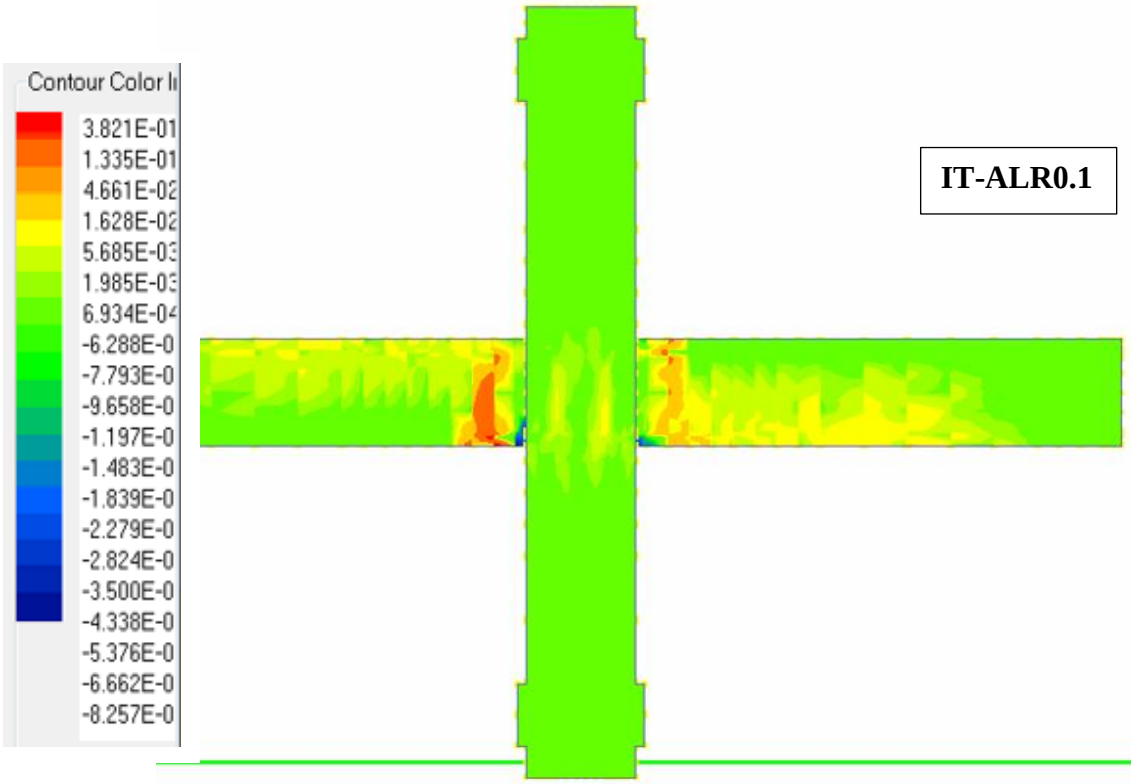
Contour Color Ii
3.821E-01
1.335E-01
4.661E-02
1.628E-02
5.685E-03
1.985E-03
6.934E-04
-6.288E-0
-7.793E-0
-9.658E-0
-1.197E-0
-1.483E-0
-1.839E-0
-2.279E-0
-2.824E-0
-3.500E-0
-4.338E-0
-5.376E-0
-6.662E-0
-8.257E-0
IT-ALR0.1

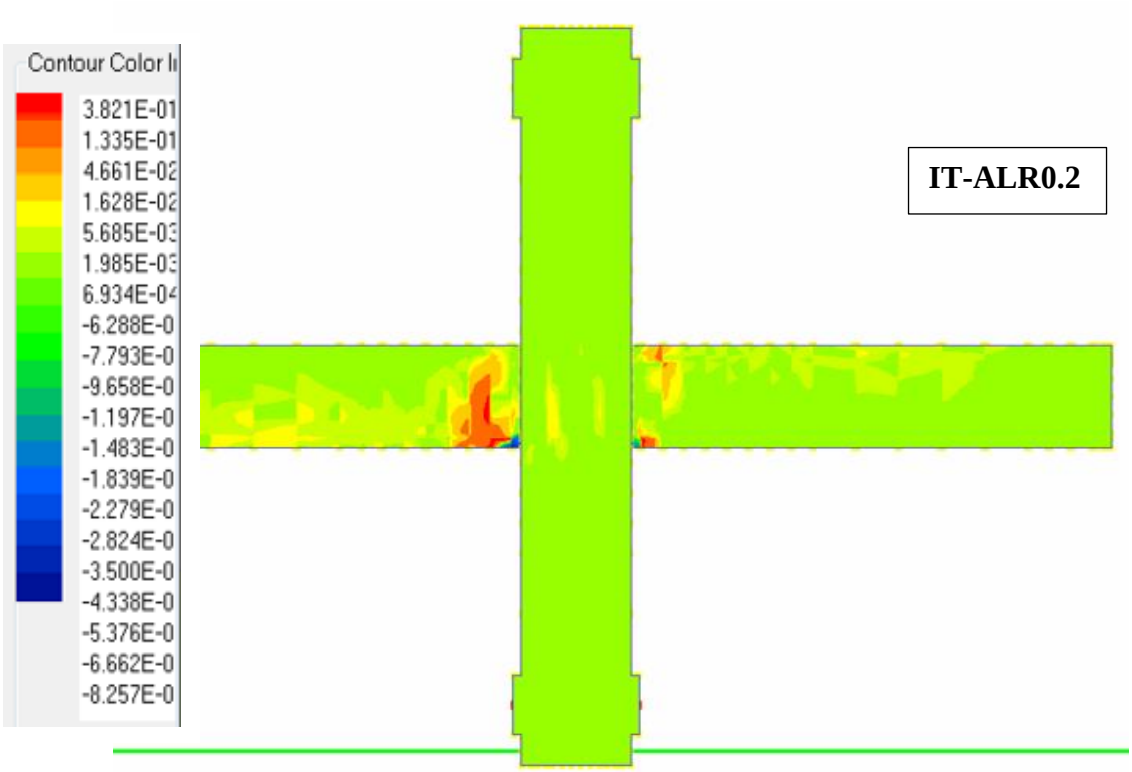
Contour Color li
3.821E-01
1.335E-01
4.661E-02
1.628E-02
5.685E-03
1.985E-03
6.934E-04
-6.288E-0
-7.793E-0
-9.658E-0
-1.197E-0
-1.483E-0
-1.839E-0
-2.279E-0
-2.824E-0
-3.500E-0
-4.338E-0
-5.376E-0
-6.662E-0
-8.257E-0
IT-ALR0.2

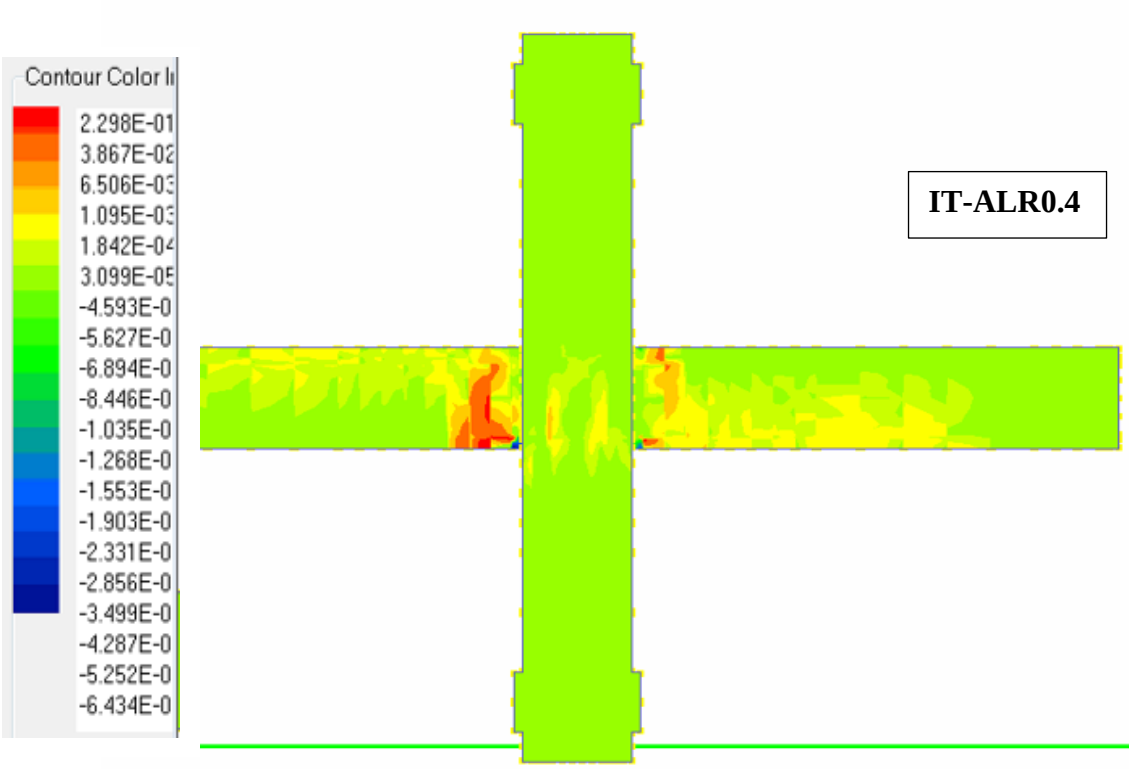
Contour Color li
2.298E-01
3.867E-02
6.506E-03
1.095E-03
1.842E-04
3.099E-05
-4.593E-0
-5.627E-0
-6.894E-0
-8.446E-0
-1.035E-0
-1.268E-0
-1.553E-0
-1.903E-0
-2.331E-0
-2.856E-0
-3.499E-0
-4.287E-0
-5.252E-0
-6.434E-0
IT-ALR0.4

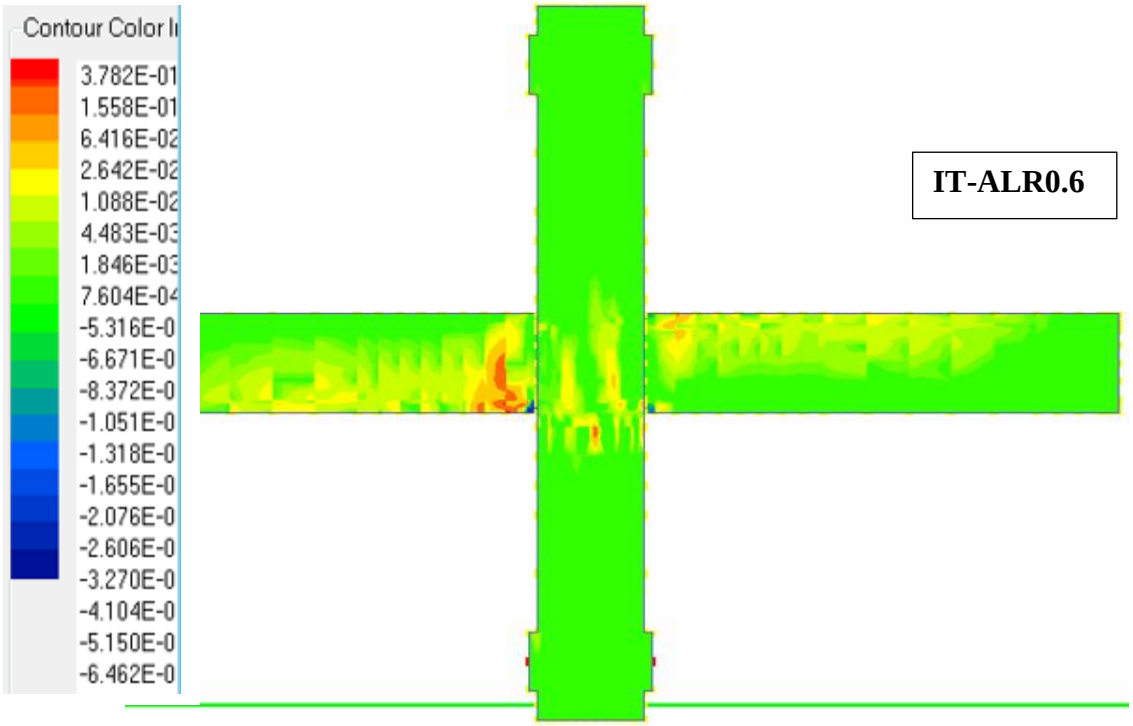
Contour Color I
3.782E-01
1.558E-01
6.416E-02
2.642E-02
1.088E-02
4.483E-03
1.846E-03
7.604E-04
-5.316E-0
-6.671E-0
-8.372E-0
-1.051E-0
-1.318E-0
-1.655E-0
-2.076E-0
-2.606E-0
-3.270E-0
-4.104E-0
-5.150E-0
-6.462E-0
IT-ALR0.6

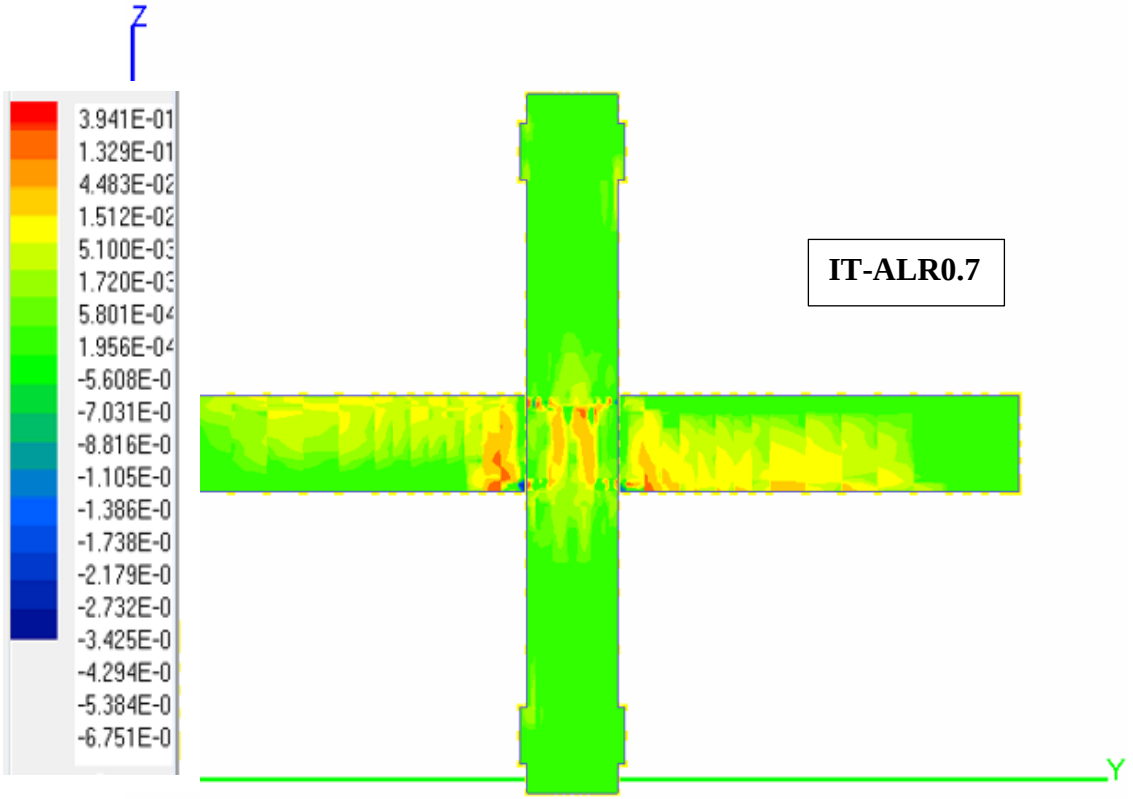
Z
3.941E-01
1.329E-01
4.483E-02
1.512E-02
5.100E-03
1.720E-03
5.801E-04
1.956E-04
-5.608E-0
-7.031E-0
-8.816E-0
-1.105E-0
-1.386E-0
-1.738E-0
-2.179E-0
-2.732E-0
-3.425E-0
-4.294E-0
-5.384E-0
-6.751E-0
IT-ALR0.7
Y